

UCSF

UC San Francisco Electronic Theses and Dissertations

Title

Histone mimicry in HP1 is required for a conformational switch that regulates assembly of a minimal heterochromatin unit necessary for silencing in vivo

Permalink

<https://escholarship.org/uc/item/8fs166kg>

Author

Canzio, Daniele

Publication Date

2012

Peer reviewed|Thesis/dissertation

Histone mimicry in HP1 is required for a conformational switch that regulates assembly of a minimal heterochromatin unit necessary for silencing *in vivo*

by

Daniele Canzio

DISSERTATION

Submitted in partial satisfaction of the requirements for the degree of

DOCTOR OF PHILOSOPHY

in

Chemistry & Chemical Biology

in the

GRADUATE DIVISION

Copyright (2012)

by

Daniele Canzio

Dedication

To my mother Carla, my sister Eugenia, and my father Giovanni,
your love, your values, and your passion inspire me and my work

Acknowledgments

My graduate career at UCSF was truly rich with numerous unforgettable experiences. The most significant one was the opportunity to work with many amazing people. Those people shaped my path, day after day. And more importantly, they showed me how essential the human aspect is in establishing fun and successful scientific research. I had the true honor to collaborate with many people from the Narlikar lab, from labs at UCSF, the NIH, and Harvard University. I have collaborated with people from all over the world, from Asian, North American, South American and European countries. Not all collaborations were easy. Some were more challenging than others. But at the heart of the relationships there was one common, genuine goal: to push the scientific discovery forward.

I am tremendously grateful to my graduate advisor Geeta Narlikar. Since my rotation in her lab, I have witnessed her devotion to mentoring students and postdocs, and her passion for scientific discovery. Geeta has a genuine instinct for the next scientific question, and a profound sensitivity for people needs, both crucial aspects that a leader must have to lead a research group. These are aspects that no one is born with but can conquer if aware of their significance. Geeta has a very strong set of values that allow her to confront challenging situations, and to imagine brave and unconventional solutions when necessary. She stands by her people and at times, puts them even before herself.

She trains her students and postdocs to think outside the box and to never be afraid of taking intellectual risks. There is essentially no limit to people's imaginations in her lab

when they based on careful and rigorous thinking. This ability to think big picture is what makes significant scientific breakthroughs possible in her lab.

My thanks to Geeta also includes her husband, Alok. Alok stands by Geeta with a unique sensitivity that gives her extra motivation and strength in her work. He is also a very good friend with whom I have had many profound and significant conversations throughout my time at UCSF.

UCSF offers a special environment to nurture high quality scientific collaborations and friendships. I had the good fortune to collaborate with multiple laboratories at UCSF. In particular, I am enormously thankful to the Madhani, the Cheng and the Cooke labs. Hiten Madhani has contributed to my research as a direct collaborator in both of my stories, and as a member of my thesis committee. Smita Shankar, Diana Marina, and Jennifer Garcia are members of the Madhani lab I most closely interacted with. I learned so much from all of them and my friendship with them goes beyond school. Yifan Cheng is a fantastic researcher and a talented group leader. I had the pleasure to work with him and members of his lab, in particular Maofu Liao and Shenping Wu, whom I worked with during my last 2 years at UCSF. I have learned so much from all of them and I am very grateful for their patience and time. In particular, I truly enjoyed collaborating with Maofu. I appreciated his devotion and his rigorous science. Roger Cooke is a legend. Roger has a drive for science that spontaneously and continuously reveals in every conversation you have with him. His unconventional motivation captures and inspires people around him. He has made a huge impact in my scientific and personal life, along with two other fantastic people from his lab, Nariman

Naber and Ed Pate. Together Roger, Nariman and Ed have a unique ability to make every day in their lab special and every experiment fun and exciting. Their lab is a place where ideas flourish, and young scientists are allowed to grow and develop without fear.

I also would like to thank Kris Kuchenbecker from the Fletterick lab for his scientific efforts in our first story and for the many useful scientific discussions we had together on each other projects. A big thanks also goes to the members of the Fujimori lab for their friendship and help throughout the years.

I have had the privilege to meet and work with Peter Schuck. Peter is a professor at NIH and a world leader in Analytical Ultracentrifugation (AUC), the technique that made my second story possible. He hosted me in his lab for 2 weeks in March of 2011. Being in his lab was a really exciting experience for me. I learned so much from him and all the members of his group. I thank them all for their generosity and time.

I had the pleasure to interact with two very talented postdocs from the Kingston lab at Harvard University, Matthew Simon and Karim-Jean Armache. They are both fantastic scientists and really great friends. Matt's graduate work on MLA made my project possible. He then generously trained me and helped me with my first story. To both Matt and Karim, I owe important conversations about graduate school and science, and I thank them for all their patience and time. I wish them all the best in establishing their new labs at Yale and NYU, respectively.

I have learned a great deal from another very talented postdoc at UCSF, Jesse Zalatan from the Lim lab. I thank him for all the help and intellectual training he constantly provide to me and to my lab.

I also want to thank the members of my thesis committee, Stavros Lomvardas, Kevan Shokat and Hiten Madhani, for all their time. Every meeting with them was fun, exciting and full of new ideas for my project.

A special thank also goes to the CCB program -Charley Craik, Christine Olson, Julia Molla and Nicole Flowers- for the help thought school.

The Narlikar lab was a special place for me to grow. It interchangeably served as school and as home. I joined the lab in July 2007 and I was the last graduate student to join for the following 2 years. Maybe for that reason, everybody looked after me like if I were a little kid for while and I cannot be more grateful for all the help and time of everybody. The first three graduate students to join the lab, Janet Yang, Georgette Charles and Claire Rowe, together with our first lab manager Tina Madrid, deserve a special thanks for establishing the core of the lab in its first years. Peretz Partensky and Lisa Racki, two other graduate students, were very instrumental to me. They both look after me. In particular, Lisa was my “guardian angel.” She is an inspirational scientist and a really fine human being. Lisa supported me in my hardest times in graduate school and I thank her so much for all her help. Kalyan Sinha is a fun and resourceful postdoc. Evelyn Cheng and Bassem Al-Sady were my partners-in-crime in our first story.

Together we set up a new system in the lab and I thank them so much for all their effort and help.

A few more fantastic students joined after me. John Leonard, Coral Zhou, Adam Larson, Stefan Isaac, Caitlin Stoddard and Ahmd Nbn are very talented students. I have learned so much from all of them and look forward to seeing them develop in the years to come. As I said before, the Narlikar lab was not just school for me, but served as home many times. That was especially true thank to both Adam and Coral. I have become very close friend to them and I have felt their support in my science and my life daily. I thank them for all the great times we have together inside and outside the lab.

Three more people deserve a tremendous recognition for their effort in the lab and for their patience with all the students and postdocs: Amanda Habel, Koy Saeteurn, and Julia Tretyakova, our two former and current lab managers.

I would also like to recognize critical past mentors. Elisabetta Bellagamba was my high school teacher of chemistry. She was the person that changed my path. Before meeting her, I had never thought of a career in science. Her passion for chemistry and her teaching opened up a new door in my life. At UCSB, I was lucky to meet many great faculties. Four in particular deserve a big thank: Paola Bruice, Tom Bruice, Stanley Parsons and David Harris. In particular, David was my mentor and a very good friend. He was another person that strongly shaped my path.

I want to thank all my friends, from the ones I met at UCSB, to the ones I met here in San Francisco. You all have stood by me and supported me throughout all those years. You are a family to me.

The Kryder and the Mulligan families deserve infinite thanks! I truly would have never been able to cross the finishing line without their daily support and immense generosity. LeeAnne and Norma are my other two mothers and I love them so much.

I want to thank my partner, Idelisse, for her love and support. I have learned so much from her at work and in our daily life. She has supported me through my most challenging times and always found the energy to make me laugh. She has made me a much better person.

Finally, an immense thanks goes to my father Giovanni, my mother Carla, and my sister Eugenia. I am extremely lucky to be part of such a special family. Our love and support for each other goes beyond anything and reaches each other even when we are so far apart. I have felt their presence in my life every single day. They have pointed to me the direction, they have shaped the road, and they have moved mountains for me to pass through. Their passion for life has inspired me and their strong values have provided the means for me to deal with all the challenges I have faced.

Chapter 2 of this thesis are reprints of material previously published in *Molecular Cell* (Mol Cell. 2011 Jan 7; 41(1):67-81). This material is included here in accordance with *Molecular Cell* permission request policies for authors.

Histone mimicry in HP1 is required for a conformational switch that regulates assembly of a minimal heterochromatin unit necessary for silencing *in vivo*

by Daniele Canzio

Abstract

Long-term silencing of large regions of the genome is achieved through the formation of heterochromatin. From yeast to humans, heterochromatin is characterized by two key molecular signatures: (i) di or tri-methylation of lysine 9 of histone H3 (H3K9me_{2/3}), and (ii) heterochromatin protein 1 (HP1). The association of HP1 with H3K9-methylated chromatin drives heterochromatin assembly and spread. Yet, how HP1 assembles on methylated nucleosomal templates and how the HP1-nucleosome complex is regulated are poorly understood.

Using *S. pombe* as a model system, we show that two dimers of the HP1 protein, Swi6, binds to one nucleosome: each dimer contains one chromodomain (CD) that engages one copy of the H3K9-methyl mark, while the other CD is unoccupied. This HP1-nucleosome complex acts as a scaffold for the addition of other HP1 molecules that self-associate through a novel CD-CD interface nucleating from the unoccupied CDs. Chromodomain-mediated polymerization of HP1 on chromatin appears to (1) increase its association with methylated nucleosomes *in vitro*, (2) bridge neighboring methylated nucleosomes, and (3) increase heterochromatin assembly *in vivo*.

Our data suggests that H3K9-methyl recognition and chromatin coating by HP1 are intrinsic to the fundamental architecture of the HP1-nucleosome complex. But they also raise the question of how methylated chromatin templates HP1 assembly.

We found that two key features of heterochromatin, the H3K9me3 and the nucleosomal DNA, promote a conformational change in Swi6 that drives its association with nucleosomes. By binding to methylated nucleosomes, unbound Swi6 dimers switch from an autoinhibited state that is refractory to both methyl mark recognition and higher-order oligomerization to a state that is competent for spreading. Cryo-EM studies of the Swi6-nucleosome complex reveal the architecture of the spreading competent state. *In vivo*, mutants that disrupt such a switch also result in disruption of heterochromatin.

The coupling of a conformational switch in HP1 to the recognition of specific features of methylated chromatin provides a mechanism for how HP1 can specifically target H3K9-methylated chromatin, thus preventing its aberrant spread into euchromatin. Finally, our discovery of these different HP1 conformational states provides a basic starting point for understanding how HP1 can switch between alternative functions in heterochromatin.

Table of contents

Preface		
	Dedication	iii
	Acknowledgments	iv
	Permissions	x
	Abstract	xi
	Table of contents	xiii
	List of figures and tables	xiv
	Author contributions	xvi
Chapter 1	Introduction	1
Chapter 2	Chromodomain mediated oligomerization of HP1 suggests a nucleosome bridging mechanism for heterochromatin assembly	17
Chapter 3	A conformational switch in HP1 allows conditional activation and drives heterochromatin assembly in vivo	101
Chapter 4	Characterization of the self-association and ligand binding properties of Swi6 domains in isolation	177

List of figures and tables

Chapter 2

Figure 1: Swi6 recognizes the H3K9 methyl mark within mononucleosomes and forms oligomers on mononucleosomes	61
Figure 2: Swi6 forms distinct oligomeric states in the absence of chromatin	62
Figure 3: Swi6 displays lower specificity for the H3K9me3 mark in mononucleosomes compared to that in H3 tail peptides	63
Figure 4: The core unit of Swi6 binding to a mononucleosome is a tetramer	64
Figure 5: Amplification of Swi6 specificity towards H3K9me3 occurs on nucleosome arrays and is sensitive to nucleosomal placement	65
Figure 6: The chromodomain contains the Swi6 tetramerization interface and couples tetramerization on the nucleosome surface to H3K9me3 recognition	66
Figure 7: Increased tetramerization of Swi6 translates into increased silencing and heterochromatin spreading at an artificial heterochromatic locus	67
Supplementary Figure S1: Analysis of the SPR data	70
Supplementary Figure S2: Loss of higher-order oligomerization in L315D Swi6 mutant	71
Supplementary Figure S3: Nucleosome and DNA binding by Swi6	72
Supplementary Figure S4: Analysis methods for Swi6-nucleosome AUC data	73
Supplementary Figure S5: Quality control for nucleosome arrays	74
Supplementary Figure S6: Swi6 deletion analysis	75
Supplementary Figure S7: Silencing phenotype of <i>swi6</i> ⁺ and <i>swi6</i> ^{VY→EW}	76

Chapter 3

Figure 1: Dissecting Swi6 self-association equilibria	137
Figure 2: Identification of an H3-tail mimic in Swi6 chromodomain	138

Figure 3: The ARK loop in Swi6 chromodomain is immobilized in the closed conformation of the Swi6 dimer	139
Figure 4: Visualization of distinct Swi6 conformations and of the Swi6-H3K ₉ me ₃ nucleosome complex by EM	140
Figure 5: Energetics of methylated nucleosome recognition by Swi6	141
Figure 6: Swi6 ^{LoopX} and Swi6 ^{AcidicX} results in defects in pericentromeric heterochromatin silencing	142
Supplementary Figure 1 (S1): Analysis of Swi6 ^{WT} self-association	145
Supplementary Figure 2 (S2): Two-step isodesmic self-association model	146
Supplementary Figure 3 (S3): Monomer-dimer-tetramer and monomer-trimer model	147
Supplementary Figure 4 (S4): Studies of the self-association process of Swi6	148
Supplementary Figure 5 (S5): Characterization of Swi6 ^{3S} and Swi6 ^{probe}	149
Supplementary Figure 6 (S6): Characterization of CFP-Swi6 and Swi6-CFP	150
Supplementary Figure 7 (S7): Cryo-EM studies of Swi6-nucleosome complex	151
Supplementary Figure 8 (S8): Nucleosome and DNA binding studies	152
Supplementary Figure 9 (S9): <i>In vivo</i> characterization of Swi6 mutants	153
Supplementary Table 1: Table of all the Swi6 constructs used in this study	176
Supplementary Table 2: Table of all the <i>S. pombe</i> strains used in this study	176

Chapter 4

Figure 1: The role of the acidic stretch in the CD of Swi6	192
Figure 2: Methylation of the ARK loop its increases affinity for the CD	193
Figure 3: Thermodynamic analysis of Swi6 chromoshadow domain	194
Figure 4: The chromoshadow domain of Swi6 binds the nucleosome	195
Figure 5: Contribution of the Hinge region to DNA binding	196

Author contributions

Chapter 2:

The work presented in this chapter is the result of a close collaboration with two other members of the Narlikar lab, Bassem Al-Sady and Evelyn Cheng. Together with our advisor, Geeta Narlikar, we designed and performed the bulk of the experiments and wrote the manuscript. We also received tremendous help from all the other co-authors to which we are extremely thankful. I worked closely with Kristopher Kuchenbecker in designing and performing SPR-based assays. I performed crosslinking, MALS, ITC and SV AUC. I performed all the mono-nucleosome binding assays. I identified the chromodomain of Swi6 as the interface responsible for Swi6 oligomerization. With the help of Bassem Al-Sady, I designed mutants to further probe this interface. Bassem Al-Sady designed nucleosomal arrays and measured Swi6 binding to arrays. Together with Smita Shankar, Bassem Al-Sady performed *in vivo* silencing and Chip assays. Hiten Madhani oversaw the design and interpretation of the *in vivo* experiments. Evelyn Cheng performed the fluorescence anisotropy assay for measuring nucleosome binding by Swi6, and measured Swi6 binding to dinucleosome substrates. Matthew Simon trained Bassem Al-Sady, Evelyn Cheng and I in obtaining MLA histones.

Chapter 3:

The core questions presented in this chapter were designed, developed and addressed by me and my graduate advisor, Geeta Narlikar. Together, we designed the bulk of the experiments and wrote manuscript. I performed the bulk of the experiments and also received tremendous help from all the other co-authors to which I am extremely thankful.

Peter Schuck trained me in the use of AUC approaches and was instrumental in analyzing and interpreting the AUC data. Together with Nariman Naber, we performed the EPR experiments. And together with Ed Pate, Adam Larson and Roger Cooke, we deconvolved the EPR spectra. Diana Marina trained me in strain construction and in the use of silencing and ChIP assays. Jennifer Garcia constructed some of the *S.pombe* strains and performed some of the initial *in vivo* experiments. I worked closely with Maofu Liao to generate samples for negative stain studies of Swi6 and cryo-EM studies of the Swi6-nucleosome complex. Maofu Liao generated the 2D reconstructions of the CFP-Swi6 and Swi6-CFP constructs, and 3D reconstructions of the Swi6-nucleosome complex. Shenping Wu generated the 3D reconstruction of the nucleosome alone by cryo-EM. Yifan Cheng oversaw all the EM analysis and interpretation. Hiten Madhani oversaw the design and interpretation of the *in vivo* experiments. Roger Cook oversaw the EPR analysis and interpretation.

Chapter 4:

The core questions presented in this chapter were designed, developed and addressed by me and my graduate advisor, Geeta Narlikar. I performed most of the experiments. As in chapter 3, I received help from Peter Schuck in the use of AUC approaches and from Maofu Liao, Shenping Wu and Yifan Cheng in performing and interpreting EM studies.

Chapter 1:

Introduction

1. A. Chromatin states and chromatin dynamics

i. The origin of the term chromatin

The assembly of DNA into higher-order chromatin is central to the spatial and temporal regulation of the eukaryotic genome (Cremer and Cremer, 2001; Cavalli, 2002). A variety of nuclear processes ranging from DNA replication, recombination, repair, and transcription are highly dependent on the underlying chromatin structure (Cremer and Cremer, 2001; Cavalli, 2002).

The term chromatin comes from the Greek term *chromo* -color- and was originally used by Walther Flemming in the 1880s to term the colorable substance within the eukaryotic nuclei (Flemming, 1878). During the 1900s, Flemming and colleagues reported on the ability of chromatin to transform into higher-order chromosome structures during mitosis and to reversibly decondense into lower-order chromatin structures after cell division (Flemming, 1882).

Those early remarkable observations paved the way to the discovery that chromatin is the complex assemblage of DNA, histone proteins, and other nonhistone protein components, and that such assemblage is subjected to regulated dynamic changes that allow the eukaryotic DNA to fulfill its numerous nuclear processes (Cremer and Cremer, 2001; Cavalli, 2002; Woodcock, 2006).

ii. The nucleosome: the basic unit of chromatin

The repeating building block of chromatin is the nucleosome. The nucleosome is a large nucleo-protein complex made by a DNA fragment of defined length (147 base pairs of DNA) that is wrapped around an octamer of proteins called histones (Luger et al., 1997). The octamer is made of two copies each of four different histones (H2A, H2B, H3 and H4). The nucleosome complex is stabilized by a multitude of protein–protein interactions within the histone octamer and by numerous electrostatic and hydrogen bonding interactions between protein and DNA. In addition, histones also have flexible regions that protrude outside the core complex, known as histone tails. Those histone tails are site of an extensive array of post-translation modifications that regulate the interaction of the nucleosome with other neighboring nucleosomes or with many nuclear factors (Luger and Richmond, 1998; Taverna et al., 2007).

Nucleosome arrays have the strong tendency to fold into higher-order structures. Many different models, based on a large number of electron microscopy, single molecule and computational studies, have been proposed to describe the properties of folded nucleosome arrays *in vitro* (Robinson and Rhodes, 2006; Tremethick, 2007; Kruithof et al., 2009; Luger et al., 2012). Whether or not those exact proposed structures apply in the settings of the nucleus still remains elusive.

iii. Early structural evidence of distinct chromatin states within the nucleus

Early structural evidence of folding of nucleosomes into higher-order states *in vivo*, came from Emil Heitz in the 1920s. While studying chromatin extracted from

Drosophila salivary glands, Heitz observed the presence of at least two distinct DNA staining patterns (Heitz, 1928). He named those two states euchromatin (from the Greek *eu* -same- and *chromo* -color-) and heterochromatin (from the Greek “*hetero*” -different- and *chromo* -color-) (Heitz, 1929). Based on his observation, Heitz also posited that while euchromatin was the chromatin state containing genes, heterochromatin was the state that either did not or that it contained “somehow passive genes” (Heitz, 1929). Although such hypothesis turned out to be not entirely valid, it provided a strong motivation for numerous subsequent elegant genetic and biochemical studies aimed to understand not only the basis of the cytological differences between chromatin domains but also their distinct functional properties.

B. Heterochromatin

i. Functional properties

A breakthrough in the understanding that different chromatin states bear distinct functional outcomes came with the observation that the location of a particular gene within the genome would dictate its expression. The first evidence of such phenomena came with the observation that the gene responsible for a red eye pigmentation of a *Drosophila* fruit fly would be silenced when either located close or within an heterochromatic region (Muller and Altenburg, 1930; Spofford, 1967). This phenomena was named position effect variegation (PEV).

PEV studies immediately revealed what is known to be the hallmark of heterochromatin: its ability to spread in a region-specific, sequence-independent manner.

By propagating, heterochromatin, not only can cause gene repression and silencing, but also, prohibit illegitimate recombination, assist in sister chromatin cohesion, and maintain telomere stability, all essential aspects of genome integrity (Weiler and Wakimoto, 1995; Wallrath, 1998; Maison and Almouzni, 2004). However, mis-regulation of heterochromatin spread can lead to illegitimate gene silencing due to aberrant heterochromatin spread. Defects in heterochromatin are therefore strongly associated with uncontrolled cell growth and migration, hallmarks of cancer (Jones and Baylin, 2002).

ii. Structural properties

It became suddenly clear that chromatin packaging plays a fundamental role in PEV. In fact, when the structure of a variegating transgene was assayed by restriction enzymes, it revealed a significant reduction of DNA accessibility (Wallrath and Elgin, 1995). Moreover, micrococcal nuclease studies revealed a difference in packaging of the heterochromatic inserts compared to the euchromatic ones. In particular, the chromatin structure of the variegating insert was characterized by an evenly-spaced, regular arrangement of the nucleosomes, while for the non-variegating insert, the nucleosome arrangement was found to be less ordered and the domain less chromatinized (Wallrath and Elgin, 1995). This same signature of evenly-spaced nucleosome arrangement was also observed for endogenous heterochromatic regions (Sun et al., 2001).

Those studies, all together, suggested the existence of an underlying mechanism that imposes a specific structure to a DNA region that results in its gene suppression.

Such a mechanism must be able to spread for large regions of the genome in a sequence-independent manner. But it also must be somewhat responsible to the dynamic changes that the eukaryotic genome undergoes during cell cycle, therefore demanding some form of reversibility. Following studies identified di or tri-methylation of lysine 9 of histone H3 (H3K9me_{2/3}) and the heterochromatin protein 1 (HP1) as central players the heterochromatin machinery.

C. HP1 proteins and their role in heterochromatin formation

i. The discovery of HP1 proteins

The most conserved form of heterochromatin, from yeast to humans, is characterized by two key molecular signatures: (1) di or tri-methylation of lysine 9 of histone H3 (H3K9me_{2/3}), and (2) a class of protein called heterochromatin protein 1 (HP1) (Eissenberg and Elgin, 2000; Lachner et al., 2001; Nakayama et al., 2001; Noma K et al., 2001; Peters et al., 2001; Grewal and Elgin, 2002; Grewal and Jia, 2007).

HP1 proteins were first identified in *Drosophila* as dominant suppressors of PEV but based on their sequence conservation, they were immediately predicted to have conserved structure and function all the way from yeast to mammals (Clark and Elgin, 1992; Platero et al., 1995). Elegant genetic studies using *Drosophila* as a model system, demonstrated that tethering of HP1 to known euchromatin regions of the genome, causes nucleation and bi-directional spread of silent chromatin for more than 4 kilobases (kb) (Danzer and Wallrath, 2004). Those same studies also showed that HP1 spreading across

chromatin is accompanied by a drastic reorganization of nucleosomes into more regular arrays (Danzer and Wallrath, 2004),

ii. The HP1-nucleosome complex is central to assembly and spreading of heterochromatin

The chromodomain (CD) is the most highly conserved domain among HP1 proteins and is known to bind the H3K9 methyl mark (Bannister et al., 2001; Jacobs and Khorasanizadeh, 2002; Nielsen et al., 2002). The current model of heterochromatin spread posits that H3K9 methylation by the Suvar3-9 family of histone methyltransferases provides a binding site for the CD of HP1 (Rea et al., 2000; Nakayama et al., 2001; Danzer and Wallrath, 2004). Upon binding to methylated chromatin, HP1 self-associates and recruits a variety of chromatin-modifiers -such as the Suv39h1 itself, histone deacetylases (HDACs) and chromatin remodeling enzymes- that participate in heterochromatin formation (Grewal and Elgin, 2002; Hall et al., 2002; Zhang et al., 2002; Yamamoto and Sonoda, 2003; Eskeland et al., 2007; Grewal and Jia, 2007). Thus, central to the spread of heterochromatin lies the formation of the HP1-nucleosome complex. Yet how methylated chromatin templates HP1 assembly is not understood.

Interestingly, the association of HP1 proteins with methylated chromatin *in vivo* is known to be highly dynamic (Cheutin et al., 2003, 2004). Distinct on- and off-rates from chromatin have been measured for HP1 (Cheutin et al., 2003, 2004), raising the

interesting question of what is the nature of the interactions that governs the HP1-nucleosome complex.

In addition to gene silencing, the HP1-chromatin platform is important for other fundamental processes such as centromere formation, repression of recombination, sister chromatid cohesion, and maintenance of telomere stability (Fanti and Pimpinelli, 2008; Vermaak and Malik, 2009; Zeng et al., 2010). Some clues to the versatility of the function of HP1-nucleosome complex can be found in the biochemical properties of its individual domains of HP1. In addition to the CD domain, HP1 proteins also contain an evolutionarily related chromoshadow (CSD) domain and an unstructured hinge region (H). The CSD domain is involved in homodimerization of HP1 proteins (Yamada et al., 1999; Brasher et al., 2000; Cowieson et al., 2000) and in reading PxVxL peptapeptide motifs and other sequences present in different proteins partners (Smothers and Henikoff, 2000; Mendez et al., 2011). The hinge region is implicated in sequence-independent RNA and DNA binding (Zhao et al., 2000; Muchardt et al., 2002; Meehan et al., 2003). It can therefore be imagined that, depending on the specific ligands of these domains, the HP1-chromatin platform can recruit different regulatory factors. Yet, how the different HP1 domains work together to create a regulatable HP1-chromatin complex is not known.

D. *S. pombe* as a model system to study HP1-mediated heterochromatin formation

Fission yeast *S. pombe* contains three main heterochromatic regions: the centromere, the mating-type locus and the telomere (Grewal and Elgin, 2002; Grewal

and Jia, 2007). All the major components involved in H3K9 methylated heterochromatin formation and spreading in higher eukaryotes are conserved in this system (Grewal and Elgin, 2002; Grewal and Jia, 2007). These include, for example, the HP1 family of proteins Swi6 and Chp2, the histone H3K9 methyltransferase, Clr4, member of the Suvar39 family, conserved HDACs of class II, Clr3 and Clr6, and the chromatin remodeling complex SHREC reminiscent of the Mi-2 class of chromatin remodeling NuRD (Nakayama et al., 2001; Min et al., 2002; Yamada et al., 2005; Grewal and Jia, 2007; Sugiyama et al., 2007; Sadaie et al., 2008).

Based on the high conservation between the fission yeast and the human system, we set to exploit the *S. pombe* system to investigate the mechanism of HP1-mediated heterochromatin assembly and spread. We believe that understanding the molecular interplay of the main components of heterochromatin in fission yeast will provide direct insight into the mechanism of their human counterparts.

E. Work presented here

The focus of this thesis is on the fission yeast HP1 protein, Swi6. Swi6 is the most abundant HP1 protein in *S. pombe* and a central player involved in recombination and gene expression of all three main heterochromatic regions (Klar and Bonaduce, 1991; Lorentz et al., 1992, 1994; Nakayama et al., 2000; Wang et al., 2000; Grewal and Elgin, 2002; Grewal and Jia, 2007).

Our approach was to investigate how the biochemical and structural properties of Swi6 would translate into the formation of a functional heterochromatin structure *in vivo*. To do so, we established an *in vitro* system to study Swi6 association to methylated nucleosomes templates and used known genetic tools to test our biochemical and biophysical predictions in fission yeast.

i. Chromodomain-mediated oligomerization of HP1 suggests a nucleosome bridging mechanism for heterochromatin assembly

In Chapter 2, we showed that CD of Swi6 bears an interface that mediates its self-association beyond dimers in addition to its binding site for the H3K9 methyl mark. Increased CD-CD self-association correlates with (1) increased specificity for methylated nucleosomes *in vitro*, and (2) increased heterochromatin assembly *in vivo*. We also measured the stoichiometry of the Swi6-nucleosome complex where two dimers of Swi6 bind to one nucleosome. Each dimer contains one CD that engages one copy of an H3K9 methyl mark, while the other CD is unoccupied. We hypothesized that the two unoccupied CDs serve as sticky ends to bridge neighboring methylated nucleosomes that can either be adjacent or located on different chromatin fibers.

The data presented in this Chapter supported a model in which methyl mark recognition on chromatin by the HP1 CD is structurally and energetically coupled to its ability to oligomerize.

ii. A conformational switch in HP1 allows for conditional activation and heterochromatin assembly *in vivo*

In Chapter 3, we present data showing that unbound Swi6 dimers exist in an auto-inhibited state that simultaneously blocks H3K9 methyl mark recognition and higher-order oligomerization. This auto-inhibition arises from a histone mimic sequence in one Swi6 monomer that blocks methyl mark recognition by the chromodomain of another monomer. Binding to methylated nucleosomes pays the energetic cost for switching Swi6 dimers to a spreading competent state. We provide evidence of such a spreading competent state by obtaining a cryo-EM structure of the Swi6-H3K9me3 nucleosome complex. This structure also reveals the two unbound CD sticky ends, described in Chapter 2. Finally, this switch between an auto-inhibited state and a spreading competent state appears central to heterochromatin assembly *in vivo*. Mutants that disrupt such a switch also result in disruption of heterochromatin structures *in vivo*.

The data presented in this Chapter uncovered a new strategy by which the nucleosomal template controls HP1 oligomerization and provide a basic starting point for understanding how HP1 molecules can switch between different conformational states that bear alternative functions.

iii. Characterization of the self-association and ligand binding of Swi6 domains in isolation

In Chapter 4, we present data that describe the self-association, H3K9me3 tail, DNA, and nucleosome binding properties of the different Swi6 domains.

We aimed to understand how the specific functions of the different domains are integrated in the context of the full-length protein.

References

- Bannister, A.J., Zegerman, P., Partridge, J.F., Miska, E.A., Thomas, J.O., Allshire, R.C., and Kouzarides, T. (2001). Selective recognition of methylated lysine 9 on histone H3 by the HP1 chromo domain. *Nature* *410*, 120–124.
- Brasher, S. V, Smith, B.O., Fogh, R.H., Nietlispach, D., Thiru, a, Nielsen, P.R., Broadhurst, R.W., Ball, L.J., Murzina, N. V, and Laue, E.D. (2000). The structure of mouse HP1 suggests a unique mode of single peptide recognition by the shadow chromo domain dimer. *The EMBO Journal* *19*, 1587–1597.
- Cavalli, G. (2002). Chromatin as a eukaryotic template of genetic information. *Current Opinion in Cell Biology* *14*, 269–278.
- Cheutin, T., Gorski, S., and May, K. (2004). In vivo dynamics of Swi6 in yeast: evidence for a stochastic model of heterochromatin. *Molecular and Cellular Biology* *24*, 3157–3167.
- Cheutin, T., McNairn, A.J., Jenuwein, T., Gilbert, D.M., Singh, P.B., and Misteli, T. (2003). Maintenance of stable heterochromatin domains by dynamic HP1 binding. *Science (New York, N.Y.)* *299*, 721–725.
- Clark, R.F., and Elgin, S.C. (1992). Heterochromatin protein 1, a known suppressor of position-effect variegation, is highly conserved in *Drosophila*. *Nucleic Acids Research* *20*, 6067–6074.
- Cowieson, N.P., Partridge, J.F., Allshire, R.C., and McLaughlin, P.J. (2000). Dimerisation of a chromo shadow domain and distinctions from the chromodomain as revealed by structural analysis. *Current Biology : CB* *10*, 517–525.
- Cremer, T., and Cremer, C. (2001). Chromosome territories, nuclear architecture and gene regulation in mammalian cells. *Nature Reviews. Genetics* *2*, 292–301.
- Danzer, J.R., and Wallrath, L.L. (2004). Mechanisms of HP1-mediated gene silencing in *Drosophila*. *Development (Cambridge, England)* *131*, 3571–3580.
- Eissenberg, J.C., and Elgin, S.C. (2000). The HP1 protein family: getting a grip on chromatin. *Current Opinion in Genetics & Development* *10*, 204–210.

Eskeland, R., Eberharter, A., and Imhof, A. (2007). HP1 binding to chromatin methylated at H3K9 is enhanced by auxiliary factors. *Molecular and Cellular Biology* 27, 453–465.

Fanti, L., and Pimpinelli, S. (2008). HP1: a functionally multifaceted protein. *Current Opinion in Genetics & Development* 18, 169–174.

Flemming, W. (1878). Beitrage zur Kenntniss der Zelle und ihrer Lebenserscheinungen. *Arch. Mikroskop* 16, 302–436.

Flemming, W. (1882). *Zellsubstanz, Kern und Zelltheilung* (Leipzig, Germany).

Grewal, S.I., and Elgin, S.C. (2002). Heterochromatin: new possibilities for the inheritance of structure. *Current Opinion in Genetics & Development* 12, 178–187.

Grewal, S.I.S., and Jia, S. (2007). Heterochromatin revisited. *Nature Reviews. Genetics* 8, 35–46.

Hall, I.M., Shankaranarayana, G.D., Noma, K.-I., Ayoub, N., Cohen, A., and Grewal, S.I.S. (2002). Establishment and maintenance of a heterochromatin domain. *Science (New York, N.Y.)* 297, 2232–2237.

Heitz, E. (1928). Das Heterochromatin der Moose, 1. Jahrb. *Wiss. Bot.* 69, , 762–818.

Heitz, E. (1929). Heterochromatin, Chromocentren, Chromomeren. *Ber. Dtsch. Bot. Ges.* 47, 274–284.

Jacobs, S. a, and Khorasanizadeh, S. (2002). Structure of HP1 chromodomain bound to a lysine 9-methylated histone H3 tail. *Science (New York, N.Y.)* 295, 2080–2083.

Jones, P.A., and Baylin, S.B. (2002). The fundamental role of epigenetic events in cancer. *Nature Reviews. Genetics* 3, 415–428.

Klar, A., and Bonaduce, M. (1991). *swi6*, a gene required for mating-type switching, prohibits meiotic recombination in the *mat2-mat3* “cold spot” of fission yeast. *Genetics*.

Kruithof, M., Chien, F.-T., Routh, A., Logie, C., Rhodes, D., and Van Noort, J. (2009). Single-molecule force spectroscopy reveals a highly compliant helical folding for the 30-nm chromatin fiber. *Nature Structural & Molecular Biology* 16, 534–540.

Lachner, M., O’Carroll, D., Rea, S., Mechtler, K., and Jenuwein, T. (2001). Methylation of histone H3 lysine 9 creates a binding site for HP1 proteins. *Nature* 410, 116–120.

Lorentz, a, Heim, L., and Schmidt, H. (1992). The switching gene *swi6* affects recombination and gene expression in the mating-type region of *Schizosaccharomyces pombe*. *Molecular & General Genetics : MGG* 233, 436–442.

- Lorentz, a, Ostermann, K., Fleck, O., and Schmidt, H. (1994). Switching gene *swi6*, involved in repression of silent mating-type loci in fission yeast, encodes a homologue of chromatin-associated proteins from *Drosophila* and mammals. *Gene* *143*, 139–143.
- Luger, K., Dechassa, M.L., and Tremethick, D.J. (2012). New insights into nucleosome and chromatin structure: an ordered state or a disordered affair? *Nature Reviews. Molecular Cell Biology* *13*, 436–447.
- Luger, K., Mäder, A.W., Richmond, R.K., Sargent, D.F., and Richmond, T.J. (1997). Crystal structure of the nucleosome core particle at 2.8 Å resolution. *Nature* *389*, 251–260.
- Luger, K., and Richmond, T.J. (1998). The histone tails of the nucleosome. *Current Opinion in Genetics & Development* *8*, 140–146.
- Maison, C., and Almouzni, G. (2004). HP1 and the dynamics of heterochromatin maintenance. *Nature Reviews. Molecular Cell Biology* *5*, 296–304.
- Meehan, R.R., Kao, C.-F., and Pennings, S. (2003). HP1 binding to native chromatin in vitro is determined by the hinge region and not by the chromodomain. *The EMBO Journal* *22*, 3164–3174.
- Mendez, D.L., Kim, D., Chruszcz, M., Stephens, G.E., Minor, W., Khorasanizadeh, S., and Elgin, S.C.R. (2011). The HP1a disordered C terminus and chromo shadow domain cooperate to select target peptide partners. *Chembiochem : a European Journal of Chemical Biology* *12*, 1084–1096.
- Min, J., Zhang, X., Cheng, X., Grewal, S.I.S., and Xu, R.-M. (2002). Structure of the SET domain histone lysine methyltransferase Clr4. *Nature Structural Biology* *9*, 828–832.
- Muchardt, C., Guilleme, M., Seeler, J.-S., Trouche, D., Dejean, A., and Yaniv, M. (2002). Coordinated methyl and RNA binding is required for heterochromatin localization of mammalian HP1alpha. *EMBO Reports* *3*, 975–981.
- Muller, H.J., and Altenburg, E. (1930). The Frequency of Translocations Produced by X-Rays in *Drosophila*. *Genetics* *15*, 283–311.
- Nakayama, J., Klar, a J., and Grewal, S.I. (2000). A chromodomain protein, *Swi6*, performs imprinting functions in fission yeast during mitosis and meiosis. *Cell* *101*, 307–317.
- Nakayama, J., Rice, J.C., Strahl, B.D., Allis, C.D., and Grewal, S.I. (2001). Role of histone H3 lysine 9 methylation in epigenetic control of heterochromatin assembly. *Science (New York, NY)* *292*, 110–113.

- Nielsen, P.R., Nietlispach, D., Mott, H.R., Callaghan, J., Bannister, A., Kouzarides, T., Murzin, A.G., Murzina, N. V, and Laue, E.D. (2002). Structure of the HP1 chromodomain bound to histone H3 methylated at lysine 9. *Nature* *416*, 103–107.
- Noma K, Allis, C.D., and Grewal, S.I. (2001). Transitions in distinct histone H3 methylation patterns at the heterochromatin domain boundaries. *Science (New York, N.Y.)* *293*, 1150–1155.
- Peters, A.H.F.M., O’Carroll, D., Scherthan, H., Mechtler, K., Sauer, S., Schöfer, C., Weipoltshammer, K., Pagani, M., Lachner, M., Kohlmaier, A., et al. (2001). Loss of the Suv39h Histone Methyltransferases Impairs Mammalian Heterochromatin and Genome Stability. *Cell* *107*, 323–337.
- Platero, J.S., Hartnett, T., and Eisenberg, J.C. (1995). Functional analysis of the chromo domain of HP1. *The EMBO Journal* *14*, 3977–3986.
- Rea, S., Eisenhaber, F., O’Carroll, D., Strahl, B.D., Sun, Z.W., Schmid, M., Opravil, S., Mechtler, K., Ponting, C.P., Allis, C.D., et al. (2000). Regulation of chromatin structure by site-specific histone H3 methyltransferases. *Nature* *406*, 593–599.
- Robinson, P.J.J., and Rhodes, D. (2006). Structure of the “30 nm” chromatin fibre: a key role for the linker histone. *Current Opinion in Structural Biology* *16*, 336–343.
- Sadaie, M., Kawaguchi, R., Ohtani, Y., Arisaka, F., Tanaka, K., Shirahige, K., and Nakayama, J. (2008). Balance between distinct HP1 family proteins controls heterochromatin assembly in fission yeast. *Molecular and Cellular Biology* *28*, 6973–6988.
- Smothers, J.F., and Henikoff, S. (2000). The HP1 chromo shadow domain binds a consensus peptide pentamer. *Current Biology : CB* *10*, 27–30.
- Spofford, J.B. (1967). Single-locus modification of position-effect variegation in *Drosophila melanogaster*. I. White variegation. *Genetics* *57*, 751–766.
- Sugiyama, T., Cam, H.P., Sugiyama, R., Noma, K., Zofall, M., Kobayashi, R., and Grewal, S.I.S. (2007). SHREC, an effector complex for heterochromatic transcriptional silencing. *Cell* *128*, 491–504.
- Sun, F.L., Cuaycong, M.H., and Elgin, S.C. (2001). Long-range nucleosome ordering is associated with gene silencing in *Drosophila melanogaster* pericentric heterochromatin. *Molecular and Cellular Biology* *21*, 2867–2879.
- Taverna, S.D., Li, H., Ruthenburg, A.J., Allis, C.D., and Patel, D.J. (2007). How chromatin-binding modules interpret histone modifications: lessons from professional pocket pickers. *Nature Structural & Molecular Biology* *14*, 1025–1040.

Tremethick, D.J. (2007). Higher-order structures of chromatin: the elusive 30 nm fiber. *Cell* 128, 651–654.

Vermaak, D., and Malik, H.S. (2009). Multiple roles for heterochromatin protein 1 genes in *Drosophila*. *Annual Review of Genetics* 43, 467–492.

Wallrath, L.L. (1998). Unfolding the mysteries of heterochromatin. *Current Opinion in Genetics & Development* 8, 147–153.

Wallrath, L.L., and Elgin, S.C. (1995). Position effect variegation in *Drosophila* is associated with an altered chromatin structure. *Genes & Development* 9, 1263–1277.

Wang, G., Ma, A., Chow, C.M., Horsley, D., Brown, N.R., Cowell, I.G., and Singh, P.B. (2000). Conservation of heterochromatin protein 1 function. *Molecular and Cellular Biology* 20, 6970–6983.

Weiler, K.S., and Wakimoto, B.T. (1995). Heterochromatin and gene expression in *Drosophila*. *Annual Review of Genetics* 29, 577–605.

Woodcock, C.L. (2006). Chromatin architecture. *Current Opinion in Structural Biology* 16, 213–220.

Yamada, T., Fischle, W., Sugiyama, T., Allis, C.D., and Grewal, S.I.S. (2005). The nucleation and maintenance of heterochromatin by a histone deacetylase in fission yeast. *Molecular Cell* 20, 173–185.

Yamada, T., Fukuda, R., Himeno, M., and Sugimoto, K. (1999). Functional domain structure of human heterochromatin protein HP1(Hsalpha): involvement of internal DNA-binding and C-terminal self-association domains in the formation of discrete dots in interphase nuclei. *Journal of Biochemistry* 125, 832–837.

Yamamoto, K., and Sonoda, M. (2003). Self-interaction of heterochromatin protein 1 is required for direct binding to histone methyltransferase, SUV39H1. *Biochemical and Biophysical Research Communications* 301, 287–292.

Zeng, W., Ball, A.R., and Yokomori, K. (2010). HP1: heterochromatin binding proteins working the genome. *Epigenetics : Official Journal of the DNA Methylation Society* 5, 287–292.

Zhang, C.L., McKinsey, T.A., and Olson, E.N. (2002). Association of class II histone deacetylases with heterochromatin protein 1: potential role for histone methylation in control of muscle differentiation. *Molecular and Cellular Biology* 22, 7302–7312.

Zhao, T., Heyduk, T., Allis, C.D., and Eissenberg, J.C. (2000). Heterochromatin protein 1 binds to nucleosomes and DNA in vitro. *The Journal of Biological Chemistry* 275, 28332–28338.

Chapter 2:

Chromodomain-mediated oligomerization of HP1 suggests
a nucleosome bridging mechanism for heterochromatin assembly

Chromodomain-mediated oligomerization of HP1 suggests a nucleosome bridging mechanism for heterochromatin assembly

Daniele Canzio^{1,2}, Evelyn Y. Chang^{1,3}, Smita Shankar¹, Kristopher M. Kuchenbecker^{1,4}, Matthew D. Simon⁵, Hiten D. Madhani¹, Geeta J. Narlikar^{1,*} and Bassem Al-Sady^{1,*}

¹ *Department of Biochemistry and Biophysics, University of California San Francisco, 94158, USA.*

² *Chemistry and Chemical Biology Graduate Program University of California San Francisco, 94158, USA.* ³ *Tetrad Graduate Program University of California San Francisco, 94158, USA.*

⁴ *Biophysics Graduate Group University of California San Francisco, 94158, USA.*

⁵ *Department of Molecular Biology, Massachusetts General Hospital, Boston, MA 02114 and Department of Genetics, Harvard Medical School, Boston, MA 02115.*

*To whom correspondence should be addressed geeta.narlikar@ucsf.edu, bassem.al-sady@ucsf.edu

Summary

HP1 proteins are central to the assembly and spread of heterochromatin containing histone H3K9 methylation. The chromodomain (CD) of HP1 proteins specifically recognizes the methyl mark on H3 peptides, but the same extent of specificity is not observed within chromatin. The chromoshadow domain of HP1 proteins promotes homodimerization, but this alone cannot explain heterochromatin spread. Using the *S. pombe* HP1 protein, Swi6, we show that recognition of H3K9 methylated chromatin *in vitro* relies on a newly identified interface between two CDs. This interaction causes Swi6 to tetramerize on a nucleosome, generating two vacant CD sticky ends. On nucleosomal arrays, methyl-mark recognition is highly sensitive to inter-nucleosomal distance, suggesting that the CD sticky ends bridge nearby methylated nucleosomes. Strengthening the CD-CD interaction enhances silencing and heterochromatin spread *in vivo*. Our findings suggest that recognition of methylated nucleosomes and HP1 spread on chromatin are structurally coupled, and imply that methylation and nucleosome arrangement synergistically regulate HP1 function.

Introduction

Histone H3 lysine 9 methylated (H3K9me3) heterochromatin, conserved from yeast to humans, is a highly versatile nuclear structure. It is required for centromere formation, heritable gene silencing, repression of recombination, sister chromatid cohesion, and maintenance of telomere stability (Grewal and Jia, 2007). A hallmark of this type of heterochromatin is the formation of macromolecular assemblies that can spread along chromatin from specific nucleation sites (Hall et al., 2002). The structural features that allow H3K9me3 based heterochromatin to spread and fulfill its various nuclear functions, however, are not well understood.

At the core of heterochromatic macromolecular assemblies lies the HP1-H3K9me3 chromatin complex, which is thought to mediate the many functions of heterochromatin through the recruitment of diverse sets of regulators (Grewal and Jia, 2007; Smothers and Henikoff, 2000). In gene silencing, HP1 proteins are thought to reduce RNA polymerase occupancy by both recruiting accessory silencing factors (Fischer et al., 2009) and by forming less accessible chromatin structures (Danzer and Wallrath, 2004). HP1 proteins have been proposed to enable post-transcriptional gene silencing by recruiting RNA processing machinery (Iida et al., 2008). Understanding how HP1 proteins recognize and bind H3K9me3 chromatin is thus central to understanding both the molecular mechanisms of heterochromatin assembly and how this type of heterochromatin fulfills its wide range of functions.

Previous work has described individual aspects of the HP1/H3K9me3 nucleosome complex. HP1 proteins contain three recognized protein domains: 1) a chromodomain (CD), 2) an evolutionarily related chromoshadow domain (CSD), and 3) a poorly defined hinge (H) region between the CD and CSD. The CD is part of a family of proteins that contain a specialized hydrophobic cage, formed by aromatic residues, that bind methyl marks on histones with high specificity but low affinity (Jacobs and Khorasanizadeh, 2002; Nielsen et al., 2002). The CSD is involved in dimerization of HP1 proteins (Cowieson et al., 2000) and is important for the silencing function of HP1 proteins (Sadaie et al., 2008). The H region is thought to be required for non-specific binding of HP1 proteins to DNA, as observed *in vitro* (Meehan et al., 2003; Zhao et al., 2000). Despite these key findings, several questions remain about how the functions of these individual domains are integrated to allow stable recognition of the physiological template, H3K9 methylated chromatin. For example, it is not clear whether the weak binding of the CD for methylated tail peptides observed *in vitro* is sufficient to guide heterochromatin assembly to the correct sites *in vivo*. In particular, the strong non-specific binding of HP1 proteins to inter-nucleosomal DNA (Meehan et al., 2003; Yamada et al., 1999) raises the question of how specificity for the methyl mark is attained in the context of chromatin. Finally, while HP1 proteins can dimerize via the CSD, such homodimerization alone appears insufficient to explain the ability of these proteins to spread along chromatin.

To address these questions, we used the *S. pombe* HP1 protein, Swi6, as a model system. *S. pombe* contains only a single H3K9 methyltransferase, Clr4, along with two

HP1 proteins, Chp2 and Swi6, of which Swi6 is more abundant (Grewal and Jia, 2007; Sadaie et al., 2008). We reconstituted the core Swi6-H3K9me3 chromatin complex using recombinant Swi6 and chromatin templates that are homogeneously methylated at H3K9 using methyl lysine analog (MLA) technology (Simon et al., 2007). We analyzed the biochemical properties of this complex and tested our key conclusions *in vivo*. Our results suggest a mechanism of heterochromatin formation in which HP1 proteins utilize a process of step-wise higher order oligomerization. This process is mediated by interactions between CDs to interpret information encoded in both the methylation state and the underlying nucleosomal arrangement of chromatin.

Results

Swi6 recognizes the H3K9 methyl mark within mononucleosomes and forms oligomers on mononucleosomes and in solution

Previous studies have reported on the ability of Swi6 to preferentially bind the H3K9me3 mark in the context of H3 tail peptides (Jacobs and Khorasanizadeh, 2002; Nielsen et al., 2002; Yamada et al., 2005). However, the magnitude of discrimination observed within H3 tail peptides has not been recapitulated in the context of chromatin, largely due to the challenge of generating homogeneously methylated chromatin. We produced homogeneously methylated nucleosomes using methyl lysine analogs (MLAs), then investigated the ability of recombinant Swi6 to specifically recognize methylated nucleosomes using two different equilibrium approaches. For both approaches, unmodified (H3K9) and methylated (H3Kc9me3) nucleosomes were assembled on 147 base pairs of the nucleosome positioning sequence 601 (Figure 1a).

In the first approach, surface plasmon resonance (SPR) was used to assay binding of Swi6 to H3K9 and H3Kc9me3 nucleosomes (Figure 1b). Analysis of the binding kinetics (traces in Figure 1b, inset) revealed no large differences in the association rates, but comparison of the dissociation traces reveals that Swi6 dissociates more rapidly from H3K9 nucleosomes compared to H3Kc9me3 nucleosomes, consistent with specific binding of Swi6 to methylated nucleosomes (Figure 1b). Because kinetic analysis of SPR data can be problematic and at times unreliable, we further optimized the assay for equilibrium measurements. The equilibrium binding isotherms clearly reveal two features (Figure 1c; see also Figure S1b&c). At low concentrations (10 nM – 1 μ M), there is a methylation specific interaction that approaches but does not reach saturation. At high concentrations (>1 μ M), there is apparently a weak, non-saturable interaction, and the concentration dependence of this interaction is similar for the H3K9 and the H3Kc9me3 nucleosome surfaces. We were, however, unable to fit a physically meaningful model to the data because (i) the data do not reveal saturation and therefore cannot be used to determine a final stoichiometry and (ii) HP1 proteins are known to oligomerize in solution, so the concentration will change as function of the oligomeric state of Swi6 (See Figure S1e&f for more detailed discussion).

Despite the inability to fit a quantitative model to the data, the Swi6 concentration dependence reveals interesting features of the interaction of Swi6 with nucleosomes. The results imply the presence of at least two types of Swi6 binding events: one that occurs at concentrations below 1 μ M and involves recognition of the

methyl mark, and a second that occurs primarily at higher concentrations, is less sensitive to the presence of the methyl mark and is suggestive of step-wise Swi6 oligomerization.

To further investigate the Swi6 behavior observed by SPR, we measured Swi6 binding to core nucleosomes using a fluorescence polarization based approach. Using nucleosomal DNA labeled at one end with fluorescein, we monitored the gain in fluorescence polarization as a function of Swi6 concentration (Figure 1d, schematic, also see Extended Experimental Procedures). Analogous to the SPR data, we observe a binding profile that contains a methylation specific concentration regime and a non-saturable concentration regime.

The above results raised the question of what physical processes underlie the different types of binding events implied by the unusual concentration dependence. We hypothesized that the binding events in the methyl mark specific concentration regime reflect direct binding of Swi6 to the nucleosome and the H3K9 residue while the binding events in the non-saturable concentration regime reflect mainly Swi6-Swi6 interactions that are scaffolded by the initial Swi6-nucleosome complex. The non-saturable behavior would then arise because addition of each Swi6 molecule would generate a new binding site for another Swi6 molecule, reflecting an intrinsic property of Swi6 to self-associate. To test this hypothesis, we investigated the oligomeric states adopted by Swi6 in solution under the two concentration regimes.

To determine the oligomeric state of Swi6 in the methylation specific concentration regime, we used two complementary approaches: (i) a cross-linking based approach and (ii) isothermal titration calorimetry (ITC). Over concentrations ranging from 25-5000 nM, cross-linker treated wild-type Swi6 migrates on SDS-PAGE gels at a mass consistent with a dimer, while the previously described dimer-disrupting CSD mutant, L315D, migrates at a mass consistent with a monomer (Cowieson et al., 2000) (Figure 2a). We then used ITC to obtain a more quantitative estimate of the K_d of the known dimerization domain of Swi6, the CSD (Figure 2b). Consistent with the cross-linking data, titrations of the WT Swi6 CSD into buffer produced no detectable heat release even at 17 nM indicating that K_d for CSD self-association is below 17 nM (Figure 2b, left panel). In contrast, titrations for the CSD domain containing the L315D mutation produce significant heat release and suggest a K_d for self-association of this mutant CSD in the high micromolar range (Figure 2b, right panel). Together, these two approaches suggest that at low nanomolar concentrations, Swi6 mainly exists as a dimer in the absence of nucleosomes.

We next determined the oligomeric states that can be adopted by Swi6 in the non-saturable concentration regime. We had noticed that under cross-linking conditions, Swi6 can form oligomers larger than a dimer (Figure 2a, indicated by asterisk), consistent with previous studies on HP1 (Yamada et al., 1999; Zhao et al., 2000). To investigate the formation of defined higher-order oligomers and obtain true masses independent of oligomer shape we used a multi-angle light scattering (MALS) approach (Extended Experimental Procedures). The WT Swi6 protein forms mainly dimers at 20

mM (Figure 2c). Interestingly, approximately 5% of the protein is tetrameric, suggesting that Swi6 is capable of forming oligomers beyond a dimer. In contrast, the L315D mutation drastically reduces the ability of Swi6 to dimerize: more than 90% of the L315D is monomeric at 20 mM, in agreement with the ITC data (Figure 2b). The intermolecular cross-linking approach described above enabled further stabilization of the higher order oligomeric states for analysis by MALS. Using this approach we found that WT Swi6 can form discrete complexes corresponding to dimeric, tetrameric, and octameric states (Figure 2d), whereas the L315D mutant is strongly impaired in forming such oligomeric states (Figure S2a). These data indicate that Swi6 can form well-defined higher order complexes in solution. Further, the Swi6 concentration regime in which states beyond dimer become populated correlates with the non-saturable concentration regimes of Figures 1c and d, suggesting that the non-saturable concentration regime mainly reflects Swi6-Swi6 interactions.

The above characterization of the oligomeric states of Swi6 indicates that Swi6 exists as a preformed dimer in the concentration regime in which we observed discrimination between H3Kc9me3 and H3K9 mononucleosomes. Further, the intrinsic property of Swi6 to form higher order oligomers suggests a potential for such oligomerization in binding across multiple nucleosomes within a nucleosomal array. To examine this possibility, we isolated the steps involved in direct recognition of the H3 tail within a mononucleosome, then used the information derived from these studies to better understand how Swi6 functions in the context of multiple nucleosomes.

Swi6 displays lower specificity for the H3K9me3 mark in mononucleosomes compared to H3 tail peptides

We reasoned that, by following the disappearance of the unbound nucleosomes in a gel mobility shift assay, we could better separate direct binding of Swi6 to the nucleosome from subsequent binding events that might entail mainly Swi6-Swi6 contacts. We measured the Swi6 concentration dependence for disappearance of unbound nucleosomes and obtained a value for $K_{1/2}$, which represents the concentration of Swi6 at which half of the nucleosomes remain unshifted. Most of the unbound MLA nucleosomes completely disappear by 1 mM Swi6 (Figure 3a). At higher concentrations we observe further, apparently continuous upshifting of the complexes, consistent with the nucleosome-scaffolded oligomerization behavior inferred from Figures 1c and d.

Using the above approach of quantifying $K_{1/2}$ values, we found that Swi6 prefers H3K9me3 over H3K9 nucleosomes by 5-fold (Figure 3a, right panel; specificity is expressed as a ratio of $K_{1/2}$ for H3K9 to that for H3K9me3 nucleosomes). Swi6 binds H3K9me0 nucleosomes with the same affinity as H3K9 nucleosomes (Figure S3a). We obtained the same 5-fold specificity for H3K9me3 over H3K9 nucleosomes using an equilibrium binding assay, in which the two types of nucleosomes compete with a fluorescently labeled DNA molecule for binding to Swi6 (Figure S3e).

Both the above assays indicate that the specificity for the methyl mark on core nucleosomes is substantially lower than that observed for the methyl mark on H3 tail peptides (Figures 3b&c and S3b). The results suggest a model in which Swi6 can bind to

a core nucleosome in alternative orientations that lack interactions between the H3K9 residue and the CD, in addition to orientations that recognize the H3K9 residue. The binding orientations that lack interactions between the CD and H3K9 could arise from the previously described abilities of the hinge and the CSD domains to interact with other regions of the nucleosome, such as the DNA and a globular region of H3, respectively (Dawson et al., 2009; Lavigne et al., 2009; Meehan et al., 2003). The above model predicts that increasing alternative binding interactions between Swi6 and the nucleosome will decrease the observed specificity for the methyl mark, as a smaller proportion of Swi6 molecules would bind in H3K9 recognizing orientations. At the same time we expect that the overall affinity will increase, as increasing the number of alternative binding orientations will increase the binding options of Swi6. Given that the affinity of HP1 proteins for free DNA increases with DNA length (Zhao et al., 2000) and our observations for Swi6 (Figure S3d), increasing the flanking DNA could be one way to increase the number of alternative binding modes. Consistent with these predictions, we find that increasing the flanking DNA length on one or both sides of a nucleosome results in a reduction in specificity but a gain in overall affinity (Figure 3d and Figure S3c).

Application of a simple quantitative model suggests that, for Swi6-H3Kc9me3 core nucleosome complexes, 94% of the Swi6 molecules are bound in H3K9-specific orientations and 6% are bound in alternative orientations (Extended Experimental Procedures). In contrast, for Swi6-H3K9 core nucleosome complexes, only 0.1% of the Swi6 molecules are bound in H3K9-specific orientations and >99% are bound in

alternative orientations. Thus, in the context of H3K9 nucleosomes, the large fraction of Swi6 molecules bound in alternative orientations is expected to mask the binding contributions from molecules bound in H3K9-specific orientations. Together, the above observations raise the possibility that the specificity of HP1 proteins for the H3K9me3 mark could be controlled in part by regulating alternative binding orientations. The experiments that follow provide a structural and energetic framework to understand how such regulation might occur.

The core unit of Swi6 binding to a mononucleosome is a tetramer

Quantification of the gel mobility shifts results suggests that binding of Swi6 to either H3K9me3 or H3K9 core nucleosomes occurs cooperatively with Hill coefficients of ~1.7 and 2.0, respectively (Figure 3b) suggesting that at least two molecules of Swi6 bind to one nucleosome. Further, the analysis in figures 2a and b indicates that, at the concentrations used in the native gel-shift assay, Swi6 is a dimer in solution. The cooperative binding could then reflect an additional interaction between two or more Swi6 dimers on the nucleosome. Indeed, the MALS data from Figure 2 indicate that Swi6 can form tetramers and octamers in the absence of nucleosomes at high concentrations. Alternatively, the two Swi6 dimers may not directly interact, but binding by two or more dimers may be required to stably upshift the nucleosomes on a native gel.

To directly determine the stoichiometry of the Swi6-core nucleosome complex in solution, under the methylation specific concentration regimes of Figures 1c, 1d and 3a, we used sedimentation velocity analytical ultracentrifugation (SV-AUC). SV-AUC

allows the differentiation of multiple species present in the sample based on their mass dependent migration. Recent improvements in the analysis tools for SV-AUC data allow the determination of masses of multi-protein complexes while directly accounting for differences in shapes (Brown and Schuck, 2006). We performed three independent experiments each for samples containing H3Kc9me3 core nucleosomes alone (Figure 4a), H3Kc9me3 core nucleosomes bound by L315D Swi6 (Figure 4b), or H3Kc9me3 core nucleosomes bound by WT Swi6 (Figure 4c). We used Swi6 and nucleosome concentrations based on titration experiments (See Experimental Procedures). Each experiment was analyzed using two independent models for data fitting: (i) a continuous two-dimensional function $c(s, f/f_0)$ for sedimentation coefficient s and hydrodynamic translational frictional ratio f/f_0 , (Figure S4a), and (ii) a continuous function $c(s)$ for sedimentation coefficient s with a bi-modal f/f_0 distribution (Figure S4b) (f/f_0 is a measure of the shape of the complex, see Experimental Procedures).

Both analysis methods indicate that the majority of the complexes have a stoichiometry of four WT Swi6 proteins to one core nucleosome (Figure 4c). These findings suggest that two WT Swi6 dimers bind to the nucleosome to form a tetramer. Further, the molar mass obtained for the core nucleosome-L315D Swi6 complex reveals a stoichiometry of two Swi6 proteins to one core nucleosome (Figure 4b).

These observations suggest a model in which the two unoccupied Swi6 chromodomains in the Swi6 tetramer can serve as sticky ends (Figure 4c, black arrows) that can bind methyl marks on nearby nucleosomes. Binding of proximal nucleosomes

via this specific type of sticky ends architecture would be predicted to energetically favor H3K9-specific binding orientations of the Swi6 tetramer over alternative binding orientations, resulting in greater specificity for the methyl mark. To test this hypothesis, we determined whether Swi6 binds with greater specificity to methylated di- and polynucleosome constructs compared to mononucleosomes.

Swi6 binds with similar specificity to mono and dinucleosomes

Dinucleosomes were first assembled on a DNA construct containing 15 base pairs of linker DNA (L15) between two 601 positioning sequences (Figure 5a, diagram). The relatively short linker length is designed to mimic inter-nucleosomal distances prevalent in *S. pombe* (Godde and Widom, 1992; Lantermann et al., 2010). Native gel mobility shift assays show that Swi6 binds to methylated 2N(L15) with approximately 2.5-fold higher affinity than to the unmethylated control (Figure 5a). This specificity is comparable to that observed for mononucleosomes containing 20 bp of flanking DNA and is likely due to nonspecific binding of Swi6 to the linker DNA (Figure 3d and Fig. S3c). These results suggest that L15 dinucleosomes do not increase specific binding by Swi6. To test if these closely spaced nucleosomes sterically interfere with Swi6 binding to the H3 tails of both nucleosomes, we also measured Swi6 binding to a 2N(L47) dinucleosome, linked by 47 base pairs of DNA. Swi6 binds to methylated 2N(L47) with 2.5-fold higher affinity than unmethylated 2N(L47), ruling out a simple steric interference model (Figure 5b).

The above results suggest that, in the context of Swi6 binding, a dinucleosome substrate behaves like two unlinked mononucleosomes with flanking DNA and does not show any amplification of specificity. *In vivo*, however, Swi6 binds along many nucleosomes (Noma et al., 2001), leaving the possibility that the sticky ends mechanism may have evolved to have a larger effect in the context of a long stretch of nucleosomes.

Nucleosome arrays provide a highly specific substrate for Swi6

We next measured Swi6 binding to a 12 nucleosome array containing the same 15 base pair linker length as used in the dinucleosome construct (Figure 5c, diagram and Figure S5a). Native gel mobility shifts show that this 12N(L15) array substrate substantially increases Swi6 specificity for the methyl mark, to ~25-fold (Figure 5c). This represents a ~10-fold amplification in specificity compared to that measured for the corresponding dinucleosome construct. The large gain in specificity on nucleosomal arrays is consistent with our model (Figure 4c), in which bridging interactions between nucleosomes, mediated by vacant CD sticky ends, favor binding of Swi6 in H3K9-specific orientations over alternative orientations. The observation that H3K9me specificity is amplified only in the context of 12N arrays but not dinucleosome substrates, suggests that Swi6 bridging requires nucleosome conformations that cannot be accessed by dinucleosomes.

If bridging nearby nucleosomes is required for correctly orienting Swi6 complexes, then increasing the distance between nucleosomes on a 12N array is expected to reduce such bridging and result in lower specificity. We therefore measured

the specificity of Swi6 for the methyl mark in the context of arrays with more widely spaced nucleosomes, containing 47 base pair linker DNA (Figure S5b). As predicted, Swi6 binds to the methylated 12N(L47) substrate with lower specificity (5.4-fold) than to methylated 12N(L15) arrays (Figure 5d). These results indicate the importance of appropriate nucleosome placement for achieving high specificity.

Our finding that specificity for the methyl mark is amplified in a manner that is sensitive to internucleosomal distance is consistent with model in which the tetrameric Swi6 architecture depicted in Figure 4c enables bridging across nucleosomes. In this context, the intrinsic ability of Swi6 to form a tetrameric state (Figure 2c,d) suggests that, in addition to the CSD-CSD interface, there are other Swi6-Swi6 interfaces that promote tetramerization.

Swi6 tetramerization is mediated by the chromodomain

Because the CSD domain alone shows no oligomer formation beyond a dimer, even at concentrations where the intact Swi6 protein forms tetrameric species (Figure 2c and S2b), we used a domain deletion approach using Swi6 constructs lacking the CSD domain to identify the domain responsible for Swi6 tetramer formation. We used gel filtration to measure the extent of protein self-association for these proteins. At high concentrations, the CD alone (aa 81-137) is able to dimerize in solution, to the same extent as a Swi6 protein lacking only the CSD (NCDH) (Figure S6a). This suggested that the CD is the major component of the additional protein-protein interface. The weak CD self-association could be further stabilized by cross-linking (Figure 6a). The CD-CD

interaction also helps explain the non-saturable addition of Swi6 to nucleosomes observed by SPR and fluorescence anisotropy.

Our data agree with previous reports that the CD of human HP1 forms higher-order oligomers when cross-linked (Yamada et al., 1999). However, the interface through which such CD-CD interactions occur has not yet been identified. Given the high level of structural similarity between the CD and the evolutionary related CSD (Figure 6b), we hypothesized that the region of the CD corresponding to the sole alpha helix in the CSD that is primarily responsible for CSD dimerization might play a similar role in CD self-association. This hypothesis was further supported by analysis of the previously determined crystal structure of the dHP1 CD (Jacobs and Khorasanizadeh, 2002). The crystallographic unit of this structure contains two CD monomers that appear to engage in contacts via the alpha helix (Figure S6b). Over 30 different point mutants were made in an attempt to reduce CD dimerization, but all of these also resulted in a loss of H3K9me3 peptide binding function (data not shown). We were, however, able to obtain two gain-of-function mutants that increase CD dimerization without significantly, or not all, disrupting peptide binding: the single mutant Y131W and the double mutant V82E-Y131W (Figures 6b). The single mutant V82E replaces a Swi6 residue with a residue normally found at this location in Chp1, another chromodomain containing protein in *S. pombe* (Schalch et al., 2009).

When introduced in the full-length protein, the Y131W single and the V82E-Y131W double mutant respectively displayed ~ 1.6-fold and ~3.5-fold increased

tetramer formation over WT as determined by MALS, suggesting that this region of the CD is involved in Swi6 tetramerization (Figure 6c&d and S6c). The V82E single mutant by itself does not significantly increase tetramer formation (Figure S6c). We find that the V82E single substitution increases binding to H3K9me3 tail peptides by ~ 3-fold, consistent with previous work (Schalch et al., 2009). The double mutant V82E-Y131W however displays similar affinity for the H3K9me3 tail peptide as WT (Figure 6d).

Specificity for the methyl mark is dependent on both the CD-CD and the CSD-CSD interactions

The observation that CD-CD self association helps form Swi6 tetramers was particularly intriguing because our model, in which both H3K9 methyl marks are bound by CDs of different Swi6 dimers, places those two CDs in close proximity to self-associate (Figure 4c). We therefore hypothesized that binding in the specific orientation would strongly favor Swi6 tetramerization via CD-CD self-association and conversely, Swi6 tetramerization via self-association of two CDs would strongly favor binding in the specific orientation. If so, any disruption of the tetramer architecture depicted in Figure 4c would reduce specific recognition of the H3K9me3 mark on the nucleosome, while any strengthening of the specific architecture would increase specificity for the H3K9me3 mark.

To test these predictions, we measured specificity towards H3K9me3 core nucleosomes for WT Swi6 and for the L315D and V82E-Y131W mutants (Figures 6e & S6c). The L315D mutation, which significantly decreases higher-order oligomerization

by disrupting CSD self-association (Figures 2c and S2a), displays 2.5-fold reduced specificity for methylated core nucleosomes relative to WT Swi6 (Figure 6e). Conversely, the V82E-Y131W double mutant, which increases tetramer formation 3.5-fold in solution by increasing CD self-association (Figure 6c&d), displays 2-fold increased specificity for methylated core nucleosomes (Figure 6e). Interestingly, both the L315D and the V82E-Y131W mutant proteins bind the H3K9me3 tail peptide with specificities comparable to the WT protein (Figure 6d). The observation that the mutations alter methyl mark discrimination only in the nucleosomal context suggests that the effects are a result of altered oligomerization states. These results indicate that specific recognition of the nucleosomal H3K9me3 mark by Swi6 is dependent on both CSD-mediated dimerization and CD-mediated tetramerization on the nucleosome surface.

A specific CD-CD interface implies that the sticky ends that bridge nearby nucleosomes would entail CD-CD interactions in addition to interactions between the unoccupied CD and a nearby methyl mark. Therefore, in the context of nucleosomal arrays, the CD-CD interaction would further promote the H3K9 specific orientations via bridging interactions with nearby nucleosomes (see also Supplementary discussion). Such a model then makes two key predictions: (i) strengthening the CD-CD interaction would increase the specificity on nucleosomal arrays to a greater extent than on mononucleosomes, and (ii) any amplification of specificity would be very sensitive to the inter-nucleosomal distance. To test these predictions, we compared the specificity of

the V82E-Y131W mutant to that of WT Swi6 on the 12N(L15) and 12N(L47) nucleosomal arrays.

As predicted by the model, we found that the V82E-Y131W mutant shows a large increase in specificity (~7-fold) on the 12N(L15) arrays compared to WT Swi6 (Figure 6e). Interestingly, this raises the specificity for the H3K9me3 mark to the ~130 fold observed on H3 tail peptides (Figure 3c). Further, most of the observed gain in specificity arises from a large decrease in binding to the H3K9 array and a small increase in binding to the H3K9me3 array (Figure S6d). These results suggest that the combination of strengthening the CD-CD interface and binding across multiple nucleosomes eliminates most of the alternative binding modes adopted by Swi6. No significant amplification of specificity is observed in the context of the 12N(L47), confirming that the CD-CD nucleosome bridging interaction is sensitive to inter-nucleosomal distance (Figure 6e).

To further investigate the role of Swi6 oligomerization in the context of nucleosomal arrays, we tested the effects of disrupting the CSD-CSD interface, which is also expected to disrupt the ability of Swi6 dimers to bridge across nucleosomes (Figure 6e). The L315D mutant shows greatly reduced specificity on the 12N(L15) template. Intriguingly, the L315D mutant discriminates between methylated and unmethylated 12N(L15) arrays to a similar degree (2-3 fold) as in the context of 12N(L47) arrays and mononucleosomes (Figure 6e). Therefore, the L315D Swi6 mutant is insensitive to the distance between nucleosomes. The L315D mutant thus uncovers the baseline ability of

HP1 proteins to recognize a nucleosomal H3K9 methyl mark in the absence of significant oligomerization and nucleosome bridging-dependent effects.

Increased tetramerization of Swi6 results in increased silencing at an artificial heterochromatic locus and higher recruitment to centromeres

To test whether these biochemically derived mechanistic conclusions are relevant to the ability of Swi6 to form functional heterochromatin *in vivo*, we investigated whether strengthening the CD-CD interface via the V82E-Y131W double mutant causes enhanced silencing and Swi6 occupancy *in vivo*.

To test for such an effect, we utilized a reporter system that measures silencing of the *ura4+* gene at its endogenous location on Chromosome 3 (S.S., K. Finn, H.D.M., unpublished). In this reporter construct, a centromeric fragment, under control of a promoter, is inserted 1.8 kb downstream of the *ura4+* gene (Figure 7a). We chose a 1.7 kb fragment (Fragment A; Fr A) from a library of fragments derived from the centromeric *dh* repeats. Fr A shows very weak silencing of the *ura4+* gene, leading to minimal growth of cells on 5-FOA, which provides a sensitive assay for mutants that enhance silencing (Figure 7b). We introduced the *swi6*^{V82E, Y131W} allele by chromosomal integration into strains containing Fr A. As a control, we constructed isogenic *swi6+* strains. To control for strain-to-strain variability, we isolated and characterized 6 independent genetic isolates for both *swi6*^{V82E, Y131W} and *swi6+* alleles in the Fr A background. As shown in Figure 7b for two independent strains, *swi6*^{V82E, Y131W} increased Fr A-dependent silencing of *ura4+* (compare rows 6 and 8 to rows 5 and 7). A side by

side comparison of all 6 independent isolates of the *swi6*⁺ and *swi6*^{V82E, Y131W} alleles further confirms stronger growth on 5-FOA for all the *swi6*^{V82E, Y131W} strains (Fig. S7). The mutant Swi6 protein is not expressed at a higher level than the WT Swi6 protein, ruling out a trivial explanation for the gain of silencing effects (Figure 7c).

We next probed the molecular features of the silenced region using ChIP. We first examined Swi6 localization across the Fr A cassette locus, and found a reproducible 2-3 fold increase in Swi6 enrichment in the *swi6*^{V82E, Y131W} alleles versus the *swi6*⁺ alleles (Figure 7d), consistent with the increased specific binding observed on nucleosomal arrays *in vitro*. However, the overall enrichment was low, probably reflecting the low degree of silencing at this artificial locus. Next, we examined H3K9me2 levels at and around the Fr A locus. Since Fr A-dependent Swi6 localization spreads beyond Fr A into adjacent euchromatic regions at the unbounded 5' end (Figure 7d), H3K9 methylation may also exhibit some Swi6-dependent spread (Hall et al., 2002). Indeed, we found that H3K9me2 levels are robustly increased in the *swi6*^{V82E, Y131W} alleles, and remain elevated at regions well outside (~20 kb) the Fr A initiating element (Figure 7e). The fact that H3K9me2 enrichment can be observed outside the zone of detectable Swi6 enrichment is likely due to the differential sensitivity of the two ChIP experiments. Increased localization of Swi6 in the context of the V82E-Y131W mutation, concomitant with robustly increased H3K9me2 levels and elevated *ura4*⁺ silencing, suggests that increasing the oligomerization capacity of the Swi6 protein enhances the ability of Swi6 to establish and spread heterochromatin at the artificial locus.

Next we asked whether the V82E-Y131W mutation has an effect on Swi6 activity at endogenous heterochromatin loci. We examined recruitment of Swi6 by ChIP at the *dg* repeat of centromere 1. Since H3K9 methylation at the centromere is Swi6-independent (Nakayama et al., 2001) examining centromeric heterochromatin should allow us to uncouple Swi6 recruitment from deposition of H3K9 methylation. In such a situation, changes in Swi6 recruitment should directly report on the ability of the protein to recognize H3K9 methylated chromatin *in vivo*. Indeed, when we examined H3K9me2 methylation at the *dg* repeat in the no Fr A control, *swi6+* and *swi6*^{V82E, Y131W} Fr A-containing alleles, we found no change in the enrichment level of H3K9me2 at the *dg* repeat (Figure 7f, top panel). In contrast, when we tested for Swi6 recruitment, we found a small but reproducible increase of Swi6 residence at the *dg* repeat only in the context of the Swi6 V82E-Y131W mutant (Figure 7f, bottom panel). This result suggests that when Swi6 oligomerization is increased, Swi6 recruitment is increased at endogenous heterochromatin loci where H3K9 methylation is Swi6-independent. These data help strengthen our model that CD-mediated oligomerization is critical for Swi6-dependent heterochromatin formation.

Discussion

To understand how HP1 proteins assemble on physiological chromatin templates, we reconstituted and characterized the core HP1-H3K9me3 chromatin complex. Our data suggest that recognition of H3K9me3 by HP1 proteins is coupled to its oligomerization on the nucleosome through a chromodomain-chromodomain interface that promotes silencing *in vivo*. The mechanistic implications of these observations are

discussed below.

A new role for the HP1 chromodomain in heterochromatin formation

Swi6 mutants that have increased tetramerization mediated via the CD-CD interaction exhibit increased specificity for H3K9me3 nucleosomes, suggesting that interactions between two CDs on a nucleosome restricts the number of non-H3K9me3 specific binding modes. Mutants that increase tetramerization, and thus H3K9me3 specificity *in vitro*, also exhibit increased heterochromatin spread and silencing at an artificially induced heterochromatic locus *in vivo*. The CD of HP1 proteins was previously known to recognize peptides containing methylated H3K9 (Jacobs and Khorasanizadeh, 2002; Nielsen et al., 2002). Our work suggests that the CD has an additional critical role in the context of chromatin: orienting HP1 proteins via CD-CD interactions to ensure that HP1 proteins can distinguish the methyl mark from other overlapping binding surfaces presented by a nucleosome.

Sticky end chromodomains in the Swi6 tetramer-nucleosome complex present polymerizable surfaces for higher order oligomerization across chromatin

Our data imply that H3K9me3 recognition and chromatin coating by Swi6 are mechanistically coupled and intrinsic to the fundamental architecture of the tetrameric HP1/Swi6 complex on the nucleosome (Figure 6f) as follows: i) Dimerization via the strong CSD-CSD interaction and tetramerization via the weaker CD-CD interaction couples recognition of the two methyl marks in a nucleosome to the generation of two unoccupied CDs. These unoccupied CDs can serve as sticky ends that bridge and recruit

neighboring methylated nucleosomes, which might be either adjacent or located on different chromatin fibers. ii) Interactions between the CD of a chromatin bound HP1 dimer and that of an incoming HP1 dimer can promote deposition of the incoming HP1 dimer in an H3K9me3-recognizing orientation.

This ability to bridge nucleosomes via polymerizable CDs may represent the primary underlying mechanism that allows HP1 proteins to spread (Hall et al., 2002) along the chromatin fiber and establish the extent of the heterochromatic domain. Further, since this mechanism is dependent on a high density of H3K9me3 methylation on chromatin (Nakayama et al., 2001; Noma et al., 2001), it may enable Swi6 to sense regions of high local Clr4 methylase activity, preventing ectopic heterochromatin formation. Coupling between oligomerization and recognition of H3K9methyl marks has also been proposed in the context of the vertebrate chromodomain containing protein CDYL1b (Franz et al., 2009).

Chromatin architecture and implications for heterochromatin spread

The bridging architecture depicted in Figure 6f places specific steric and distance constraints on any Swi6-mediated heterochromatin assembly and spread, restricting the number of chromatin architectures accessible to heterochromatin assembly by Swi6. In fact, we find that Swi6 gains specificity on nucleosome arrays over unlinked nucleosomes only in the context of short DNA linkers (Figures 5c&d and 6e). We therefore hypothesize that HP1 proteins assess both the nucleosome arrangement in addition to the H3K9me3 mark, thereby integrating two signals for heterochromatin

assembly.

If only a subset of chromatin architectures is permissive to template the assembly of HP1 proteins on H3K9me3 chromatin, such architectures might be regulated *in vivo* to allow specification of HP1 protein binding sites. In fact, in metazoans, the nucleosome architecture of heterochromatic loci shows significant differences compared to euchromatin sites. For example, in *Drosophila melanogaster*, constitutive heterochromatin is characterized by more evenly spaced nucleosomes (Danzer and Wallrath, 2004; Wallrath and Elgin, 1995) compared to euchromatin. It has been suggested that the ACF chromatin remodeling complex is involved in generating such chromatin architectures in *Drosophila* (Fyodorov et al., 2004). In *S. pombe*, there is some evidence that local nucleosome arrangement in heterochromatin impacts Swi6 association. Several protein complexes collaborate in *S. pombe* to maintain heterochromatin regions. A key such effector is a bi-functional enzyme complex called SHREC, containing both the histone deacetylase (HDAC) Clr3 and the SNF2 chromatin-remodeling factor homolog Mit1 (Sugiyama et al., 2007). The Clr3 subunit of SHREC is required for Swi6 localization, in a manner that appears uncoupled from its effects on H3K9 methylation (Nakayama et al., 2001; Yamada et al., 2005); S.I.S. Grewal, personal communication). This effect may result either from 1) the absence of Clr3's HDAC activity, resulting in an increase in acetylated and phosphorylated histones that may affect Swi6's ability to associate with those nucleosomes (Yamada et al., 2005), or 2) effects of the SHREC complex on nucleosome arrangement (Sugiyama et al., 2007). We speculate that SHREC and/or other chromatin regulators may promote a nucleosome

arrangement that enables Swi6 to bridge H3K9me3-marked nucleosomes and therefore to spread. Further work will be needed to identify what exact chromatin architectures are compatible with Swi6 bridging and how such structures may be generated and maintained *in vivo*.

Experimental Procedures

(Detailed Methods are described in “Extended Experimental Procedures” in Supplementary Information)

Protein cloning and purification

Full length Swi6 was cloned into pET30a (Novagen), mutants made using site directed mutagenesis and proteins purified from *E. coli*. Tagged Swi6 containing N-terminal 6xHis and C-terminal FLAG tags was used for the MALS, AUC, cross-linking, native gel-shift, nucleosome competition and peptide binding assays. Untagged Swi6 was used for the SPR-based and polarization-based nucleosome binding measurements. Removing the tags slightly increases overall affinity for nucleosomes and arrays (~2.5 fold) but does not affect specificity (data not shown).

Mononucleosome, dinucleosome, and array reconstitution

Gradient salt dialysis was used to assemble mononucleosomes on DNA templates containing the 147 bp long 601 positioning sequence, dinucleosomes on DNA templates containing two 601 sequences linked by 15 or 47 bp of DNA and arrays on DNA templates containing 12 copies of the 601 nucleosome positioning sequence separated by either 15 or 47 bp linkers. H3Kc9me3, H3Kc9me0 and H3K9 histones were prepared as described (Luger et al., 1999; Simon et al., 2007). Arrays with >95% assembly were used for gel shift assays.

Surface plasmon resonance

A BiaCore T100 instrument was used for SPR analysis of Swi6 interaction with the mononucleosome substrates. H3K9 and H3Kc9me3 substrates assembled on a 5' biotinylated 601 sequence were immobilized to 25 to 60 RU on active flow cells . Immobilization levels of mononucleosomes ranged from 25 to 60 RU. Surface stability and assay quality were judged by the reproducibility of a 10 μ L control sample (100 nM Swi6) injection that followed each sample concentration (Figure S1d).

Fluorescence polarization binding measurements

All H3 tail peptides were produced as described (Simon et al., 2007). Nucleosomes for polarization-based binding measurements were assembled on a 6-carboxyfluorescein-labeled 601 positioning sequence.

Native gel mobility shift assays

Different concentrations of Swi6 protein were incubated with 5-10 nM mononucleosome or 1.25 nM dinucleosome. Samples were run on native polyacrylamide gels, stained with SyBR Gold (Invitrogen), visualized on a Molecular Dynamics Typhoon scanner and quantified using Image Quant software. The $K_{1/2}$ for each binding curve and Hill coefficient were calculated with Kaleidograph software using a simple equilibrium model. Swi6 gel shifts with 12N arrays were performed using agarose gels with 1 nM array (12 nM nucleosomes) and analyzed as described for mononucleosomes.

Protein cross-linking

Cross-linking assays were performed using EDC/NHS cross-linking (Pierce) (see Extended Experimental Procedures). The samples were boiled and analyzed on 4-12% NuPAGE gradient gels (Invitrogen) under denaturing conditions, then visualized on a Typhoon scanner by Sypro Red staining or by anti-FLAG western blotting.

Isothermal titration calorimetry

The heat released by dissociation of CSD dimers into monomers was measured with a Microcal, Inc., Omega microcalorimeter. Dilution ITC experiments involved sequential injections from a concentrated protein stock (5 mM for WT Swi6 and 625 mM for L315D Swi6) in 5 ml increments into the 1.4 ml calorimeter cell initially containing only buffer.

Size-exclusion chromatography coupled to multi-angle light scattering (SEC-MALS/UV/RI)

Protein samples were injected into an analytical size exclusion silica gel KW804 chromatography column (Shodex). The chromatography system was coupled to an 18-angle light scattering detector (DAWN HELEOS II, Wyatt Technology) and a differential refractometer (Optilab rEX, Wyatt Technology).

Sedimentation velocity analytical ultracentrifugation

Sedimentation velocity experiments were conducted using an analytical ultracentrifuge (Beckman Coulter) equipped with an absorption optical scanner. The

binding reaction was set up such that a) both nucleosome and Swi6 concentrations were above the $K_{1/2}$ value measured by native gel and b) the Swi6 concentration was sufficient to titrate all the nucleosomes as assayed by native gel shift.

Data were analyzed using the Sedfit software (Schuck, 2004). Three independent analyses: $c(s)$, $c(s,fr)$, and $c(s,bi-modal\ fr)$ were used to study the sedimentation properties and the molar mass of each sample. Solution density (ρ), solution viscosity (η) were calculated in SEDNTERP (Schuck, 2004).

***In vivo* silencing assays**

A fragment of the *dh* centromeric repeat was placed 1.8 kb downstream of the *ura4+* gene on chromosome III using homologous recombination. Transcription of this fragment is driven by the *padh1+* promoter and is sufficient to induce silencing of *ura4+* in a manner that requires *clr4+* and *dcr1+* (S.S., K. Finn and H.D.M., unpublished). Silencing of *ura4+* gene was assayed by growth on 2 mg/mL 5-fluoroorotic acid (5-FOA). The endogenous *swi6+* was replaced with either *swi6*^{V82E,Y131W} marked with a 5' *G418^R* selectable marker, or the wild-type allele and the same marker.

Chromatin immunoprecipitation (ChIP)

ChIP experiments with *Fr A*⁻, *swi6+* and *swi6*^{V82E,Y131W} strains were performed using anti-H3K9me2 (Abcam) or anti-Swi6 (Nakayama et al., 2000) antisera. Details see Extended Experimental procedures.

References

- Cowieson, N.P., Partridge, J.F., Allshire, R.C., and McLaughlin, P.J. (2000). Dimerisation of a chromo shadow domain and distinctions from the chromodomain as revealed by structural analysis. *Curr Biol* *10*, 517-525.
- Danzer, J.R., and Wallrath, L.L. (2004). Mechanisms of HP1-mediated gene silencing in *Drosophila*. *Development* *131*, 3571-3580.
- Dawson, M.A., Bannister, A.J., Gottgens, B., Foster, S.D., Bartke, T., Green, A.R., and Kouzarides, T. (2009). JAK2 phosphorylates histone H3Y41 and excludes HP1 alpha from chromatin. *Nature* *461*, 819-U879.
- Fischer, T., Cui, B., Dhakshnamoorthy, J., Zhou, M., Rubin, C., Zofall, M., Veenstra, T.D., and Grewal, S.I.S. (2009). Diverse roles of HP1 proteins in heterochromatin assembly and functions in fission yeast. *Proc Natl Acad Sci USA* *106*, 8998-9003.
- Franz, H., Mosch, K., Soeroes, S., Urlaub, H., and Fischle, W. (2009). Multimerization and H3K9me3 binding are required for CDYL1b heterochromatin association. *J Biol Chem* *284*, 35049-35059.
- Fyodorov, D.V., Blower, M.D., Karpen, G.H., and Kadonaga, J.T. (2004). Acf1 confers unique activities to ACF/CHRAC and promotes the formation rather than disruption of chromatin in vivo. *Genes Dev* *18*, 170-183.
- Godde, J.S., and Widom, J. (1992). CHROMATIN STRUCTURE OF SCHIZOSACCHAROMYCES-POMBE - A NUCLEOSOME REPEAT LENGTH THAT IS SHORTER THAN THE CHROMATOSOMAL DNA LENGTH. *Journal of Molecular Biology* *226*, 1009-1025.
- Grewal, S.I.S., and Jia, S. (2007). Heterochromatin revisited. *Nat Rev Genet* *8*, 35-46.
- Hall, I.M., Shankaranarayana, G.D., Noma, K.I., Ayoub, N., Cohen, A., and Grewal, S.I.S. (2002). Establishment and maintenance of a heterochromatin domain. *Science* *297*, 2232-2237.
- Iida, T., Nakayama, J.-i., and Moazed, D. (2008). siRNA-mediated heterochromatin establishment requires HP1 and is associated with antisense transcription. *Mol Cell* *31*, 178-189.
- Jacobs, S.A., and Khorasanizadeh, S. (2002). Structure of HP1 chromodomain bound to a lysine 9-methylated histone H3 tail. *Science* *295*, 2080-2083.
- Lantermann, A.B., Straub, T., Stralfors, A., Yuan, G.C., Ekwall, K., and Korber, P. (2010). *Schizosaccharomyces pombe* genome-wide nucleosome mapping reveals positioning mechanisms distinct from those of *Saccharomyces cerevisiae*. *Nature Structural & Molecular Biology* *17*, 251-U215.

- Lavigne, M., Eskeland, R., Azebi, S., Saint-Andre, V., Jang, S.M., Batsche, E., Fan, H.Y., Kingston, R.E., Imhof, A., and Muchardt, C. (2009). Interaction of HP1 and Brg1/Brm with the globular domain of histone H3 is required for HP1-mediated repression. *PLoS Genet* 5, e1000769.
- Luger, K., Rechsteiner, T.J., and Richmond, T.J. (1999). Preparation of nucleosome core particle from recombinant histones. In *Chromatin* (San Diego, Academic Press Inc), pp. 3-19.
- Meehan, R.R., Kao, C.F., and Pennings, S. (2003). HP1 binding to native chromatin in vitro is determined by the hinge region and not by the chromodomain. *Embo Journal* 22, 3164-3174.
- Nakayama, J., Klar, A.J., and Grewal, S.I. (2000). A chromodomain protein, Swi6, performs imprinting functions in fission yeast during mitosis and meiosis. *Cell* 101, 307-317.
- Nakayama, J., Rice, J.C., Strahl, B.D., Allis, C.D., and Grewal, S.I. (2001). Role of histone H3 lysine 9 methylation in epigenetic control of heterochromatin assembly. *Science* 292, 110-113.
- Nielsen, P.R., Nietlispach, D., Mott, H.R., Callaghan, J., Bannister, A., Kouzarides, T., Murzin, A.G., Murzina, N.V., and Laue, E.D. (2002). Structure of the HP1 chromodomain bound to histone H3 methylated at lysine 9. *Nature* 416, 103-107.
- Noma, K., Allis, C.D., and Grewal, S.I.S. (2001). Transitions in distinct histone H3 methylation patterns at the heterochromatin domain boundaries. *Science* 293, 1150-1155.
- Sadaie, M., Kawaguchi, R., Ohtani, Y., Arisaka, F., Tanaka, K., Shirahige, K., and Nakayama, J. (2008). Balance between Distinct HP1 Family Proteins Controls Heterochromatin Assembly in Fission Yeast. *Molecular and Cellular Biology* 28, 6973-6988.
- Schalch, T., Job, G., Noffsinger, V.J., Shanker, S., Kuscu, C., Joshua-Tor, L., and Partridge, J.F. (2009). High-affinity binding of Chp1 chromodomain to K9 methylated histone H3 is required to establish centromeric heterochromatin. *Mol Cell* 34, 36-46.
- Schuck, P. (2004). A model for sedimentation in inhomogeneous media. I. Dynamic density gradients from sedimenting co-solutes. *Biophysical Chemistry* 108, 187-200.
- Simon, M.D., Chu, F., Racki, L.R., de la Cruz, C.C., Burlingame, A.L., Panning, B., Narlikar, G.J., and Shokat, K.M. (2007). The site-specific installation of methyl-lysine analogs into recombinant histones. *Cell* 128, 1003-1012.

Smothers, J.F., and Henikoff, S. (2000). The HP1 chromo shadow domain binds a consensus peptide pentamer. *Curr Biol* 10, 27-30.

Sugiyama, T., Cam, H.P., Sugiyama, R., Noma, K.-i., Zofall, M., Kobayashi, R., and Grewal, S.I.S. (2007). SHREC, an effector complex for heterochromatic transcriptional silencing. *Cell* 128, 491-504.

Wallrath, L.L., and Elgin, S.C.R. (1995). Position Effect Variegation in *Drosophila* Is Associated with an Altered Chromatin Structure. *Genes & Development* 9, 1263-1277.

Yamada, T., Fischle, W., Sugiyama, T., Allis, C.D., and Grewal, S.I.S. (2005). The nucleation and maintenance of heterochromatin by a histone deacetylase in fission yeast. *Mol Cell* 20, 173-185.

Yamada, T., Fukuda, R., Himeno, M., and Sugimoto, K. (1999). Functional domain structure of human heterochromatin protein HP1 (Hsalpha): involvement of internal DNA-binding and C-terminal self-association domains in the formation of discrete dots in interphase nuclei. *J Biochem* 125, 832-837.

Zhao, T., Heyduk, T., Allis, C.D., and Eisenberg, J.C. (2000). Heterochromatin protein 1 binds to nucleosomes and DNA in vitro. *J Biol Chem* 275, 28332-28338.

Acknowledgements

We thank Shiv I.S. Grewal for a generous gift of anti-Swi6 antisera, Christine Rumpf for help with ITC measurements, Dan Southworth and Janet Yang for assistance with MALS set-up, Kalyan Sinha and Peter Schuck for critical advice and comments on the AUC experiments and data interpretation and Robert Fletterick for critical advice and comments on the SPR experiments and data interpretation. We thank Barbara Panning, Jonathan Weissman, Karim-Jean Armache and members of the Narlikar Lab for helpful discussion and comments on the manuscript. This work was supported by grants from the National Institutes of Health (5R01GM071801 to H.D.M. and 1R01GM073767 to G.J.N.), the UCSF Program for Breakthrough Biomedical Research (PBBR) Award to G.J.N., and the Beckman Foundation (to G.J.N.). G.J.N. and H.D.M. are Scholars of the Leukemia and Lymphoma Society. D.C. is a Genentech, Inc. Predoctoral Fellow. E.C. is a ARCS Foundation, Inc. Fellow. S.S. is a fellow of the Leukemia and Lymphoma Society. K.M.K is supported by a training grant to the Biophysics Graduate Group (NIH T32GM008284).M.D.S. is a fellow of the Helen Hay Whitney foundation. B.A. is a fellow of the Jane Coffin Childs Memorial Fund for Medical Research.

Supplemental Data

Supplementary Figures **S1-S7**

Figure Legends:

Figure 1: Swi6 recognizes the H3K9 methyl mark within mononucleosomes and forms oligomers on mononucleosomes

(A) Schematics of the unmodified K9 and methyl lysine analog (MLA) Kc9me0 and Kc9me3 substrates (top panel) and of the unmodified (H3K9) and MLA methylated (H3Kc9me3) mononucleosomes assembled on the 147 bp 601 sequence (bottom).

(B) Bottom Panels: Representative dose responses for H3K9 (black) and H3Kc9me3 (red) mononucleosomes. Schematic: H3K9 and H3Kc9me3 mononucleosomes captured on a streptavidin derivatized SPR chip. Top panels: Close up of the kinetics of association and dissociation.

(C) Scaled isotherms for three independent dose responses of Swi6 against H3K9 (open diamonds) and H3Kc9me3 (filled circles) mononucleosome surfaces plotted on a semi-log scale. Plotted points represent the response at equilibrium, determined by averaging the signal over the final ten seconds of the sample injection. Inset: isotherms plotted on a linear scale.

(D) Schematics: Mononucleosomes with fluorescein (green star) attached by a flexible linker at one end of the 147 bp DNA template. Average of three independent fluorescent polarization experiments for H3K9 (open diamonds) and H3Kc9me3 (filled circles) mononucleosomes are shown. Error bars represent s.e.m. All Swi6 concentrations represent monomer concentrations.

Figure 2: Swi6 forms distinct oligomeric states in the absence of chromatin

(A) Wild-type Swi6 (schematic on top) is largely a pre-formed dimer at low nM concentrations. Swi6 WT (left) and L315D (right) were treated at indicated concentrations with EDC and NHS cross-linkers. Treated proteins were separated by SDS-PAGE and detected by anti-FLAG western. Swi6 concentrations: uncross-linked 50 nM, cross-linked 25, 50, 100, 200, 500, 1000 and 5000 nM.

(B) The CSD-CSD dimerization $K_d < 17$ nM. Top: Representative ITC thermogram profiles for the dissociation of WT CSD dimer (left) and L315D CSD dimer (right) at 15°C. Bottom: Graphs represent the respective binding isotherms plotted as heat changes per injection (q_i) vs. total monomer concentration.

(C) Multiangle light scattering (MALS) measurements for 20 μ M WT Swi6 (blue) and 20 μ M L315D mutant (red). Relative refractive index signals (solid lines, left y-axis) and derived molar masses (dotted lines, right y-axis) shown as a function of the elution volume. M: monomer, D: dimer, T: tetramer. (D) Top panel: Higher order oligomeric species of Swi6 stabilized by cross-linking. MALS measurements conducted as in (A). M: monomer, D: dimer, T: tetramer, O: octamer. Bottom panel: Aliquots of fractions collected from chromatography in (Top) were separated by denaturing SDS-PAGE and visualized by Sypro Red staining. The distribution of distinct oligomeric states thus visualized directly correlates with the oligomeric masses observed by MALS, while the presence of un-cross-linked Swi6 demonstrates Swi6 is not over cross-linked. All Swi6 concentrations represent monomer concentrations.

Figure 3: Swi6 displays lower specificity for the H3K9me3 mark in mononucleosomes compared to that in H3 tail peptides

(A) Representative gel shift using H3K9 or H3Kc9me3 mononucleosomes. Swi6 concentrations vary from 0 to 12 μM (0.6 fold dilutions). Unbound nucleosomes (N).

(B) Quantification of three gel shift experiments using H3K9 (open diamonds) and H3Kc9me3 (filled circles) to determine $K_{1/2}$ and specificity ($K_{1/2} \text{ H3K9} / K_{1/2} \text{ H3Kc9me3}$). Hill coefficient = 1.7 (H3Kc9me3) and = 2 (H3K9).

(C) Swi6 specificities for H3Kc9me3 mononucleosome and H3K9me3 peptide. $K_{1/2}$ values (μM) for peptides were measured by fluorescence anisotropy and $K_{1/2}$ (μM) for nucleosomes are from (B) with $n=3$.

(D) Increasing linker DNA length (L, in “bp”) decreases Swi6's ability to discriminate the methyl mark on mononucleosomes. Left graph: Swi6 discrimination for H3Kc9me3 over unmodified mononucleosomes. Right graph: Swi6 affinity for H3Kc9me3 mononucleosomes, normalized to core (L=0) nucleosomes. All error bars represent s.e.m. All Swi6 concentrations represent monomer concentrations.

Figure 4: The core unit of Swi6 binding to a mononucleosome is a tetramer

(A) Sedimentation Velocity Analytical Ultracentrifugation (SV-AUC) on H3Kc9me3 core nucleosomes. Left: The $c(M, f/f_0)$ distribution generated from SV-AUC experiments shown as a two-dimensional distribution. x-axis: molecular weight (Mwt); y-axis: hydrodynamic translational frictional ratio (f/f_0). Below, the $c(M, f/f_0)$ surface is shown as a contour plot of the distribution projected onto the M - f/f_0 plane, where the magnitude of $c(M, f/f_0)$ is indicated by contour lines at constant $c(M, f/f_0)$ for equidistant

intervals of c . Right: Table showing measured average masses (versus theoretically predicted masses) from three independent experiments using either a continuous two-dimensional function $c(s, f/f_0)$ for sedimentation coefficient s and hydrodynamic translational frictional ratio f/f_0 , or a continuous function $c(s)$ with a *bi-modal* f/f_0 distribution $c(s, bimodal f/f_0)$. Errors represent s.e.m.

(B) SV-AUC on H3Kc9me3 core nucleosome with L315D Swi6. Representation and table as in (A). Red asterisk: free L315D Swi6.

(C) SV-AUC on H3Kc9me3 core nucleosome with WT Swi6. Representation and table as in (A). Blue asterisk: free WT Swi6. Black arrows represent sticky ends.

The measured masses are used to derive structural models for the stoichiometry of the complexes as shown.

Figure 5: Amplification of Swi6 specificity towards H3Kc9me3 occurs on nucleosome arrays and is sensitive to nucleosomal placement

Dinucleosome (2N) or 12-nucleosome arrays (12N) constructs contain either 15 bp (L15) or 47 bp (L47) internucleosomal linkers.

(A) Swi6 displays 2.5 fold specificity towards 2N(L15) H3Kc9me3 dinucleosomes.

Representative gel shift shown. $K_{1/2}$ for H3Kc9me3 and H3K9 2N(L15) substrates are 62 and 156 nM, respectively. Specificity = $K_{1/2} \text{ H3Kc9me3} / K_{1/2} \text{ H3K9}$.

(B) Swi6 displays similar specificity towards H3Kc9me3 2N(L47) as for 2N(L15)

dinucleosomes. Gel shift and analysis as in (A). $K_{1/2}$ for H3Kc9me3 and H3K9 2N(L47) substrates were 12 and 32 nM, respectively.

(C) Swi6 displays ~10x amplified specificity towards H3Kc9me3 12N(L15) arrays vs. H3Kc9me3 2N(L15) dinucleosomes. Swi6-bound and unbound arrays were separated by agarose gel electrophoresis. Representative gel shift shown. $K_{1/2}$ and specificity were determined as above.

(D) Amplification of Swi6 specificity on 12N(L15) arrays is reduced on 12N(L47) arrays. Gel shift and analysis as in (C).

$K_{1/2}$ for array substrates: see Figure S6d. All error bars represent s.e.m. Swi6 concentrations represent monomer concentrations.

Figure 6: The chromodomain contains the Swi6 tetramerization interface and couples tetramerization on the nucleosome surface to H3K9me3 recognition

(A) The chromodomain of Swi6 can homodimerize. MALS measurements for uncross-linked (black) and cross-linked (green) Swi6 chromodomain (CD) showing UV absorbance signal in mA (solid lines, left y-axis) and derived molar masses (dotted lines, right y-axis) as a function of the elution volume. The CD was injected at ~50 μ M. M: monomer, D:dimer. Cross-linked CD shows increased D. Inset: SDS-PAGE analysis for the uncross-linked (-) and cross-linked (+) samples used in the MALS measurements.

(B) Top: Superimposition of the structure of monomeric dHP1 CD (black, pdb 1KNE) with dimeric Swi6 CSD (light brown, pdb 1E0B) shows structural similarity between the two evolutionarily related domains. Bottom: Alignment of the CD of the three HP1-like proteins in *S. pombe* with dHP1 CD and Swi6 CSD. Yellow boxes: conserved residues V82 and Y131. Purple box: hydrophobic residue (L or I) central to CSD dimerization.

Red star: CD hydrophobic cage residues required for H3K9me3 recognition. Gray: secondary structure schematic for dHP1 CD and Swi6 CSD.

(C) MALS measurements for WT Swi6 (blue) and V82E Y131W Swi6 (yellow), shows UV absorbance signal (solid lines, left y-axis) and derived molar masses (dotted lines, right y-axis) as a function of the elution volume. WT and V82E-Y131W Swi6 were injected at $\sim 20 \mu\text{M}$. The V82E-Y131W protein shows a higher proportion of species in tetrameric (T) and octameric (O) oligomeric states.

(D) Relationship between peptide specificity and oligomeric states (tetramer and beyond) for WT, CSD mutant (L315D) and the CD double mutant V82E-Y131W. H3K9me3 specificity for each protein is calculated as $K_{1/2}\text{H3K9}/K_{1/2}\text{H3K9me3}$. All data are reported as fold differences relative to the WT protein. Errors represent s.e.m.

(E) H3K9me3 specificity is regulated by the oligomeric state of Swi6.

y-axis: Fold specificity for methylated mononucleosome (1N) and indicated 12N array substrates.

(F) A model to depict how the CSD-CSD and CD-CD interactions enable orientation of Swi6 to correctly recognize the methyl mark in a nucleosome and generate sticky ends that bridge nearby nucleosomes and further enhance specific orientations. Swi6 concentrations represent monomer concentrations.

Figure 7: Increased tetramerization of Swi6 translates into increased silencing and heterochromatin spreading at an artificial heterochromatic locus

(A) Schematic of the reporter cassette integrated downstream of endogenous *ura4+* gene. Cassette contains a promoter (P) driving the expression of a centromeric *dh* fragment (Fr

A), an intergenic region from two convergent regions (t), a boundary element (B) that contains synthetic TFIIC binding sites (known to limit the spread of heterochromatin in *S. pombe*) and a Nat drug resistance marker (Nat^R).

(B) The V82E-Y131W mutant shows increased silencing of the fragment A cassette (Fr A). Serial dilutions of indicated *S. pombe* strains. Strains containing Fr A show silencing of *ura4+* and are able to grow on media containing 5-FOA. *swi6+* or *swi6*^{VYDEW} alleles were introduced into strains containing the whole cassette with or without Fr A (Fr A⁻); 2 independent clones are shown for each *swi6* allele. Fr A⁻ strains contain the entire cassette as shown in (A) but lack the centromeric fragment.

(C) The V82E-Y131W mutant expresses slightly lower levels of Swi6 than WT.

Extracts from respective strains were separated on SDS-PAGE gels and probed for α -tubulin (green) or Swi6 (red). Quantification of the Swi6 band normalized for the α -tubulin control is shown relative to the value obtained for *swi6+* clone 1.

(D) The Swi6 V82E-Y131W mutation induces increased Swi6 recruitment to the Fr A locus. Chromatin immunoprecipitation (ChIP) with anti-Swi6 antisera was performed in *swi6+*, *swi6*^{VYDEW} or Fr A⁻ backgrounds. Fr A specific Swi6 enrichment is represented as the ratio of the actin-normalized signal at indicated amplicons in *swi6+* or *swi6*^{VYDEW} strains divided by the actin-normalized signal in the Fr A⁻ strain. Error bars represent s.e.m. of unicate ChIP experiments from the 6 genetic isolates of *swi6+* or *swi6*^{VYDEW} alleles. X-axis: distance in base pairs relative to the Fr A cassette promoter (P). Genomic features near the Fr A cassette insertion site are aligned below the graph.

(E) The Swi6 V82E-Y131W mutation increases H3K9 methylation at and beyond the Fr A cassette. ChIP experiments were performed with anti-H3K9me2 antisera. The Fr A specific H3K9me2 enrichment is calculated as in (D). Error bars as in (D).

(F) The Swi6 V82E-Y131W mutation leads to increased Swi6 recruitment at endogenous heterochromatin. Top: H3K9me2 ChIP. H3K9me2 fold enrichment over actin at the centromeric *dg* repeat for the Fr A⁻ strain and *swi6*⁺ or *swi6*^{VYDEW} alleles. Bottom: Swi6 ChIP. Swi6 fold enrichment over actin at the centromeric *dg* repeat for the same strains as (Top). Error bars for *swi6*⁺ and *swi6*^{VYDEW} as in (D). Error bar for Fr A⁻ (bottom) represents s.e.m. for three independent IPs from the Fr A⁻ strain.

Figure 1

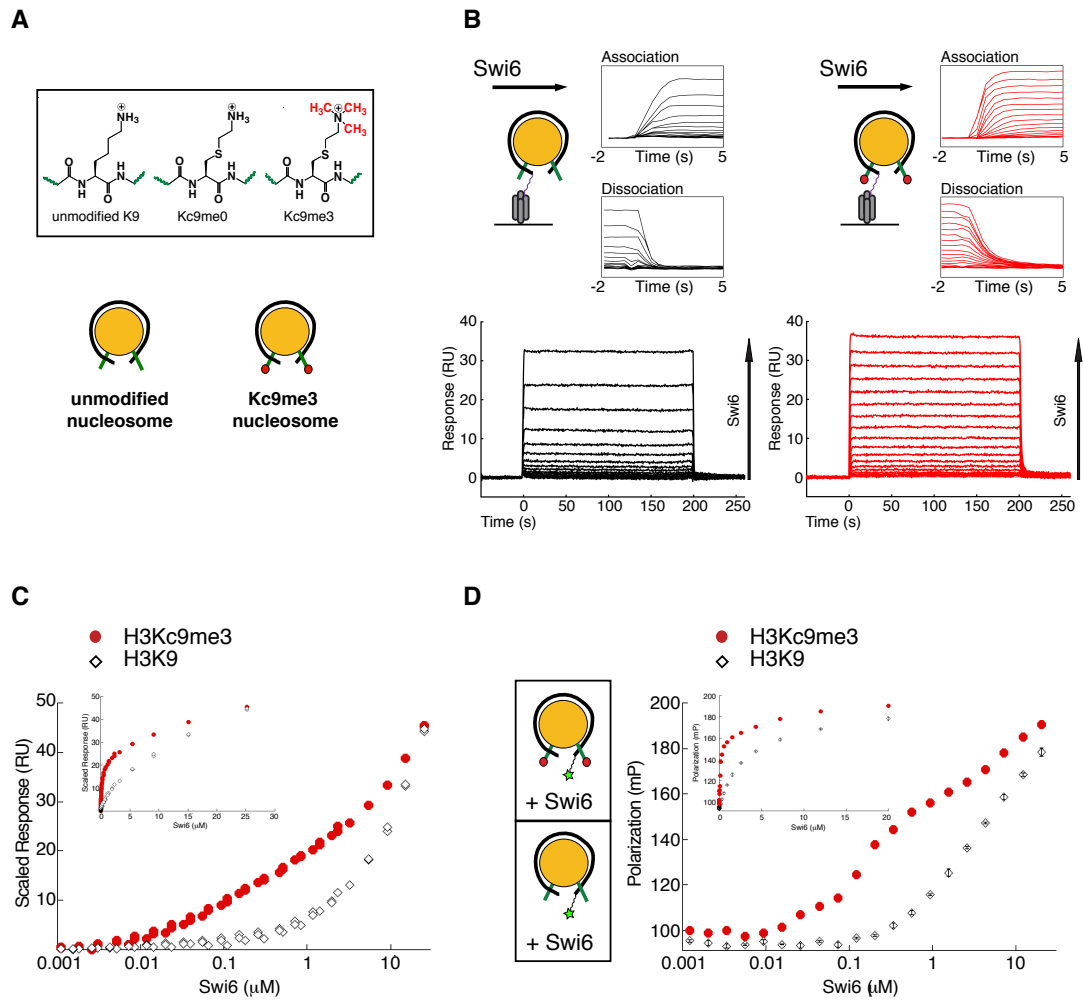


Figure 2

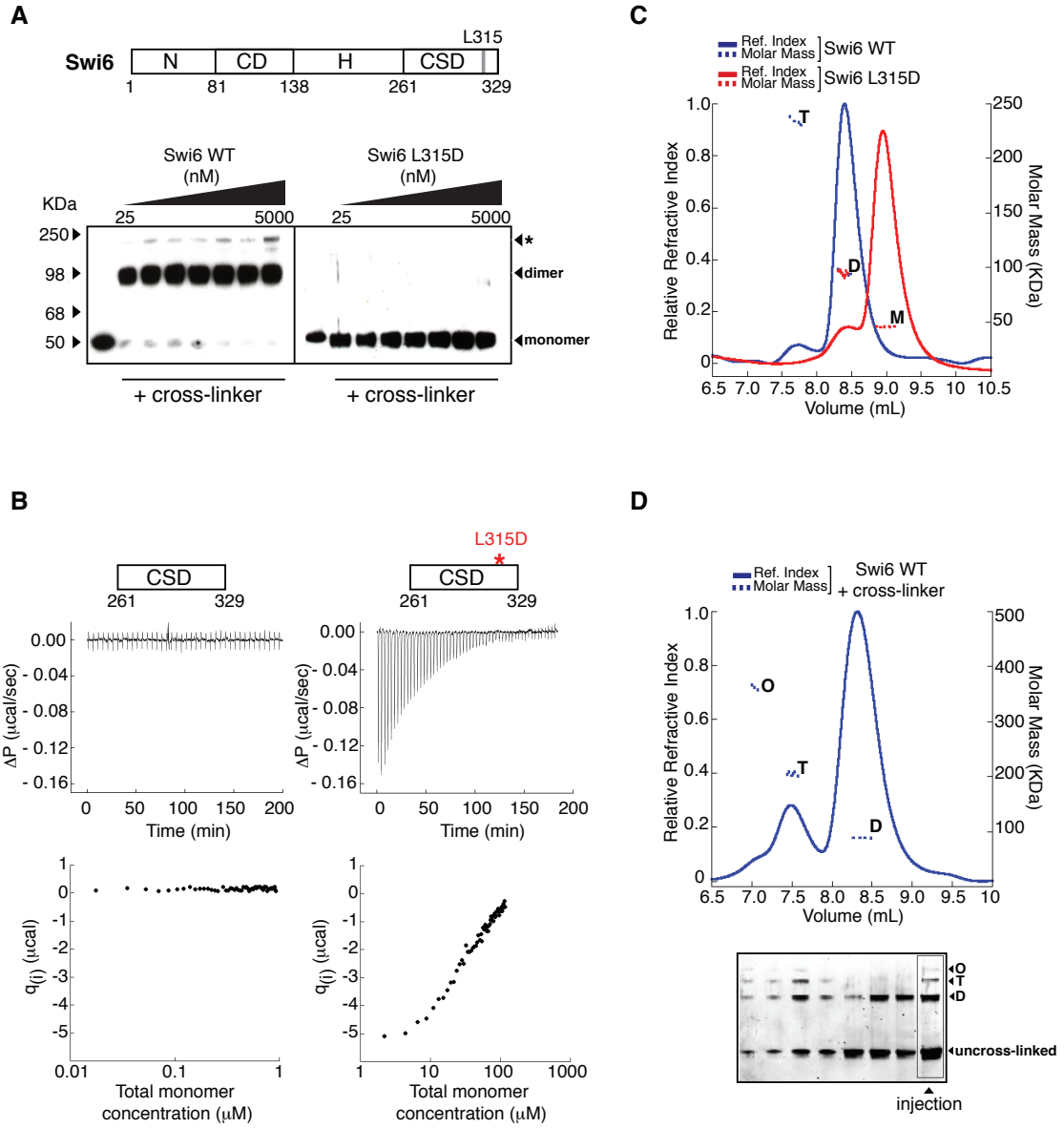


Figure 3

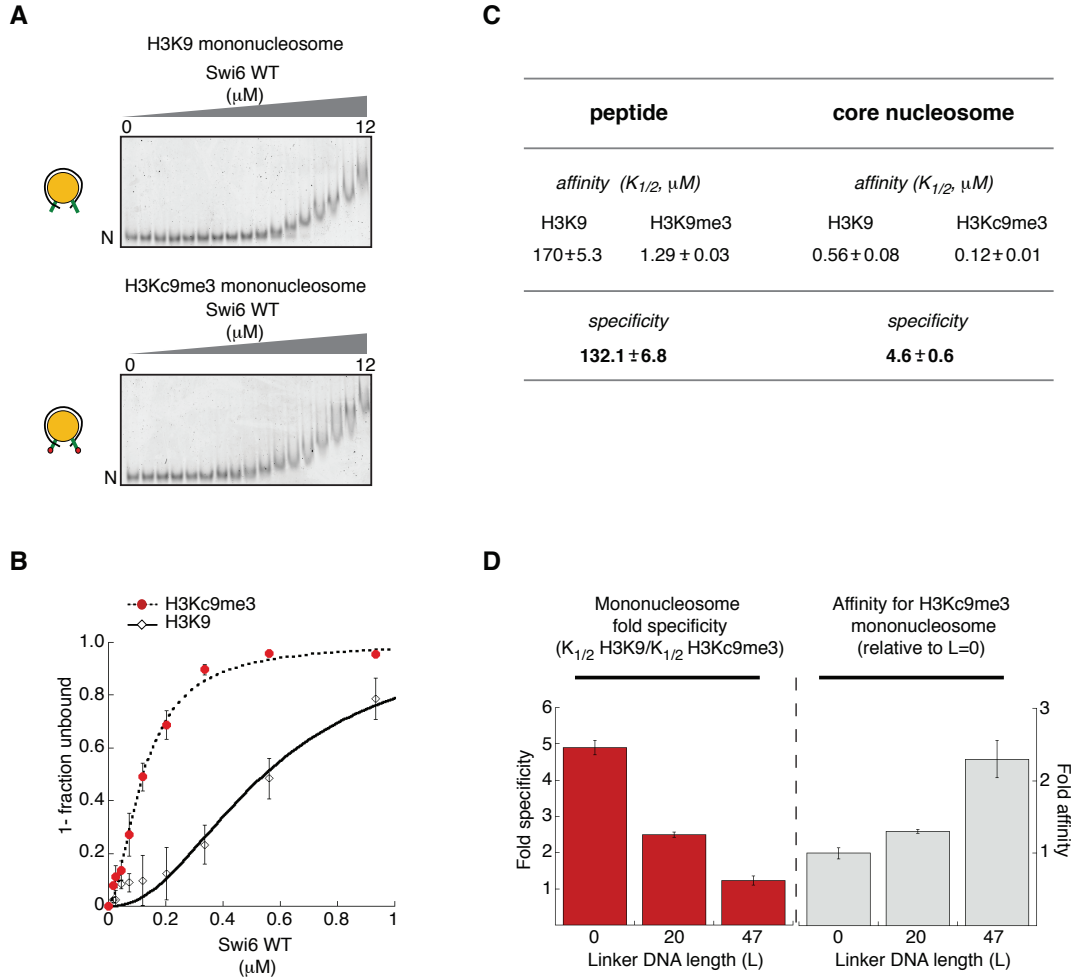


Figure 4

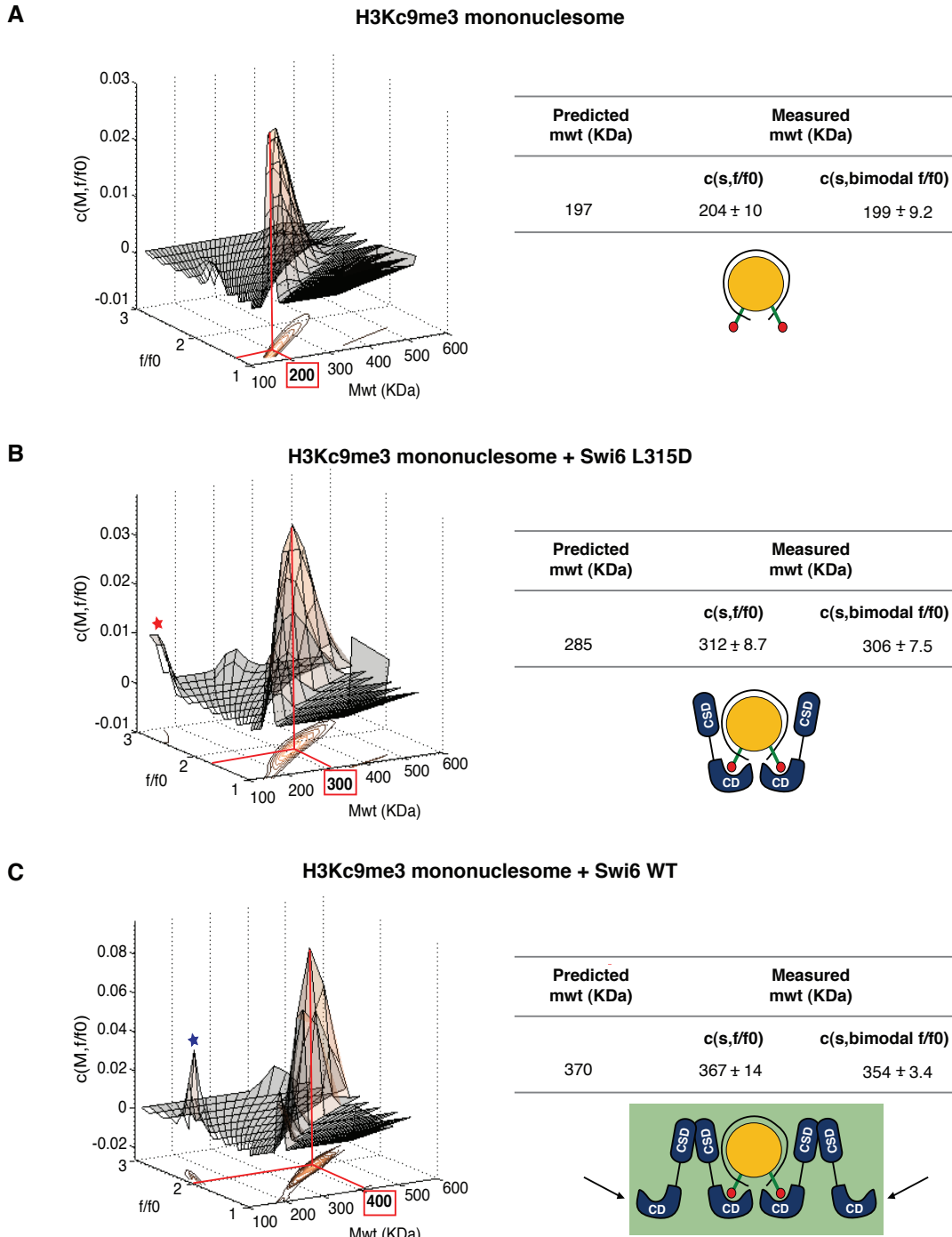


Figure 5

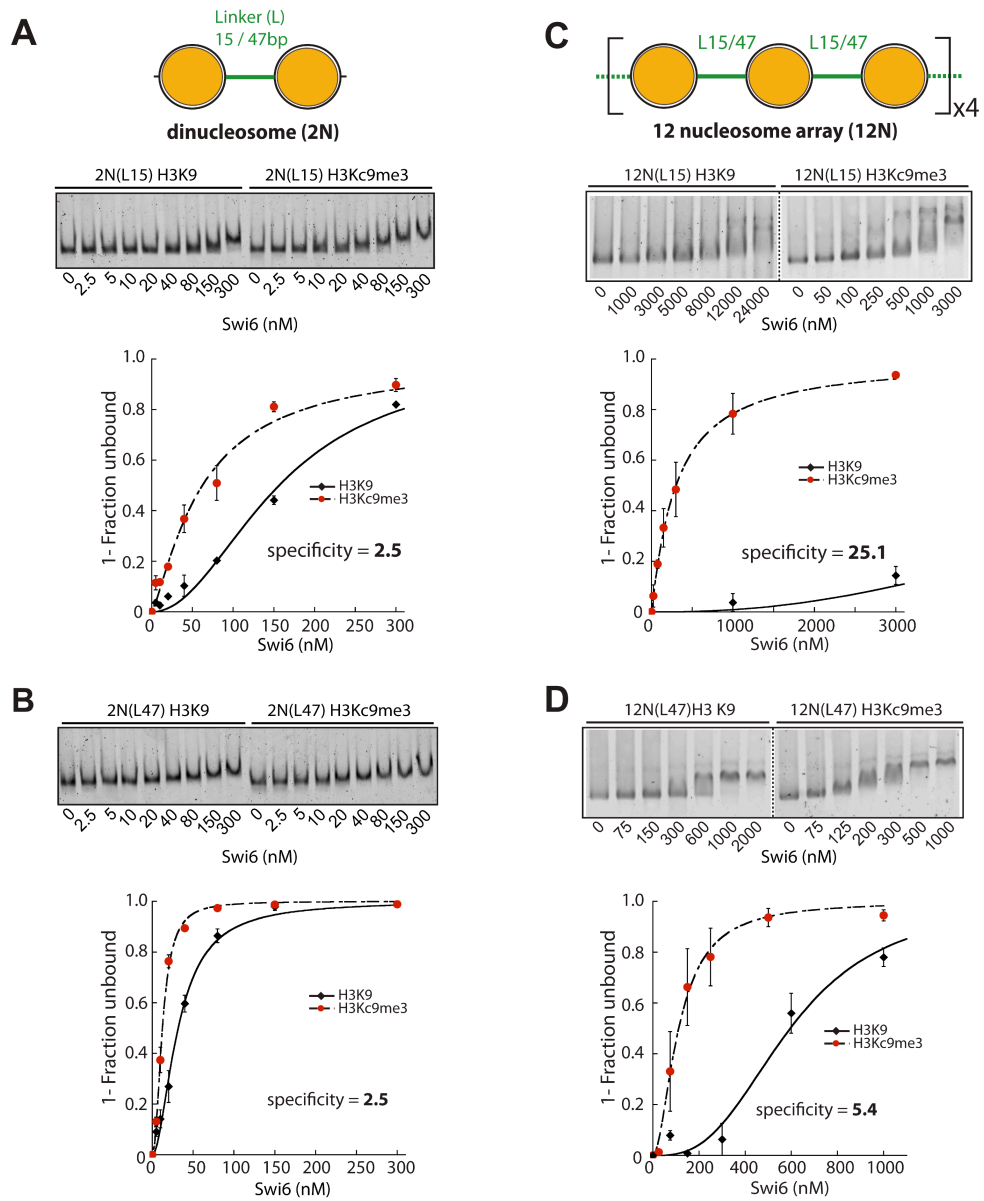


Figure 6

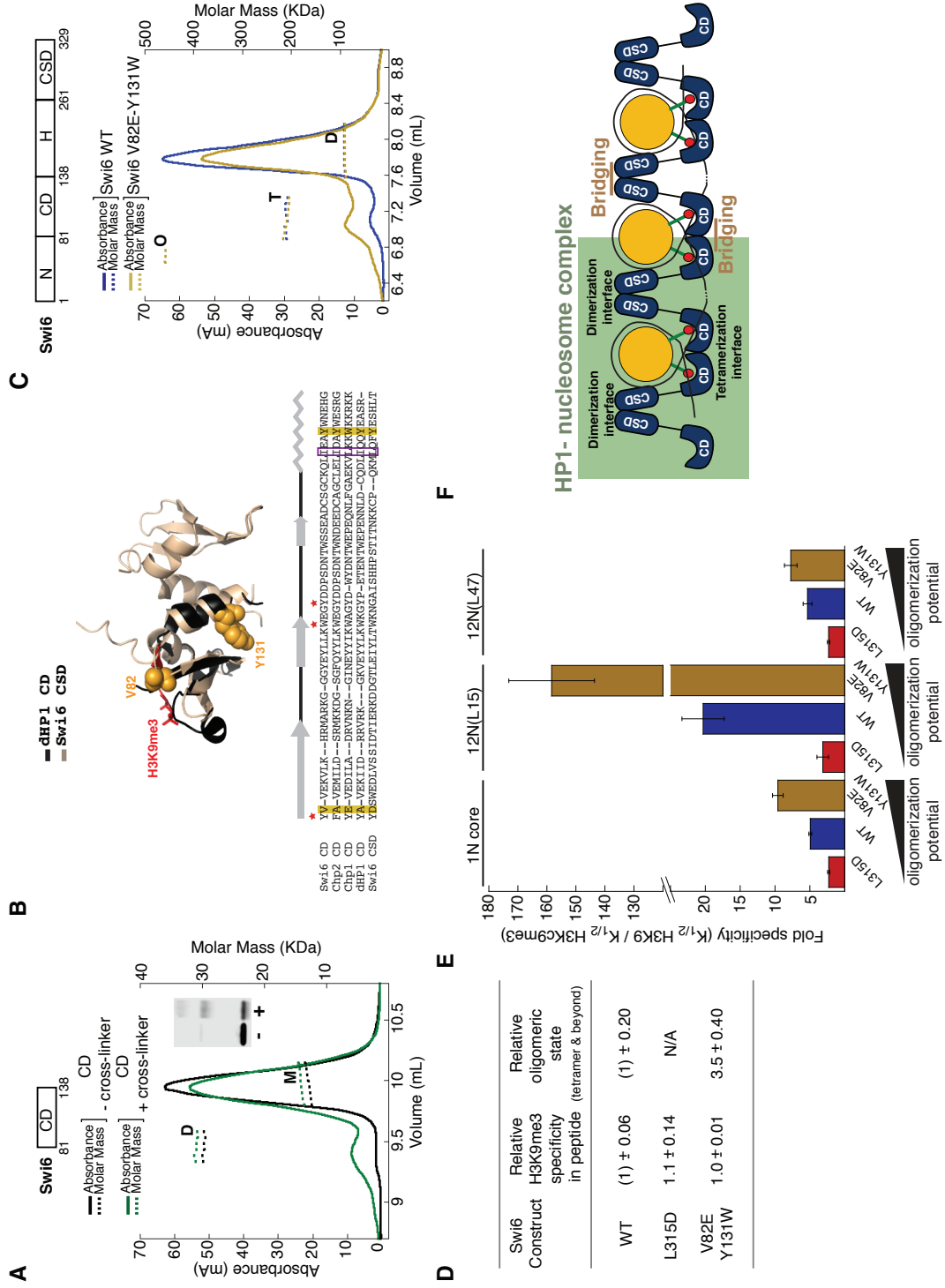
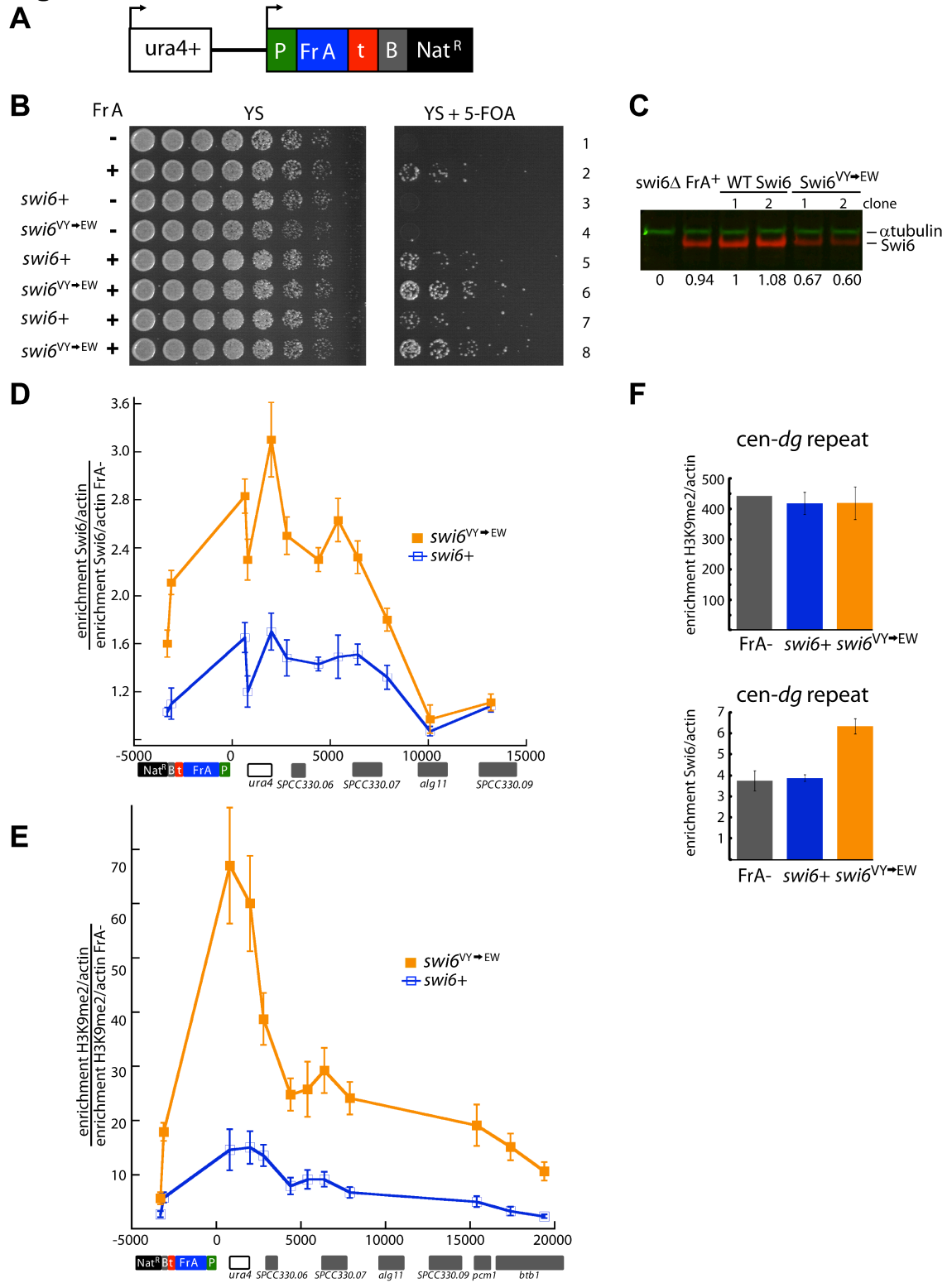


Figure 7



Supplementary Information

Chromodomain-mediated oligomerization of HP1 suggests a nucleosome bridging mechanism for heterochromatin assembly

Daniele Canzio, Evelyn Y. Chang, Smita Shankar, Kristopher M. Kuchenbecker, Matthew D. Simon, Hiten D. Madhani, Geeta J. Narlikar and Bassem Al-Sady

Inventory of Supplementary Information

Figure S1 (related to Figure 1)

Raw data and analysis of the surface plasmon resonance assay

Figure S2 (related to Figure 2)

Loss of higher-order oligomerization in L315D Swi6 mutant

Figure S3 (related to Figure 3)

Comparison of H3K9 and H3K9me0 nucleosome:Swi6 affinities by gel mobility shift assay. Quantification of H3K9 and H3K9me3 tail peptide:Swi6 interactions by fluorescence polarization. Quantification of gel mobility shift assays of Swi6 with mononucleosomes containing varying linker DNAs on both sides of 147bp 601 sequence and Swi6 with DNA constructs of varying length. Estimation of Swi6 binding specificity for H3K9me3 over H3K9 core nucleosomes using a DNA - nucleosome competition assay

Figure S4 (related to Figure 4)

Details of two analysis methods for mononucleosome:Swi6 SV-AUC data

Figure S5 (related to Figure 5)

Quality control for arrays used in Figure 5. Gel mobility shift assay based co-operativity estimates for Swi6:H3Kc9me3 12N array interactions. Sensitivity analysis for gel mobility shift assays in Figure 5c.

Figure S6 (related to Figure 6)

Swi6 deletion analysis. Analysis of dHP1 chromodomain crystallographic unit. H3K9me3 peptide affinities and specificities of Swi6 mutants. Affinity of Swi6 for H3Kc9me3 and H3K9 12N arrays.

Figure S7 (related to Figure 7)

Fr A cassette silencing phenotype of 6 *swi6*⁺ and 6 *swi6*^{VY→EW} isolates.

Supplementary Figure legends

Extended Experimental Procedures

Supplementary discussion

Estimation of the fraction of Swi6 molecules bound in H3K9 recognizing orientations. Detailed description of model for the role of CD-CD interactions and the effects of altering flanking DNA.

Supplementary information references

Figure S1

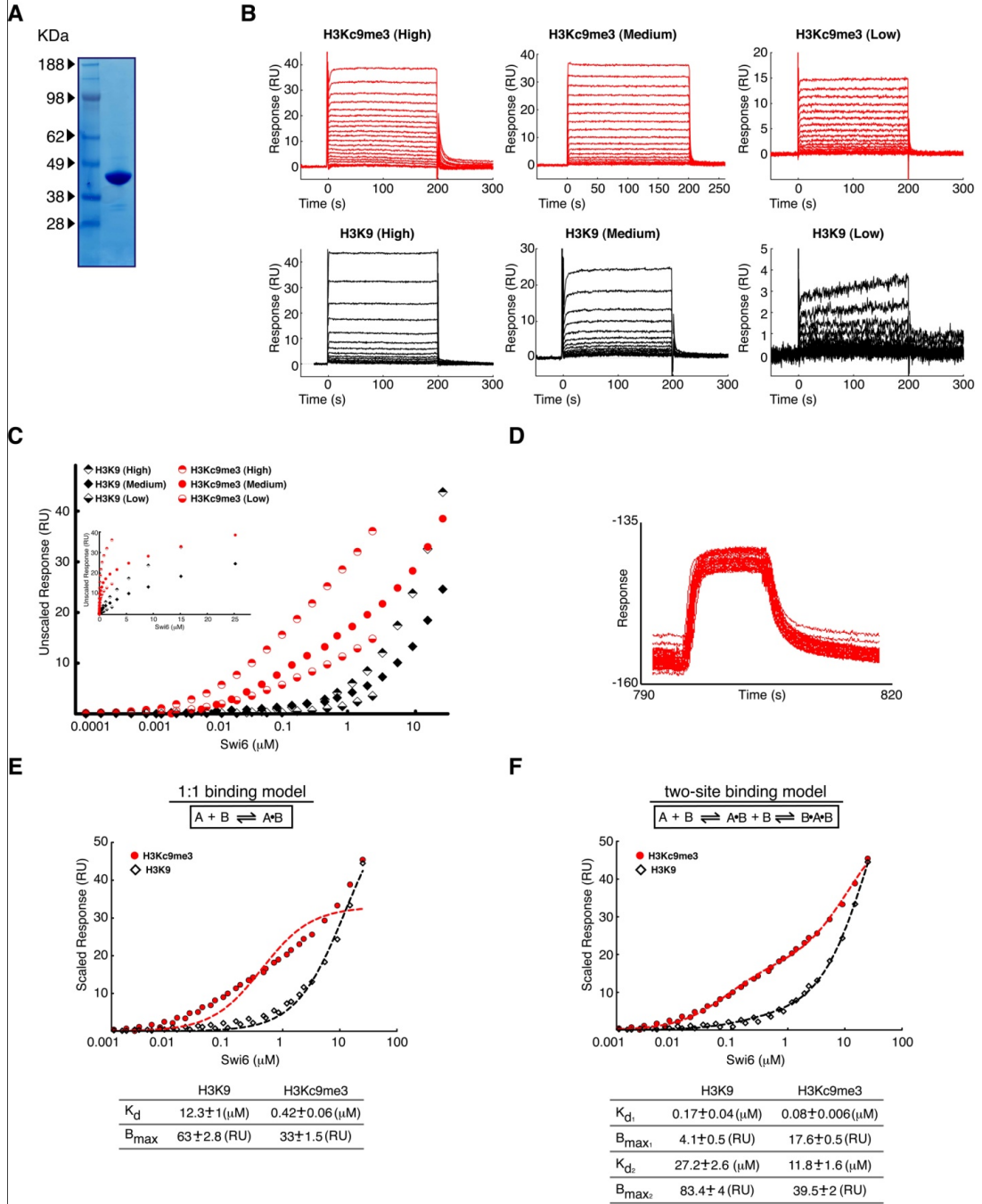


Figure S2

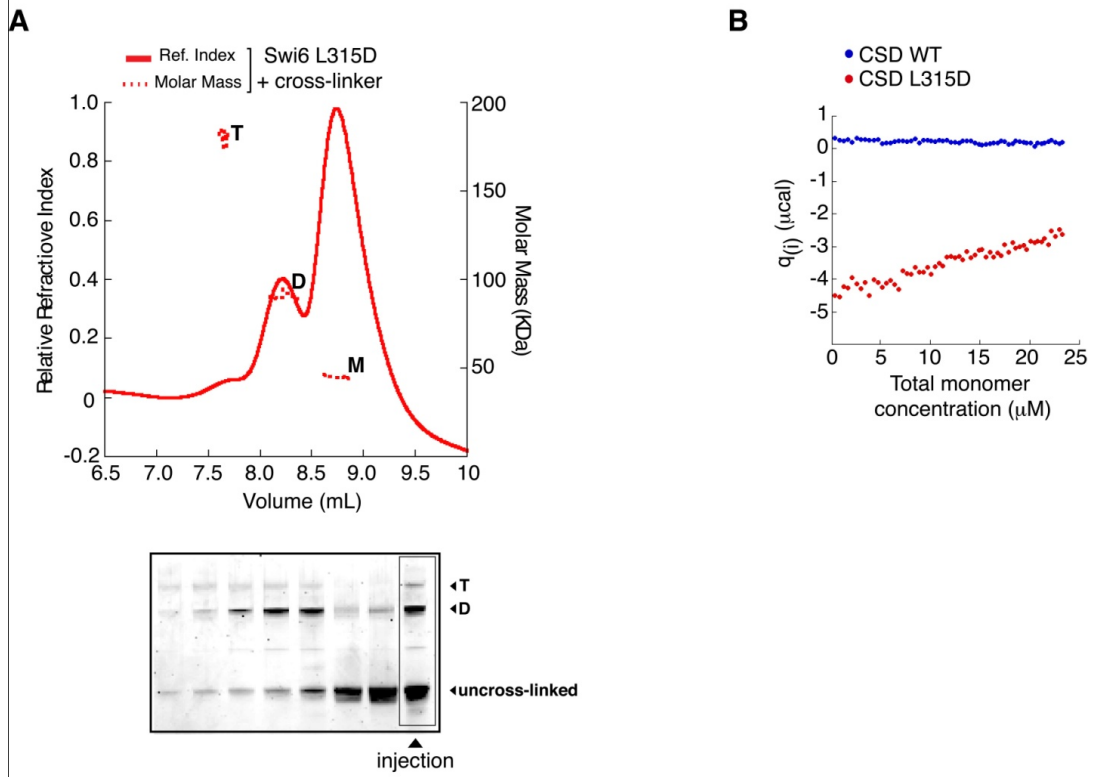


Figure S3

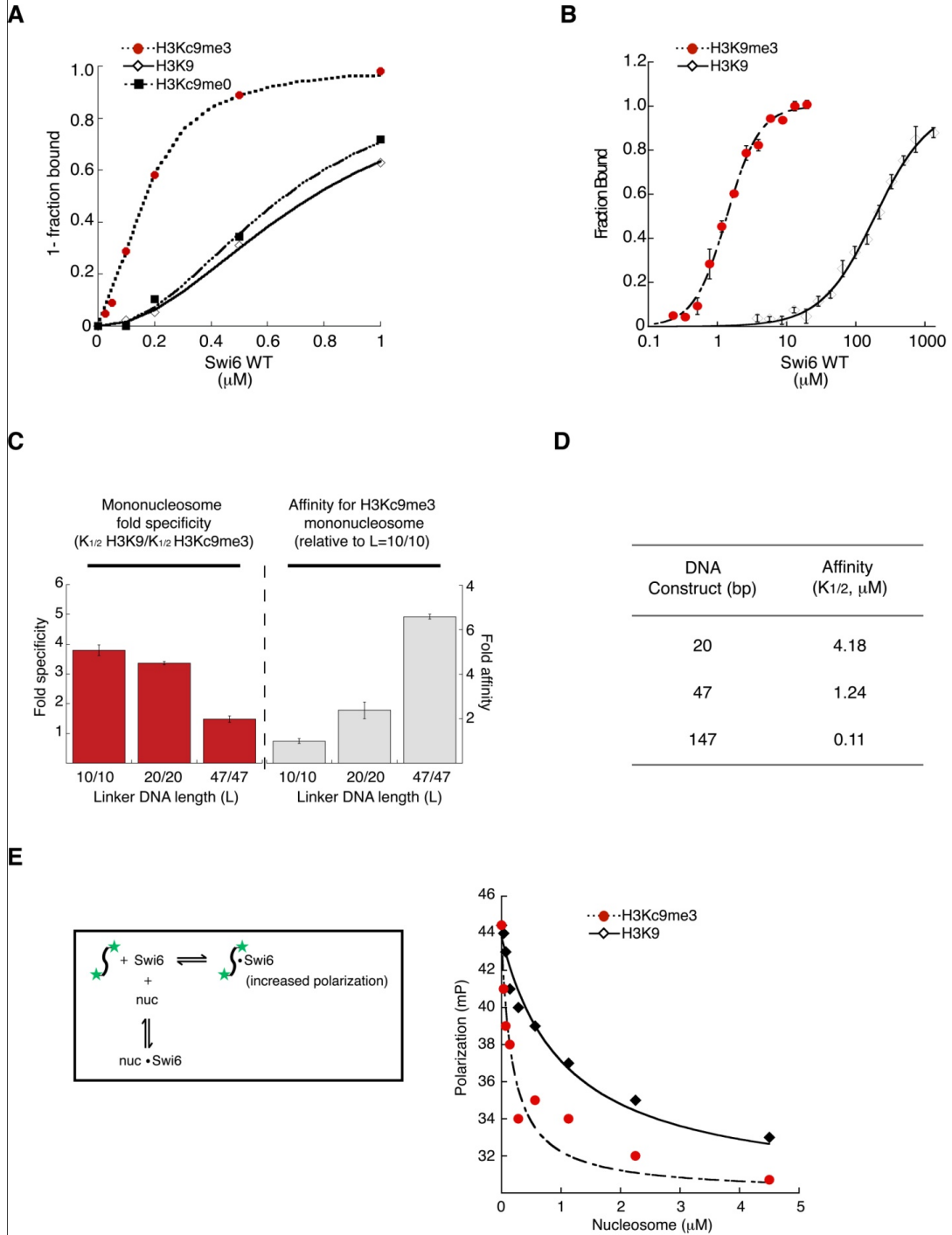


Figure S4

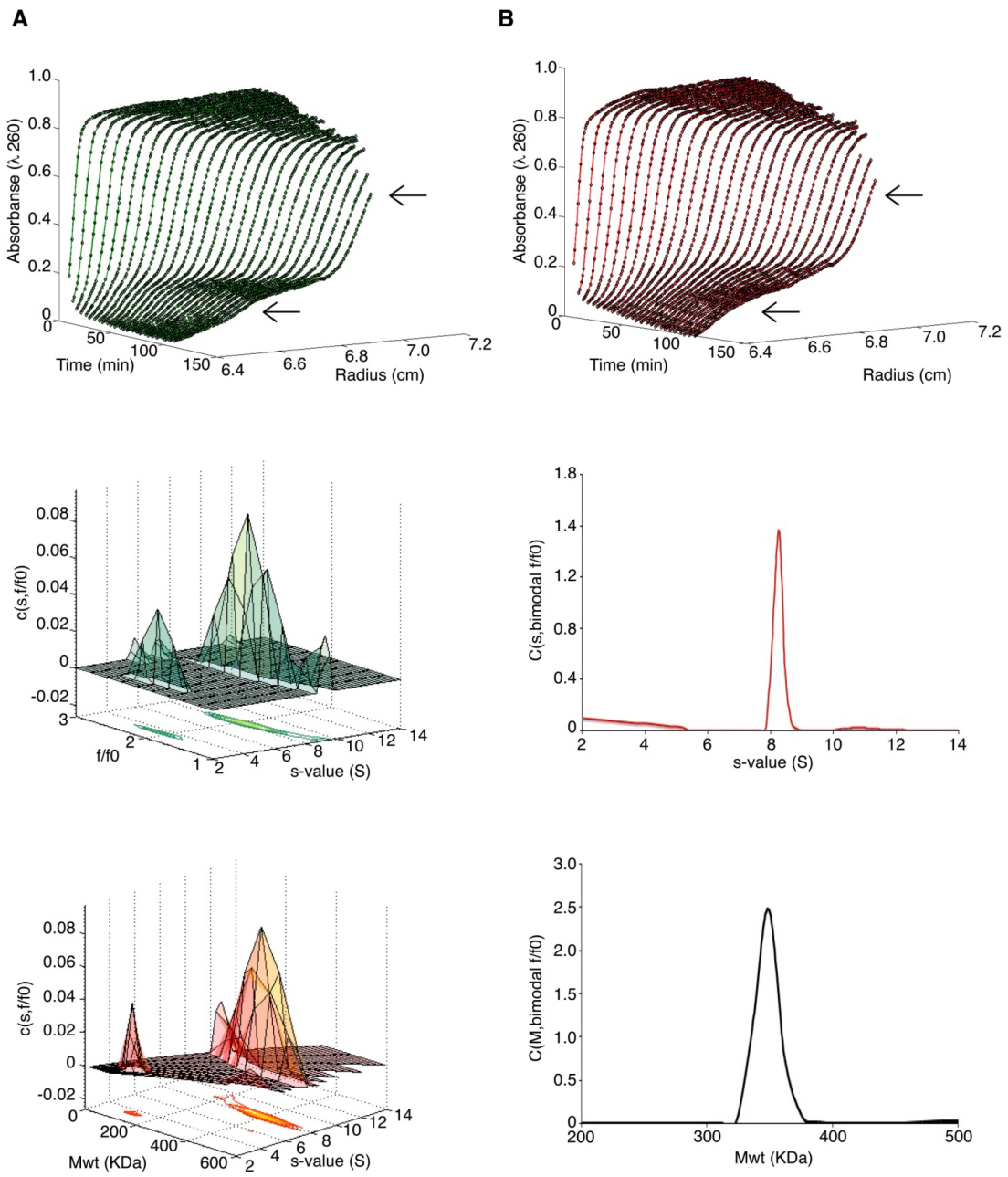


Figure S5

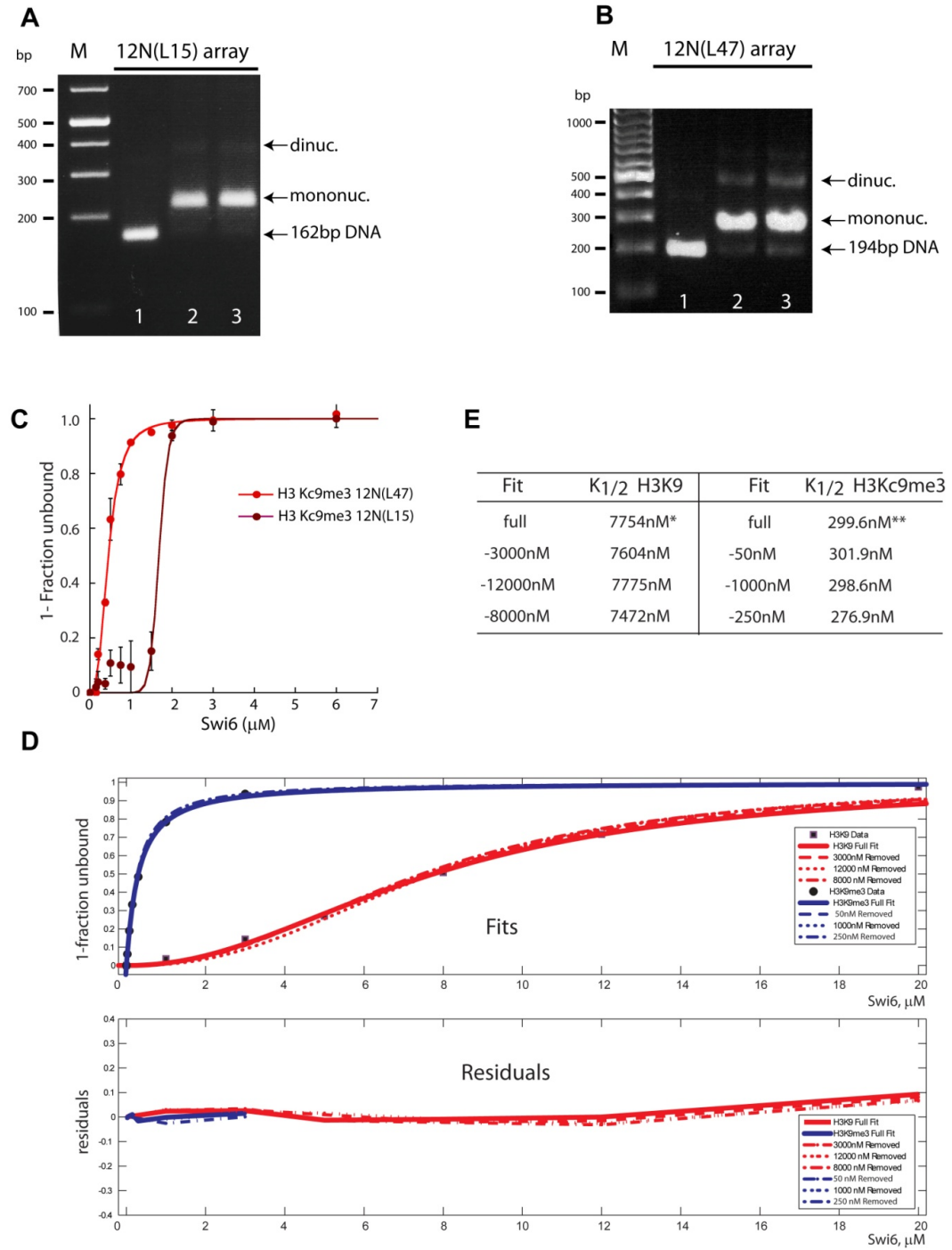


Figure S6

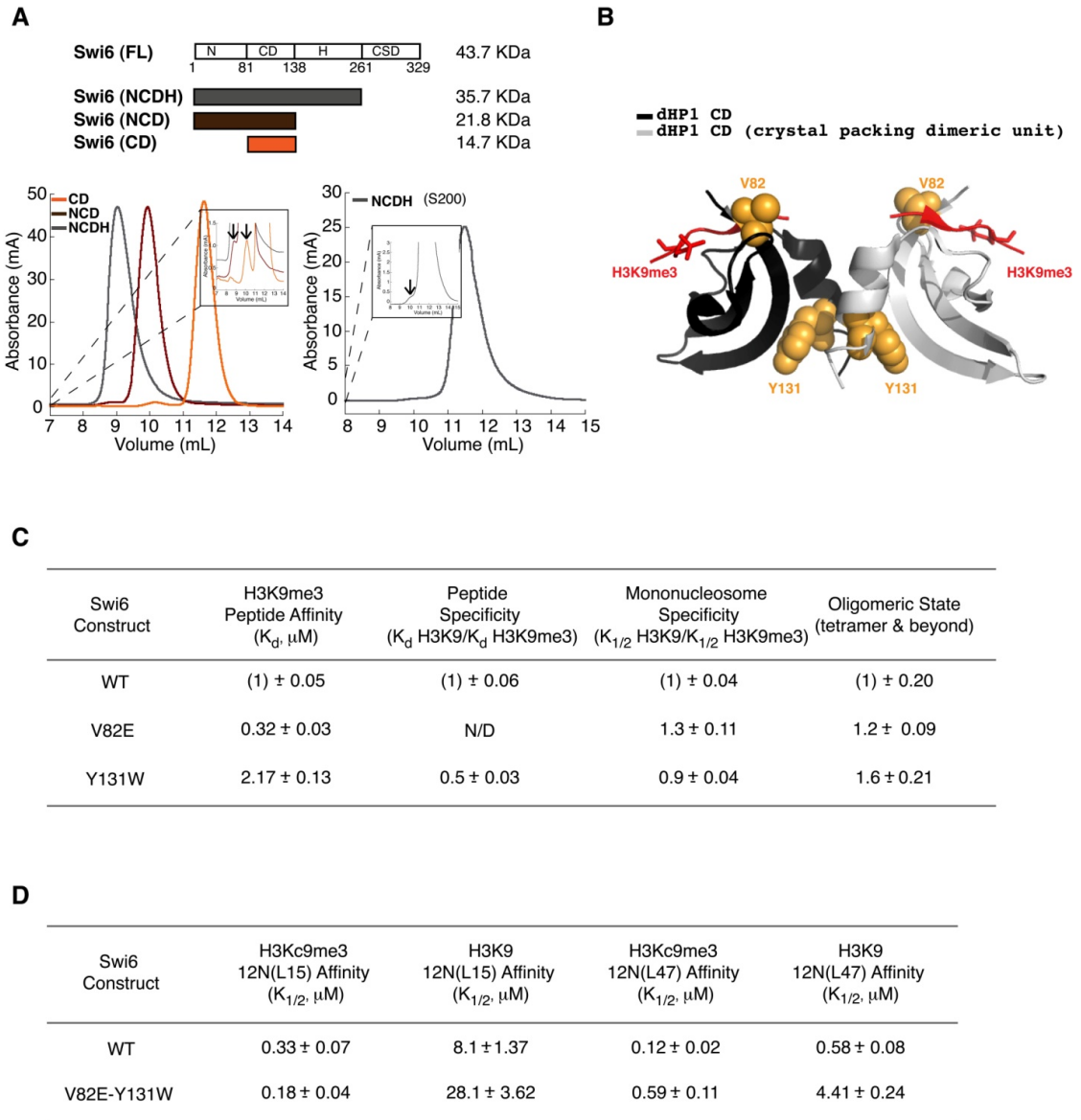
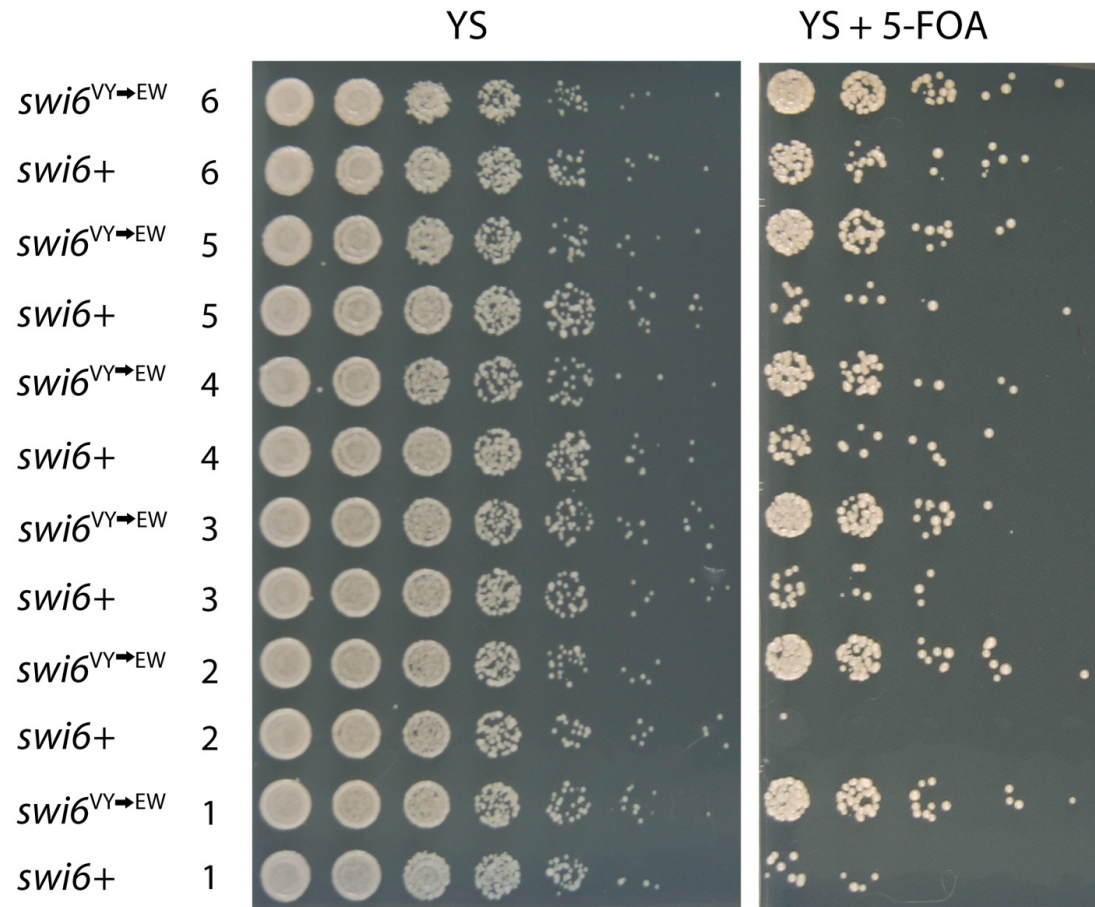


Figure S7



Supplemental Figure Legends

Figure S1

Raw data and analysis of the surface plasmon resonance assay

(A) Coomassie-stained SDS-PAGE protein gel loaded with ~4mg of the cleaved, recombinant Swi6 protein used in the SPR assay.

(B) Data from three independent dose responses of Swi6 to nucleosomes captured on the streptavidin derivatized SPR chip, carried out at different nucleosome densities (Low, Medium and High) for both H3Kc9me3 (red) and H3K9 (black) nucleosomes.

(C) Unscaled binding isotherms plotted on a semi-log scale for H3Kc9me3 (circles) and H3K9 (diamonds) of the dose response titrations from (B). The inset shows the isotherms plotted on a linear scale. The scaled isotherms for three independent dose responses of Swi6 for both H3Kc9me3 and H3K9 are shown in Figure 1c.

(D) Raw traces of the interaction between a fixed concentration of Swi6 (control sample) and H3Kc9me3 nucleosomes. The control sample was injected following every concentration of Swi6 in the titration to assay for nucleosome surface stability throughout the duration of the experiment.

(E) Fits of the scaled isotherms based on a 1:1 binding model for both H3Kc9me3 (red) and H3K9 (black) nucleosomes.

(F) Fits of the scaled isotherms based on a two-site binding model for both H3Kc9me3 (red) and H3K9 (black) nucleosomes.

As described in the main text, despite the readily apparent equilibrium and kinetic differences between Swi6's interaction with H3K9 and H3Kc9me3 nucleosomes, we cannot directly fit a model to the data for two reasons. (i) Because the data does not reveal saturation, we do not have knowledge of the final stoichiometry for this interaction. (ii) In Figure 1c, the data are plotted as a function of total Swi6 monomer concentration. However, HP1 proteins are known to oligomerize in solution. This presents a major complication as the concentration of molecules in solution will change as a function of oligomeric state. Because we are spanning over four orders of magnitude in our dose response curves, it is likely that we are titrating Swi6 at different oligomeric states. Without direct knowledge of the oligomeric partitioning and the final stoichiometry, we cannot obtain a meaningful model to extract rate and equilibrium constants from the kinetic and equilibrium measurements. The 1:1 binding model clearly does not fit well to the data, and while the two sites binding model appears to fit well to the data, we cannot compare the two K_d values for methylated and unmethylated nucleosomes. This is because the fits result in very different final stoichiometries of Swi6:nucleosome ($B_{\max,1}$ and $B_{\max,2}$) for each binding event for methylated and unmethylated nucleosomes.

K_{d1} represents the first binding step, and K_{d2} represents the second binding step.

Swi6 concentrations represent monomer concentrations.

Figure S2

Loss of higher-order oligomerization in L315D Swi6 mutant

(A) Higher order oligomeric species of L315D Swi6 can be stabilized by cross-linking.

Top panel: MALS measurements for cross-linked L315D Swi6 were conducted as in Figure 2d. L315D Swi6 was cross-linked at 100 μM using EDC/NHS chemistry and then injected at 20 μM . A mixture of masses corresponding to distinct monomer, dimer, and tetramer states was observed. Bottom panel: Aliquots from the size elution chromatography fractions analyzed in the top panel were separated on SDS-PAGE and visualized by Sypro Red staining. The distribution of distinct oligomeric states visualized by the denaturing gel directly correlates with the oligomeric masses observed with MALS, while the presence of uncross-linked Swi6 migrating at 50 kDa demonstrates that the protein was not over cross-linked. Swi6 concentrations represent monomer concentrations.

(B) The CSD does not display detectable higher order oligomerization. Graph represents the binding isotherms plotted as heat changes per injection (q_i) versus total monomer concentration for WT CSD (blue) and L315D CSD (red). Heat release for the L315D mutant reflects dimer dissociation (see Figure 2b). Concentration regime was 0.4 to 24mM CSD protein.

Figure S3

(A) Quantification of gel shift experiments using unmodified (open diamonds), H3Kc9me0 (filled squares), and H3Kc9me3 nucleosomes (filled circles). The average of three experiments is shown for H3Kc9me0 and H3K9 nucleosomes and the average of two experiments for H3Kc9me3 nucleosomes.

(B) Quantification of peptide binding experiments using H3K9 (open diamonds), and H3K9me3 (filled circle) peptide. $K_{1/2}$ (μM) for methylated and unmethylated peptide was

measured by fluorescence polarization. Error bars represent s.e.m. The Hill coefficients (n) determined for these experiments were variable, with the median n = 1.38 (6 experiments) and n = 1.1 (4 experiments), for H3K9me3 and H3K9 peptides, respectively.

(C) Increasing linker DNA length (L) on both sides of the 147 bp 601 sequence decreases Swi6's ability to discriminate the methyl mark on mononucleosomes. Three linker DNA lengths were assayed: 10bp/10bp linker DNA, 20bp/20bp linker DNA and 47bp/47bp linker DNA. Left graph: Swi6 discrimination for H3Kc9me3 over unmodified mononucleosomes decreases with the linker DNA length. Right graph: Swi6 affinity for H3Kc9me3 mononucleosomes versus linker DNA length, normalized to L=10/10 nucleosomes.

All error bars represent s.e.m.

(D) $K_{1/2}$ values for DNA constructs with 20, 47 and 147 bp. Maximum variation observed was 40%.

(E) Estimation of Swi6 binding specificity for H3Kc9me3 over H3K9 core nucleosomes using a DNA - nucleosome competition assay. Scheme: An 80 bp 5' and 3' fluorescein-labeled DNA probe (F80F) was prebound to Swi6. The extent of binding was measured by fluorescence polarization (FP). Swi6 was displaced from the F80F-Swi6 complex by the addition of H3Kc9me3 or H3K9 core nucleosomes at indicated concentrations, resulting in a decreased FP signal. K_i constants for H3Kc9me3 and H3K9 nucleosomes were determined by fitting the FP data from the competition curves (right) and determined to be 0.19 mM and 1.03 mM, respectively. These values result in a 5.3 fold

binding preference of Swi6 for H3Kc9me3 over H3K9 nucleosomes. The points represent averages of two repeats for each competition curve.

Swi6 concentrations represent monomer concentrations.

Figure S4

Two analyses of SV-AUC data by $c(s, f/f_0)$ and $c(s, \text{bimodal } f/f_0)$

(A) Application of $c(s, f/f_0)$ analysis to H3Kc9me3 mononucleosome with WT Swi6.

Top: Two dimensional representation of the raw data profiles (black dots) as a function of time (min) and radius (cm). Data were collected by following sample absorbance at 260 nm. Traces were calculated at one-minute time intervals. For clarity, only every fourth scan is shown. Solid lines represent fits of the analysis (rmsd=0.0068). The two arrows indicate two clearly separated regions in the sedimentation coefficient distribution.

Middle: The $c(s, f/f_0)$ distribution as a two-dimensional distribution with x-axis representing the sedimentation coefficient (s-values) and y-axis representing the hydrodynamic translational frictional ratio (f/f_0). Below the $c(s, f/f_0)$ surface is shown a contour plot of the distribution projected into the s- f/f_0 plane, where the magnitude of $c(s, f/f_0)$ is indicated by contour lines for equidistant intervals of c.

Bottom: The $c(s, M)$ distribution as a two-dimensional distribution with x-axis representing the sedimentation coefficient (s-values) and y-axis representing molecular weight (M, KDa). Below the $c(s, M)$ surface is shown a contour plot of the distribution projected into the s-M plane, where the magnitude of $c(s, M)$ is indicated by contour lines for equidistant intervals of c.

(B) Application of $c(s, \text{bimodal } f/f_0)$ analysis to H3Kc9me3 mononucleosome with Swi6 WT.

Top: Two dimensional representation of the raw data profiles (black dots) as a function of time (min) and radius (cm). Data were collected and traces presented as in panel A. Solid lines represent the fits of the analysis (rmsd=0.09).

Middle: The $c(s, \text{bimodal } f/f_0)$ distribution with x-axis representing the sedimentation coefficient (s-values) and y axis representing $c(s, \text{bimodal } f/f_0)$. Graph is based on a s-value window from 5 to 15.

Bottom: The $c(M, \text{bimodal } f/f_0)$ distribution as a two-dimensional distribution with x-axis representing the molecular weight (KDa) and y axis representing $c(M, \text{bimodal } f/f_0)$.

Figure S5

Quality control of assembled 12N(L15) and 12N(L47) nucleosome arrays and cooperativity of Swi6 binding on H3Kc9me3 arrays

(A) 12N(L15) array. 12N(L15) DNA alone (lane 1), H3K9 (lane 2) and H3Kc9me3 (lane 3) 12N(L15) arrays assembled at 1.3:1 (H3K9) or 1.1:1 (H3Kc9me3) histone octamer:DNA molar ratios were digested with 100 U EcoR1 for 3 hrs and separated on 2% TBE-agarose gels. Release of free 162 bp DNA from assembled arrays indicates under-assembly, while appearance of species corresponding to dinucleosomes or greater indicates over-assembly. Arrays with >90% signal deriving from mononucleosomes were chosen for gel shifts.

(B) 12N(L47) array. As above, except samples were digested with 10 U EcoR1. Histone octamer to DNA molar assembly ratios were 1.2:1 for H3K9 arrays and 1.1:1 for H3Kc9me3 arrays.

(C) Binding of Swi6 to H3Kc9me3 12N(L47) and 12N(L15) arrays appears more cooperative than on mono- and dinucleosomes as measured by native gel electrophoretic mobility shift assay. The following binding model was used to derive Hill coefficients from the binding data: (fraction bound = $[Swi6]^n / ([Swi6]^n + K_d)$ where n= Hill coefficient. n = 2.9 for H3Kc9me3 12N(L47) and n = 15 for H3Kc9me3 12N(L15). Swi6 concentrations represent monomer concentrations.

These Hill coefficients are only a qualitative estimate of cooperativity as the observed cooperativity could also arise if binding of multiple Swi6 molecules is required to observe stably upshifted arrays. The data, however, do strongly indicate that binding of Swi6 across multiple nucleosomes helps correctly orient Swi6 for recognition of the H3Kc9me3 mark.

(D) Sensitivity analysis for 12N(L15):Swi6 gel shifts in Figure 5c. TOP: Three of the seven Swi6 concentration points from H3K9 (blue) or H3Kc9me3 (red) 12N(L15):Swi6 binding curves were individually excluded and the remaining six points refitted using the equation in the extended experimental procedures. The excluded Swi6 concentration points are indicated in the legend. BOTTOM: Residuals for plots in TOP.

(E) Table of $K_{1/2}$ values. Calculated $K_{1/2}$ values for the plots in (D) are shown. * The 95% confidence interval is 278.9-320.3 nM. ** The 95% confidence interval is 6911-8597 nM.

Figure S6

Characterization of mutations in the chromodomain dimerization interface

(A) Domain deletion approach.

Top: Molecular weights of each of the three constructs analyzed for Swi6 domain mapping.

Bottom Left: Elution profile followed at 280 nm of the NCDH, NCD, CD constructs off a S-75 Superdex column. Both the CD and NCD show a main monomer peak and a relatively small dimer peak.

Bottom right: Elution profile followed at 280 nm of the NCDH construct off a S-200 Superdex column. This shows a main monomer peak and a relatively small dimer peak.

Arrows in insets represent dimer peaks.

(B) Crystallographic unit of dHP1 CD structure (pdb 1KNE) containing two dHP1 CD monomers (black and gray), which appear to engage in contacts via the CSD-homologous alpha helix.

(C) Affinity for H3K9me3 peptide, specificity for H3K9me3 over H3K9 peptide, specificity for H3Kc9me3 over H3K9 mononucleosomes and oligomerization state (tetramer and beyond) for WT, V82E and Y131W Swi6. All data are relative to WT Swi6.

All error bars represent s.e.m. Swi6 concentrations represent monomer concentrations.

(D) Affinity for H3Kc9me3 and H3K9 12N(L15) and 12N(L47) arrays for WT Swi6 and V82E-Y131W Swi6.

Note the $K_{1/2}$ measurements were determined by averaging the fits of three independent binding curves, while H3K9/H3Kc9me3 specificity is calculated as the average of three

$K_{1/2}$ ratios from independent fits. All error bars represent s.e.m. Swi6 concentrations represent monomer concentrations.

Figure S7

Characterization of 6 independent genetic isolates for *swi6+* and *swi6*^{VY→EW} alleles.

Serial dilutions of saturated *S. pombe* cultures derived from 6 independent genetic isolates for *swi6+* and 6 independent isolates for *swi6*^{VY→EW} (genetic background as in Figure 7b). Dilutions were plated either on YS media or YS media supplemented with 5-FOA to assay silencing.

Extended Experimental Procedures

Protein cloning and purification

Tagged and untagged Swi6 were cloned into pET30a at the BamH1 and Not1 sites. The constructs for both tagged and untagged Swi6 contain an N-terminal 6xHis tag encoded by the pET30a vector, but the untagged Swi6 contains a TEV cleavage site just upstream of the Swi6 coding region. Swi6 proteins were purified from *E. coli* Rosetta (DE3) pLysS strains as follows. Cells were grown to OD 0.4-0.5 at 37°C in LB medium with 100 mg/mL Kanamycin. Isopropyl- β -D-thiogalactopyranoside was added to a concentration of 0.4 mM to induce protein expression, and cells were incubated overnight at 18°C. Harvested cells were resuspended in lysis buffer (1X PBS buffer pH 7.3, 300 mM NaCl, 10% glycerol, 0.1% Igepal CA-630, 7.5 mM Imidazole, and protease inhibitors). Following sonication, cell debris was removed by centrifugation at 25,000g for 20 min. Cell lysate supernatants were incubated for 1 hour at 4°C with Cobalt-NTA affinity beads (Clontech). Beads were washed with lysis buffer and proteins eluted with 25 mM HEPES pH 7.5, 100 mM KCl, 10% glycerol and 250 mM Imidazole. Proteins were further purified by size-exclusion chromatography on a Superdex 200HR 10/300 column (GE Healthcare) into a final elution buffer containing 25 mM HEPES pH 7.5, 100 mM KCl, and 10% glycerol. Tagged Swi6 was then stored at -80°C. Untagged Swi6 underwent two additional steps: (i) TEV protease was used to cleave the N-terminal 6x-His tag; and (ii) Anion exchange chromatography on a Mono Q 4.6/100 PE column (GE Healthcare) was used to separate the cleaved product from the TEV protease. Protein concentrations of all Swi6 construct samples were measured

by UV absorption at 280 nm and calculated using the experimentally determined extinction coefficient $\epsilon = 34,776 \text{ M}^{-1} \text{ cm}^{-1}$.

EDC/NHS Protein crosslinking

Samples were incubated for 2 hours at room temperature in a total volume of 20 mL with 2 mM EDC and 5 mM NHS. EDC and NHS chemistry specifically cross-links aspartate and glutamate residues to nearby lysine residues. Reactions were quenched by adding hydroxylamine to a final concentration of 10 mM, followed by SDS loading dye.

Mono- and Dinucleosome reconstitution

The mononucleosome 601 positioning sequence, containing a Pst1 site 18 bp in from the 5' end, was amplified by PCR and gel purified. The DNA fragment was assembled into mononucleosomes with recombinant *Xenopus laevis* histones by salt dialysis over 48-60 hrs (Luger et al., 1999). Reconstituted mononucleosomes were purified using a glycerol gradient. All histone octamer assemblies, nucleosome assemblies and nucleosome purifications were performed in the presence of 2 mM DTT to maintain the MLA modification.

Dinucleosome DNA templates were cloned into the pTNT vector using the Eag1 and Xho1 restriction sites. The plasmid was amplified in a dcm and dam methylation defective *E. coli* strain and the construct released by restriction enzyme digestion, then purified by native gel electrophoresis. Subsequent dinucleosome assembly steps are as described above.

Each 601 positioning sequence of the 12N arrays were separated by an EcoR1 restriction site. The array was cloned into a pCR-0Blunt backbone with EcoRV and Xho1 sites and the plasmid amplified in a *dcm* and *dam* methylation defective *E. coli* strain. The array was released by restriction digestion and purified from the digested backbone by Sephacryl S-1000 matrix gel filtration. After assembly, arrays were dialyzed into 10 mM Tris pH 8.0, 0.25 mM EDTA, 2 mM DTT and 50 mM KCl. Quality of assembly was assessed by EcoRI digestion.

Surface plasmon resonance

Matrix-free, flat, carboxymethylated gold surfaces (Sensor Chip C1, GE Healthcare) were preconditioned with five-minute pulses of 0.25% SDS and 50 mM NaOH at 25° C. Individual flow cells were prepared with the following protocol: (i) 50 μ l injection of 1-Ethyl-3-(3-dimethylaminopropyl)carbodiimide / N-hydroxysuccinimide (0.5M:0.2M); (ii) 30 μ L injection of 0.25 mg ml⁻¹ ImmunoPure Streptavidin (Thermo Scientific) in sodium acetate buffer (pH 5.0) to a total amount of 250RU for all four flow cells; (iii) 60 μ l injection of 1M ethanolamine. Nucleosomes were assembled on 147bp of 5'biotin tagged 601 sequence DNA and immobilized by injecting 2 μ l of 25nM H3Kc9me3 or H3K9 mononucleosomes onto active flow cells.

Prior to each SPR experiment, protein samples were dialyzed against 25 mM HEPES, 150 mM KCl, and 2 mM DTT. Following dialysis, Tween 20 detergent (Sigma-Aldrich) was added to the protein solution and the dialysis buffer to achieve a final concentration of 0.005% (v/v). In order to minimize refractive index differences between sample and buffer, the dialysis buffer was then used as the assay buffer for the SPR measurements.

Swi6 concentration was determined by absorbance at 280 nm. Dose response titrations were prepared by manual 0.6 fold serial dilutions of the highest concentration into assay buffer. Individual sample cycles consisted of a 30 second buffer injection followed by a 200 second sample injection at a flow rate of 20 $\mu\text{l min}^{-1}$.

Fluorescence polarization binding measurements

Peptide polarization assays were conducted in buffer containing 1 mg/ml BSA, 50 mM HEPES pH 7.5, 100 mM KCl and 10% glycerol. Peptide concentrations were held at 50-100 nM in a reaction containing variable amounts of Swi6 protein. The binding reaction was incubated 30 min at RT and fluorescence polarization was measured using a Molecular Devices HT Analyst ($\lambda_{\text{ex}}=480\text{nm}$, $\lambda_{\text{em}}=530\text{nm}$). The following binding model was used to derive $K_{1/2}$'s for peptide binding from the polarization data:

$$FP_{\text{obs}} = \frac{[\text{Swi6}]^n * FP_{\text{max}} + K_{1/2}^n * FP_{\text{min}}}{[\text{Swi6}]^n + K_{1/2}^n}$$

FP_{obs} was then converted to fraction bound (Fr. bound) with the following equation:

$$\text{Fr. bound} = \frac{FP_{\text{obs}} - FP_{\text{min}}}{FP_{\text{max}} - FP_{\text{min}}}$$

Fr. bound was then plotted versus [Swi6] to obtain the K_d using the following equation:

$$\text{Fr. bound} = \frac{[\text{Swi6}]^n}{[\text{Swi6}]^n + K_{1/2}^n}$$

where FP_{\min} is the polarization signal for the probe alone, FP_{\max} is the polarization signal at saturating $[\text{Swi6}]$ and n = Hill coefficient.

The DNA to assemble fluorescent nucleosomes was labeled on one end by amplifying the sequence using PCR with a primer (sequences available upon request) covalently linked to 6-carboxyfluorescein by a 6-carbon linker (IDT). Nucleosome polarization assays (Chin et al., 2004) were conducted in buffer containing 10% glycerol, 80 mM KCl, 20 mM HEPES buffer, 4 mM Tris, and 0.2 mM EDTA, pH 7.5. We predicted that binding by Swi6 to the H3 tail would cause local restriction of the fluorescein dye and increase fluorescence polarization. Consistent with this hypothesis, we observed an increase in fluorescence polarization with increasing concentrations of Swi6 (Figure 1d). Each anisotropy sample contained a final nucleosome concentration of 3 nM. Untagged Swi6 was serially diluted by 0.6-fold from a maximum concentration of 20 mM. Data points from three independent Swi6 dilution curves were averaged and standard errors calculated. Polarization was measured on an Analyst AD platereader (Molecular Devices).

Native gel mobility shift assay systems

Each 20 μL sample contained buffer with 20 mM HEPES pH 7.5, 4 mM Tris pH 7.5, 80 mM KCl, 0.1% Igepal CA-630, 0.2 mM EDTA, 2 mM DTT and 4-10% glycerol. Mononucleosome samples were incubated for 45 minutes at room temperature (1 hr for

dinucleosomes), then loaded on a 0.5X TBE 6% 29:1 acrylamide:bis-acrylamide gel (0.4X TBE 4% 37.5:1 acrylamide:bis-acrylamide for dinucleosomes) and run for 5 hours at room temperature at 75 V (3 hours for dinucleosomes). Array gel shift samples were loaded on 1X Tris-Acetate 1.15% agarose gels and separated for 4 hrs at 2.5 V/cm.

Binding curves were fit with the equation, fraction bound = $[Swi6]^n / ([Swi6]^n + K_{1/2}^n)$. A description of the $K_{1/2}$ value can be found in (Ackers et al., 1982).

Isothermal titration calorimetry

Experiments for both WT and L315D Swi6 were performed in 25 mM sodium phosphate pH 7.5, 100 mM KCl at 15°C. Data were analyzed with the Microcal Origin software using a monomer-dimer model. The final dilution point, 17nM, in the experiment shown in Figure 2b (left panel) is near the recommended dilution limit for the instrument used. While this concentration is close to the recommended lower concentration limit for the calorimeter, it has been shown previously that heat release from homo-oligomer dissociations can be robustly monitored in this low concentration regime for interactions of K_d s >100nM (Luke et al., 2005). Therefore, we believe that the lack of any measureable heat release for WT Swi6 CSD in the 17-100nM range suggests that the K_d for CSD self-association is below 17nM, extending previous estimates (Brasher et al., 2000).

Size-exclusion chromatography coupled to multi-angle light scattering (SEC-MALS/UV/RI)

The SEC-MALS/UV/RI (Arakawa, 2001; Wyatt, 1993) system was equilibrated in 25 mM HEPES or sodium phosphate, pH 7.5 and 100 mM KCl at a flow rate of 0.35 ml/min. Molar mass determination was performed using the ASTRA software. Cross-linked sample reactions were quenched and diluted to 100 mL, and the buffer exchanged to the SEC-MALS buffer using MicroSpin S-400 HR Columns X 25 (Amersham Biosciences) before injection onto the SEC-MALS system. Fractions of crosslinked Swi6 eluting from the SEC-MALS/UV/RI system were denatured and separated on 4-12% NuPAGE gradient gels (Invitrogen). Gels were stained with Sypro red and visualized on a Typhoon scanner.

Sedimentation Velocity Analytical Ultracentrifugation

H3Kc9me3 mononucleosomes and Swi6 proteins were individually dialyzed into 25 mM Tris 7.5, 80 mM KCl, 10% glycerol, and 2 mM DTT. Mononucleosomes were quantified by ethidium bromide staining and Swi6 proteins by UV absorption at 280 nm. The samples were prepared in 400 ml with an overall final OD of approximately 1 at 260 nm. Samples were incubated for 45 minutes at 24°C, then placed in an AUC chamber pre-equilibrated at 24°C and kept at zero-rpm at 24°C for 1 hour under vacuum. Runs were performed at 24°C at a rotor speed of 36K rpm for 4 hours. Scans were collected at 260 nm, with a radial step size of 0.003 cm and continuous scanning mode at approximately one minute intervals.

Western blotting

Strains were grown to log phase (OD 0.5), washed in 1XTBS, and total proteins extracted under denaturing conditions (Knop et al., 1999). Aliquots representing 0.4 OD units were separated on a 4-12% NuPAGE gradient gel (Invitrogen), blotted onto PVDF membranes and probed with monoclonal anti- α -tubulin (Sigma) or polyclonal anti-Swi6 antisera (Nakayama et al., 2000), and fluorescent secondary antibodies. Blots were scanned and quantified on a LiCor Odyssey scanner.

Chromatin immunoprecipitation (ChIP)

Strain growth and chromatin immunoprecipitation was performed as previously described (Rougemaille et al., 2008), with some modifications. Cell lysis was performed in 5 beat-beating cycles and Lysis buffer was supplemented with 1 mM PMSF, 3 mg/ml leupeptin, 2 mg/ml aprotinin and 1 mg/ml pepstatin. Chromatin fractions were purified and sonicated as described (Rougemaille et al). The lysate was brought up to 1.3 ml in extraction buffer and 0.1 ml set aside as the input fraction. The rest of the lysate was agitated on a nutator overnight at 4°C with either 1.4 ml anti-H3K9me2 antibody (Abcam ab1220) or 2 ml anti-Swi6 polyclonal antisera (Nakayama et al., 2000). 30 ml of a 50% slurry of protein A-coated magnetic beads (DynaL-Invitrogen) equilibrated in Lysis buffer was added to the lysate and incubated on a nutator for 90 min at 4°C. Beads were washed 2x 5 min in Lysis buffer, 2x 5 min in High Salt Lysis buffer, 2x 2.5 min in Wash Buffer and 1x 5 min in TE (buffers as in (Rougemaille et al., 2008)). DNA was eluted and de-crosslinked as described (Rougemaille et al., 2008). DNA eluates were

quantified by RT-qPCR using Dynazyme II DNA polymerase (Finnzymes). Primers available upon request.

As normalization controls for ChIP experiment containing the silencing cassette with Fr A, we used a Fr A⁻ control that contains all the features of the insertion cassette shown in Figure 7a, including the NatR marker, and only lacks the centromeric insert (Fr A). This ensures that in the comparison between strains, the only genomic difference is the presence or absence of Fr A.

DNA-nucleosome competition assay

In this assay, binding of Swi6 by nucleosomes reduces the fraction of DNA bound by Swi6 and results in a decrease in fluorescence polarization. Measurement of the decrease in fluorescence polarization as a function of nucleosome concentration is used to obtain a dissociation constant for nucleosome binding. An 80 bp DNA fragment was amplified from a plasmid containing the 601 positioning site with the Pst18 site using forward and reverse primers both 5' labeled with 5,6 carboxy-fluorescein (F80F). The K_d and B_{max} (maximal polarization value at saturation) for the F80F interaction with Swi6 were determined by fluorescence polarization assays as described above. The F80F probe was incubated with Swi6 in 25 mM HEPES pH 7.5, 100 mM KCl, 10% glycerol and 0.1 mg/ml BSA, with [F80F] = 10 nM and [Swi6] = 190 nM. This regime results in ~ 3.5% of the maximal polarization signal for the F80F-Swi6 interaction and is at ~ $K_{1/2}$ as assayed by gel shift. Duplicate, 2-fold dilutions of unmodified or H3Kc9me3 core nucleosomes were titrated into the F80F-Swi6 reactions and incubated 45 min at RT.

Fluorescence polarization was measured as above. The K_i for unmodified or H3Kc9me3 nucleosomes was determined by fitting the data to the following equation:

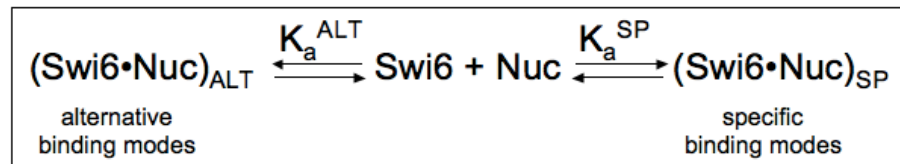
$$FP_{obs} = \frac{K_i^{NUC} (FP_{max} + [Swi6]) + FP_{min} K_d^{DNA} [nuc]_t}{K_i^{NUC} (K_d^{DNA} + [Swi6]) + K_d^{DNA} [nuc]_t}$$

where FP_{max} is the FP value for Swi6-F80F binding at saturating Swi6, FP_{min} is the FP value for F80F alone; K_i^{NUC} is the K_i for H3Kc9me3 or H3K9 nucleosomes and K_d^{DNA} is the K_d for the F80F-Swi6 interaction.

Supplementary discussion

Estimation of the fraction of Swi6 molecules bound in H3K9 recognizing orientations

We have used the simple model depicted below to estimate the proportions of Swi6 molecules bound in orientations that recognize the H3K9 residue (specific) vs. orientations that do not recognize the H3K9 residue (alternative).



We make the following initial simplifying assumptions:

- (i) Swi6 binds with the same molecularity in the specific and alternative orientations.
- (ii) Binding in the specific and alternative orientations is mutually exclusive.
- (iii) The alternative orientations are the same in the context of H3K9 and H3Kc9me3 nucleosomes.

We can then describe the observed association constant for binding in the context of H3Kc9me3 nucleosomes, $K_a^{\text{obs(M)}}$ as follows:

$$K_a^{\text{obs(M)}} = K_a^{\text{SP(M)}} + K_a^{\text{ALT}} \quad (1)$$

Where $K_a^{\text{SP(M)}}$ is the association constant for binding in the specific mode for the H3Kc9me3 nucleosomes and K_a^{ALT} is the sum of all association constants for binding in the different alternative modes.

The observed association constant for binding to H3K9 nucleosomes, $K_a^{\text{obs(U)}}$ is:

$$K_a^{\text{obs(U)}} = K_a^{\text{SP(U)}} + K_a^{\text{ALT}} \quad (2)$$

Where $K_a^{\text{SP(U)}}$ is the association constant for binding in the specific mode for the H3K9 nucleosomes.

We then make the further assumption that the methyl mark contributes the same amount of free energy when bound by Swi6 on the H3 tail peptide and when bound by Swi6 in the specific orientation on the nucleosome. Mathematically, this can be expressed by the equation:

$$K_a^{\text{SP(M)}} / K_a^{\text{SP(U)}} = \text{the specificity of binding to H3 tail peptides}$$

Using the above formalisms and our experimental measurements, we obtain the following:

$$K_a^{\text{SP(M)}} / K_a^{\text{SP(U)}} = 130 \quad (3)$$

The observed specificity on nucleosomes is obtained from the reciprocal ratio of $K_{1/2}$ values, which represent aggregate dissociation constants, to give:

$$K_a^{\text{obs(M)}} / K_a^{\text{obs(U)}} = 4.6 \quad (4)$$

Using eq. 3, we obtain:

$$K_a^{\text{SP(M)}} = 130K_a^{\text{SP(U)}} \quad (5)$$

Using eq. 5 in eq. 1 and eq. 2 we obtain the following from eq. 4:

$$(130K_a^{SP(U)} + K_a^{ALT}) / (K_a^{SP(U)} + K_a^{ALT}) = 4.6$$

Simplifying, $K_a^{SP(U)} = 0.03 K_a^{ALT}$

From eq. 5: $K_a^{SP(M)} = 130 \times 0.03 K_a^{ALT} = 3.9 K_a^{ALT}$

Using these relationships between the specific and alternative mode association constants, we can then derive the fraction of molecules that are bound in the specific mode.

The fraction of molecules bound in the specific modes for H3K9 nucleosomes is:

$$Fr(sp)^U = K_a^{SP(U)} / (K_a^{SP(U)} + K_a^{ALT}) = 0.03 / (0.03 + 1) = 0.03, \text{ or } \mathbf{3\%}$$

The fraction of molecules bound in the specific modes for H3Kc9me3 nucleosomes is:

$$Fr(sp)^M = K_a^{SP(M)} / (K_a^{SP(M)} + K_a^{ALT}) = 3.9 / (3.9 + 1) = 0.8, \text{ or } \mathbf{80\%}$$

Detailed description of model for the role of CD-CD interactions and the effects of altering flanking DNA

We hypothesize that Swi6 oligomerization mediated by CSD-CSD and CD-CD interactions promotes recognition of the H3K9 methyl mark in three ways (Figure 6f): (i) it correctly orients Swi6 on a nucleosome to recognize the H3K9 residues as implied by our results with mononucleosomes, (ii) it further promotes the H3K9 specific orientations via bridging interactions with nearby nucleosomes and (iii) it sterically and energetically disfavors binding in alternative orientations, which include binding to linker DNA. The above formulation allows a better understanding the origin of the observed specificity decrease concomitant with increased flanking DNA. Increasing flanking DNA in the context of the arrays is expected to: (i) reduce the ability of Swi6 CDs to bridge nearby nucleosomes and (ii) increase non-specific orientations by increasing available free DNA sites. In contrast, decreasing flanking DNA in the context of a mononucleosome substrate will only result in a decrease in non-specific orientations without affecting bridging, as there are no adjacent nucleosomes. The model thus predicts that increasing flanking DNA in the context of arrays will cause a greater reduction in specificity than in the context of mononucleosomes. Consistent with this prediction, we observe that Swi6 displays ~5-fold decreased specificity when the 15 bp linker DNA in arrays is increased to 47 bp (Figure 5c&d), but only a ~1.5-fold reduction in specificity when the linker DNA in mononucleosomes is increased from zero or 10 bp on either side to 20 bp on either side (Figures 3c & S3d).

Supplementary Information References

Ackers, G.K., Johnson, A.D., and Shea, M.A. (1982). Quantitative model for gene regulation by lambda phage repressor. *Proc Natl Acad Sci U S A* 79, 1129-1133.

Arakawa, T., Wen J. (2001). Size-exclusion chromatography with on-line light scattering. In *Current Protocols in Protein Science* (Hoboken, NJ, John Wiley and Sons, Inc.), pp. 1-21.

Brasher, S.V., Smith, B.O., Fogh, R.H., Nietlispach, D., Thiru, A., Nielsen, P.R., Broadhurst, R.W., Ball, L.J., Murzina, N.V., and Laue, E.D. (2000). The structure of mouse HP1 suggests a unique mode of single peptide recognition by the shadow chromosome domain dimer. *Embo Journal* 19, 1587-1597.

Chin, J., Langst, G., Becker, P.B., and Widom, J. (2004). Fluorescence anisotropy assays for analysis of ISWI-DNA and ISWI-nucleosome interactions. In *Chromatin and Chromatin Remodeling Enzymes, Pt B* (San Diego, Academic Press Inc), pp. 3-16.

Knop, M., Siegers, K., Pereira, G., Zachariae, W., Winsor, B., Nasmyth, K., and Schiebel, E. (1999). Epitope tagging of yeast genes using a PCR-based strategy: More tags and improved practical routines. *Yeast* 15, 963-972.

Luger, K., Rechsteiner, T.J., and Richmond, T.J. (1999). Preparation of nucleosome core particle from recombinant histones. In *Chromatin* (San Diego, Academic Press Inc), pp. 3-19.

Luke, K., Apiyo, D., and Wittung-Stafshede, P. (2005). Dissecting homo-heptamer thermodynamics by isothermal titration calorimetry: Entropy-driven assembly of co-chaperonin protein 10. *Biophysical Journal* 89, 3332-3336.

Nakayama, J., Klar, A.J., and Grewal, S.I. (2000). A chromodomain protein, Swi6, performs imprinting functions in fission yeast during mitosis and meiosis. *Cell* 101, 307-317.

Rougemaille, M., Shankar, S., Braun, S., Rowley, M., and Madhani, H.D. (2008). Ers1, a rapidly diverging protein essential for RNA interference-dependent heterochromatic silencing in *Schizosaccharomyces pombe*. *J Biol Chem* 283, 25770-25773.

Wyatt, P.J. (1993). LIGHT-SCATTERING AND THE ABSOLUTE CHARACTERIZATION OF MACROMOLECULES. *Analytica Chimica Acta* 272, 1-40.

Chapter 3:

A conformational switch in HP1 allows conditional activation and
drives heterochromatin assembly in vivo

A conformational switch in HP1 allows conditional activation and drives heterochromatin assembly in vivo

Daniele Canzio^{1,2}, Maofu Liao¹, Nariman Naber¹, Ed Pate³, Adam Larson^{1,4}, Shenping Wu¹, Diana B. Marina^{1,4}, Jennifer F. Garcia^{1,4}, Hiten D. Madhani¹, Roger Cooke¹, Peter Schuck⁵, Yifan Cheng¹, Geeta J. Narlikar^{1,*}

¹ *Department of Biochemistry and Biophysics, University of California San Francisco, 94158, USA.*

² *Chemistry and Chemical Biology Graduate Program University of California San Francisco, 94158, USA.* ³ *Voiland School of Chemical Engineering and Bioengineering, Washington State University, Pullman, WA, 99164 USA.* ⁴ *Tetrad Graduate Program University of California San Francisco, 94158, USA.* ⁵ *National Institute of Biomedical Imaging and Bioengineering, National Institute of Health, Bethesda, MD, 20892, USA.*

*To whom correspondence should be addressed: geeta.narlikar@ucsf.edu

Summary

HP1 proteins play a central role in the assembly and spread of H3K9-methylated heterochromatin, a structure critical for diverse nuclear processes ranging from gene silencing to chromosome segregation. How HP1 proteins assemble on their methylated nucleosomal templates and how the resulting HP1-nucleosome complex is regulated are poorly understood. We show that binding of the major *S. pombe* HP1 protein, Swi6, to methylated nucleosomes drives a switch from an auto-inhibited state to a spreading competent state. In the auto-inhibited state, a histone mimic sequence in one Swi6 monomer blocks methyl mark recognition by the chromodomain of another monomer. Auto-inhibition is relieved by recognition of two template features, the H3K9 methyl mark and nucleosomal DNA. Cryo-EM based reconstruction of the Swi6-nucleosome complex provides the overall architecture of the spreading-competent state in which two unbound chromodomain sticky ends appear exposed. Disruption of the switch between the auto-inhibited and spreading competent state disrupts heterochromatin assembly and gene silencing *in vivo*. These findings are reminiscent of other conditionally activated polymerization processes, such as actin nucleation, and open up a new class of regulatory mechanisms that operate on chromatin *in vivo*.

Introduction

Selective and heritable silencing of large chromosomal domains is achieved through the formation of heterochromatin. The most conserved form of heterochromatin, from yeast to humans, is characterized by methylation of lysine 9 on histone H3 (H3K9me3)¹⁻⁶. A hallmark of H3K9me3 heterochromatin is its ability to spread to adjacent genomic regions⁷⁻⁹. Central to the spreading process are the HP1 proteins, which specifically bind to H3K9 methylated chromatin, oligomerize, and form a platform that recruits diverse regulatory factors^{1,7-14}. In addition to gene silencing, the HP1-chromatin platform is important for other fundamental processes such as centromere formation, repression of recombination, sister chromatid cohesion, and maintenance of telomere stability^{6,15-17}. Consistent with the multiple roles of HP1 proteins, different populations of HP1 molecules have been described *in vivo* based on distinct on- and off-rates from chromatin^{18,19}. Yet the molecular basis for how methylated chromatin templates the assembly of HP1 and how the HP1-chromatin platform achieves its functional versatility remain poorly understood.

Some clues to the versatility of HP1 function can be found in the biochemical properties of its individual domains. HP1 has two structured domains, a chromodomain (CD) and an evolutionarily related chromoshadow (CSD) domain, connected by an unstructured hinge region (H) (Fig. 1a). The CD recognizes the H3K9me3 mark^{10,20,21}, while the CSD domain is involved in homodimerization of HP1 proteins²²⁻²⁴ and in reading PxVxL peptide motifs and other sequences present in different protein partners^{25,26}. The hinge region is implicated in sequence-independent RNA and DNA

binding²⁷⁻²⁹. It can therefore be imagined that, depending on the specific ligands of these domains, the HP1-chromatin platform can recruit different regulatory factors. But how the different HP1 domains work together to create a regulatable HP1-chromatin complex is not known.

Here, we use an *in vitro* reconstitution system to thermodynamically and structurally characterize the assembly of the major *S. pombe* HP1 protein, Swi6³⁰, on methylated nucleosomes. We find that unbound Swi6 dimers exist in an auto-inhibited state that simultaneously blocks H3K9 methyl mark recognition and higher-order oligomerization. Binding to methylated nucleosomes via the CD and CSD pays the energetic cost for switching Swi6 dimers to a spreading competent state. This thermodynamic linkage uncovers a new strategy by which the nucleosomal template controls HP1 oligomerization. The specific mechanism of switching between different HP1 conformational states also provides a basic starting point for understanding how HP1 molecules can switch between alternative functions.

Regulation of Swi6 self-association by the histone H3 tail

It is hypothesized that the ability of heterochromatin to spread relies on the ability of HP1 proteins to self-associate^{31,32}. In such a model, limiting the self-association of HP1 proteins to chromatin would be crucial to prevent non-functional aggregates. To better understand how Swi6 self-association is regulated by chromatin, we first characterized the individual oligomerization equilibria in the absence of nucleosomes. Previous work has characterized at least three types of Swi6 oligomeric states: a monomer, a dimer

mediated by CSD-CSD interactions, and higher-order oligomers mediated by CD-CD interactions between dimers^{22,24,27,33,34}. To measure and isolate the equilibrium constants for these oligomeric transitions we chose to use Analytical Ultracentrifugation (AUC) based approaches. Recent advances have enabled global analysis of Sedimentation Equilibrium (SE) and Sedimentation Velocity (SV) AUC data, allowing both thermodynamic and hydrodynamic properties of proteins to be included in the overall analysis^{35,36}.

Our analysis of the AUC data best describes the system as a two-step self-association process: first, a tight association of two Swi6 monomers with an affinity constant, K_{obs}^{dim} , ($1/K_{obs}^{dim} < 1\text{nM}$, at 8°C), followed by a rapidly reversible progressive self-association of Swi6 dimers with an identical chain elongation affinity constant, K_{obs}^{iso} , ($1/K_{obs}^{iso} \sim 70\mu\text{M}$, at 8°C) (Fig. 1b, c, d and Supplementary Fig. 1, 2 and 3). This process, also known as isodesmic self-association, is analogous to the self-association process of tubulin dimers during the formation of the first ring^{37,38}.

We next tested if the most distinguishing feature of the chromatin template, the H3K9 methyl mark, directly regulates Swi6 oligomerization. Specifically, we asked if occupancy of the CD by the methylated H3 tail alone increased oligomerization. We used SV AUC and followed the change in the overall weighted average sedimentation coefficient (s_w) as a function of H3K9me3 peptide concentration (Fig. 1e). The experiment was performed at a concentration of Swi6 at which Swi6 is mainly dimeric but also exhibits some higher-order oligomeric states. Any increase in oligomerization

can thus be detected by an increase in the value of s_w . In contrast to our simplest expectation, addition of the methylated peptide reduced the value of s_w , implying that Swi6 self-association is inhibited by the methylated H3 tail peptide. The s_w -value decreased to a value that is similar to the sedimentation coefficient of a Swi6 dimer (Fig. 1e). The effect was specific for the methyl mark, as an unmethylated peptide had a negligible effect at comparable concentrations.

An H3-tail mimic in the chromodomain of Swi6 inhibits binding of the H3K9me3 mark

The above result suggested that the methylated H3-tail peptide and the CD-CD interface may compete for the same site. In exploring the sequence of the Swi6 protein, we noticed that the CD contains a sequence (ARK₉₄GGG) on a loop that resembles the amino acid sequence of the H3-tail surrounding the K9 position (ARK₉STG) (Fig. 1f). Interestingly, the histone mimic sequence in Swi6 degenerates in higher organisms, but the corresponding lysine and proximal glycine are conserved (Fig. 1g, top panel). Further, in human HP1 isoforms the corresponding lysine is known to be subject to post-translation modifications found on H3K9 such as monomethylation and acetylation³⁹. We therefore hypothesized that the ARK loop from the CD of one Swi6 could occupy the H3K9 binding site in another CD and thereby mediate CD-CD self-association in solution (Fig. 1g, bottom panel). This model explains why addition of the H3-tail peptide disrupts higher-order Swi6 oligomerization. Such a mechanism is also consistent with recent interesting observations that the HP1 CD can bind ARK-containing motifs present in histone H1 and G9a proteins^{40,41}.

To test this model, we replaced the R93 and the K94 residues with alanines (Swi6^{LoopX}, Fig. 2a, Supplementary Table 1) and asked if these mutations destabilized higher order oligomerization. As predicted by the model, the Swi6^{LoopX} mutant showed a small but reproducible decrease in the isodesmic affinity constant (K_{obs}^{iso}) compared to Swi6, also referred to as Swi6^{WT} (Fig. 2b and Supplementary Fig 4, 3-fold). Interestingly, we noticed a substantially larger reduction in the association constant for dimerization (K_{obs}^{dim}) (Fig. 2c and Supplementary Fig 4, 14-fold). The dimerization constant of the Swi6^{LoopX} mutant was comparable to the dimerization constant for the Swi6^{ΔNCD} mutant (Supplementary Fig 4), which lacks both the N- and CD domains (Fig. 1a, Supplementary Table 1). This result suggested that, in addition to the previously identified CSD-CSD interface, the ARK loop-CD interaction also participates in stabilizing a Swi6 dimer.

Based on the above thermodynamic characterization we propose that a Swi6 dimer can exist in at least two states: a closed state in which the ARK loop engages the CD of its partner Swi6 and an open state in which the ARK loop-CD interaction is broken (Fig. 2d). Self-association of dimers will then consist of at least two steps: (1) a conformational step between closed and open states (K^{conf}) and (2) a self-association step between dimers in the open state (K^{oligo}). The two-step process implies that in Swi6^{WT} the magnitude of the measured isodesmic association step (K_{obs}^{iso}) is a product of K^{conf} and K^{oligo} (Fig. 2d). This model explains the smaller observed effect of the loop

mutations on oligomerization versus dimerization. The loop mutations destabilize the closed state and drive the equilibrium towards the open state of Swi6, increasing the population of dimers that is capable of oligomerizing (Fig. 2d, $K_{obs}^{iso} \sim K^{oligo}$ for Swi6^{LoopX}). The effect on dimerization thus masks the destabilizing effect of the loop mutations on the actual oligomerization step (K^{oligo}) (Fig. 2d).

The above model predicts that the ARK loop-CD interaction is mutually exclusive with H3 tail binding. To test this prediction we determined if weakening the ARK loop-CD interaction via the Swi6^{LoopX} mutant increases binding of a methylated tail peptide. We find that Swi6^{LoopX} binds tail peptides ~6-fold more strongly than Swi6^{WT} (Fig 2e). Consistent with the model we further find that Swi6 dimerization is weakened in the presence of saturating methylated H3 tail peptide (Supplementary Fig. 4).

We next investigated the extent of similarity between the ARK loop-CD interaction and the H3-CD interaction using two additional mutants in Swi6 that are predicted to disrupt binding of the H3K9me3 peptide. The first mutant is Swi6^{CageX}, in which an aromatic cage residue previously shown to be important for H3K9me3 binding²⁰ is mutated to alanine (Fig. 2a). The second mutant is Swi6^{AcidicX}, in which an acidic stretch N-terminal to the first aromatic cage residue of the CD, is mutated to alanines (Fig. 1g and 2a)⁴². In human HP1 α , two of the glutamates in this stretch are replaced with serines (Fig. 1g) and phosphorylation of the serines increases binding to H3K9me3

peptides⁴³. We hypothesized that analogous to the phosphorylated serines in HP1 α , the acidic residues in Swi6 may stabilize H3 tail binding. Both these mutants reduce binding to H3K9me3 peptides (Fig. 2e). In addition these mutants also have destabilizing effects on Swi6 oligomerization and dimerization (Figs. 2b and c, Supplementary Fig 4), suggesting that similar interactions are involved in the H3-CD and ARK loop-CD interfaces. Deleting the N-terminus and six of the acidic residues has similar effects as the AcidicX mutant (Supplementary Fig. 4).

Impact of Swi6 mutations and H3 tail binding on the local mobility of the ARK loop

The model in Fig. 2d predicts that disruption of the loop-CD interface or binding of the H3K9me3 tail will make the loop more mobile (Fig 3a). To test these predictions we used Electron Paramagnetic Resonance (EPR) spectroscopy. Selective labeling of the loop with a spin probe allows us to directly follow changes in its mobility, as these are expected to result in well-defined changes in the EPR spectrum of the spin probe⁴⁴. To achieve site-specific labeling of the ARK loop, we generated a cys-free version of Swi6, in which all three native cysteines (two in the CD and one in the CSD, C121, C124, C310) were mutated to serines (Swi6^{3S}, Supplementary Table 1). We then mutated the G95 residue on the loop to a cysteine and covalently modified it with a maleimide spin probe (Swi6^{probe}, Supplementary Table 1). Mutating the conserved native cysteines had destabilizing effects on the oligomeric properties of Swi6, H3 peptide binding, and nucleosome binding (Supplementary Fig. 5). However, the mutants still showed

significant discrimination for the H3K9 methyl mark in H3 tail peptides and nucleosomes (Supplementary Fig. 5).

To stabilize the mutant proteins, the EPR spectra were collected at 4°C. Two spectral components were observed for Swi6^{probe-WT}, one with higher mobility and a second one with reduced mobility. Deconvolution of the two components allowed determination of the fraction of probes that are immobilized. In parallel, AUC experiments reported on the oligomeric state of the protein. We found that the Swi6^{probe-WT} protein was dimeric under our experimental conditions and ~35% of the probes were immobile (Fig. 3b). We then measured the EPR spectra of three mutants that are expected to reduce the ability of the loop from one monomer to interact with the CD of the other monomer. Two of the mutants Swi6^{probe-LoopX} and Swi6^{probe-AcidicX} disrupt the loop-CD interaction as described above (Fig 2b and c, Supplementary Table 1). The third mutant Swi6^{probe-DimerX} (L315D, Supplementary Table 1) disrupts CSD-CSD dimerization and increases the population of monomeric Swi6^{23,34}. We confirmed that the Swi6^{probe-LoopX} and Swi6^{probe-AcidicX} proteins are dimeric while the Swi6^{probe-DimerX} protein is mainly monomeric under the EPR experimental conditions (Fig. 3b, left panel). Compared to Swi6^{probe-WT}, the fraction of immobile probes decreased in all the mutants (Fig. 3b, right panel). Similar results were seen with another construct in which the probe is positioned on the K94 residue, instead of on G95 (Supplementary Fig. 5).

We next asked whether binding of an H3K9me3 tail peptide affects loop mobility in the Swi6^{probe-WT} protein (Fig. 3c). As predicted by the model (Fig 2d and 3a), we observed that addition of the H3K9me3 peptide decreased the fraction of immobile probes. The H3K9me3 peptide was ~100-fold better at decreasing the immobile probe fraction compared to an H3K9 peptide and compared to an H3K4me3 peptide, indicating that the effect was specific for the H3K9 methyl mark (Fig. 3c). Again, similar results were seen with the probe positioned on the K94 residue (Supplementary Fig. 5). These EPR data provided structural evidence to correlate the increased mobility of the ARK loop with occupancy of the CD by the methylated H3 tail.

Structural analysis of Swi6 and the Swi6-nucleosome complex

The above results provide evidence for two different conformational states of the ARK loop that are regulated through interactions with the CD. Since the ARK loop-CD interaction would bring two CDs in a dimer in close proximity (Fig. 2d), we hypothesized that the two states may be accompanied by global conformational changes. To investigate such conformational changes, we used negative stain Electron Microscopy (EM). The relatively small size of a Swi6 dimer (~74KDa) makes visualization difficult. To increase the overall mass of the dimer and identify the N-terminus of Swi6 in the EM structures, we first fused a CFP molecule to the N-terminus of Swi6 (total mass ~130KDa) (Fig. 4a and Supplemental Fig. 6). The CFP-Swi6 construct showed an extended conformation (Fig. 4a). We reasoned that the CFP-tag may be disrupting the ARK loop-CD interaction due to its proximity to the CD. If this is the case, we expected CFP-Swi6 to be a weaker dimer than Swi6^{WT} due to the absence

of the ARK-CD interaction. Indeed we find that CFP-Swi6 is a ~10-fold weaker dimer than Swi6^{WT} (Supplementary Fig. 6 and Fig. 2c). To further test our reasoning we moved the CFP tag to the C-terminus of Swi6 (Fig. 4b). This Swi6-CFP construct had a similar dimerization constant as Swi6^{WT}, consistent with having an intact ARK loop-CD interaction (Supplementary Fig. 6). Further, Swi6-CFP showed a more condensed overall structure compared to CFP-Swi6 and a lower sedimentation coefficient than CFP-Swi6 (Fig. 4b and Supplemental Fig. 6).

The above results raised the possibility that the extended conformation seen with the CFP-Swi6 construct may reflect the open state (Fig. 2d), that is capable of binding methylated nucleosomes. To test this possibility we directly visualized the conformation of Swi6 bound to a methylated nucleosome using cryo-electron microscopy (cryo-EM) (Fig. 4c). We used methyl lysine analog (MLA) technology to obtain homogeneously methylated nucleosomes (H3K_c9me3 nucleosomes)⁴⁵. We used SV AUC to ensure that the conditions used for EM resulted in Swi6-H3K_c9me3 nucleosome complexes with a homogenous stoichiometry of two Swi6 dimers per nucleosome³⁴. For comparison we also visualized nucleosomes alone (Fig. 4c). For the nucleosome alone structure, a total of 13629 particles were collected and further classified into 100 two-dimensional (2D) class averages (Supplementary Fig. 7). A total of 5000 particles were collected for the Swi6-nucleosome complex, which were classified into 200 2D class averages (Supplementary Fig. 7). A three-dimensional (3D) reconstruction for both was calculated using the nucleosome structure as an initial model to an overall resolution of

~15Å and ~25Å for the nucleosome and the Swi6-nucleosome complex, respectively (Fig. 4c, Supplementary Fig. 7 and Methods).

For the Swi6-nucleosome reconstruction we used our previous biochemical knowledge to guide the structural analysis. We have previously shown that the complex of Swi6 with an H3K9 methylated nucleosome contains two Swi6 dimers³⁴. Given the pseudo-two fold symmetry in the positions of the H3 tails, the simplest model posits that the Swi6 dimers also bind in a pseudo-symmetric manner with one dimer on either side of the nucleosome. Indeed in some of the 2-D class averages we observe density on either side of the nucleosome consistent with the predictions of the biochemical analysis (Supplementary Figure 7). We therefore applied 2-fold symmetry to obtain the 3D reconstruction (see also Supplementary Methods for more details).

Given the 25Å resolution of the Swi6-nucleosome complex, it is difficult to make direct conclusions from the reconstruction about the detailed conformations of Swi6 dimers bound to the nucleosome. We therefore further analyzed the difference density between the complex and nucleosome alone (Fig. 4c). Such difference density is contributed by the bound Swi6 and possibly also by any changes of the nucleosome induced by such binding. While we cannot rule out the possibility that the conformation of the nucleosome may be altered upon Swi6 binding, the difference density has roughly the mass (~125kDa) of two Swi6 dimers (~150 kDa) as determined previously by AUC³⁴. We thus assume that the difference density is mainly contributed by the bound Swi6 dimers. The extended shape of the difference density is compatible with the shape of the

Swi6 dimer visualized in the negatively stained CFP-Swi6 dimer (Fig. 4a). Such similarity suggested a model for the arrangement of the domains of Swi6 and enabled us to manually place the known crystal structures of the CD and CSD into the difference density (Fig. 4d). The putative location of the CD suggests that one CD engages an H3 tail and one CD protrudes out in solution (Fig. 4d). This arrangement of the CDs is compatible with the sticky ends architecture proposed previously (Fig. 4e)³⁴. In addition, the putative location of the CSD raises the possibility that this domain also helps stabilize nucleosome binding (Fig. 4d). This possibility is directly tested in the next section.

Functional impact of the Swi6 conformational switch on nucleosome binding

The above thermodynamic and structural data suggests that recognition of the H3K9me3 mark requires switching from an auto-inhibited, closed conformation of Swi6 to an open conformation. To test this model in the context of a nucleosome we measured the impact of disrupting the loop-CD interaction on nucleosome binding (Figs. 5a and b). In contrast to the results with the H3 tail peptides (Fig. 2e), Swi6^{LoopX} binds methylated nucleosomes 10-fold more weakly than Swi6^{WT} even though it still discriminates in favor of the methyl mark (Fig. 5b). This result suggested that, when displaced from the CD, the ARK loop may help Swi6 make additional interactions with the nucleosome.

Given the positively charged nature of the ARK loop we tested if the ARK loop assists Swi6 in interacting with DNA. We found that Swi6^{WT} binds ~4-fold tighter than Swi6^{LoopX} to a 20 bp DNA (Fig. 5c). Further, the affinity constant of Swi6^{ΔNCD} for the

same DNA is similar to that of Swi6^{LoopX} (Fig. 5c), suggesting that the ARK loop adds to the DNA interactions made by the hinge region. If the ARK loop becomes available for enhancing DNA binding in the open state (Fig. 2d), then binding to DNA should be tighter when the CD is fully occupied by the H3K9me3 peptide. We find that binding of Swi6^{WT} to the 20mer DNA is ~4-fold tighter in the presence of saturating H3K9me3 peptide and this enhancement is not observed with the same concentration of unmethylated peptide (Fig. 5c).

Based on the above data, we propose the following model for the assembly of the minimal heterochromatin unit. Binding to methylated nucleosomes has two coupled effects: (i) release of ARK loops to help DNA binding and (ii) release of two CDs that can then bridge nearby nucleosomes (Fig. 5d). Our data cannot distinguish between a direct contact of the ARK loop with DNA versus an indirect effect of facilitating the binding of the N-terminal or hinge region to DNA. It is also possible that the ARK loop stabilizes a complex of the H3 tail with DNA as suggested previously for an H4 tail interacting CD⁴⁶. Swi6^{AcidicX}, which binds methylated H3 tail peptides more weakly than Swi6^{WT}, correspondingly binds H3K9 methylated nucleosomes ~7-fold more weakly than Swi6^{WT} (data not shown).

The EM reconstruction of the Swi6-nucleosome complex raised the possibility that the CSD dimer interacts with the nucleosome, consistent with previous suggestions⁴⁷⁻⁴⁹. To test the energetic contributions of the CSD dimer we compared the affinity of

Swi6^{WT} and Swi6^{DimerX} for nucleosomes. We find that Swi6^{DimerX} binds to H3K9me3 nucleosomes with 10-fold lower affinity than Swi6^{WT} and with similar affinity as Swi6^{LoopX} (Fig. 5b and Supplementary Fig. 8). Together our data suggest that the CD, the CSD-CSD dimer, and the ARK loop cooperate to stabilize the interaction of Swi6 with a nucleosome.

Revisiting the previous model

The new data allowed us to revisit some of our previously published results and their interpretation. In our previous work we had found that Swi6 bound to the nucleosome primarily as a tetramer³⁴. We had further identified a gain of function Swi6 mutant with two mutations in its CD, V82E and Y131W (Swi6^{EW}, Supplementary Table 1) that shows increased oligomerization in solution, increased specificity for methylated nucleosomes, and increased silencing *in vivo*³⁴. Based on these observations we proposed that the minimal Swi6-nucleosome unit has two key features³⁴: (i) two CDs, one from each Swi6 dimer, that interact with the two methylated H3 tails and additionally interact with each other and (ii) two CDs that are unoccupied (sticky ends) and serve to bridge adjacent nucleosomes.

Our cryo-EM data is compatible with the presence of the two CD sticky ends. At the same time, our new thermodynamic data suggest that CD-CD interactions are mutually exclusive with H3 tail binding. This result argues against our earlier proposal that the two CDs bound to the nucleosomal H3 tails interact with one another. How then

do we explain the previous results with the Swi6^{EW} mutant, which correlated greater CD-CD association *in vitro* with greater silencing *in vivo*?

Our new methods allowed us to revisit in more detail the biophysical origins of the gain of function effects of Swi6^{EW} (Fig. 5b and Supplementary Fig. 8). Consistent with previous results, we find that Swi6^{EW} shows 2-fold higher isodesmic self-association (K_{obs}^{iso}) compared to Swi6^{WT} (data not shown). However, the mutant also shows 2-fold weaker dimerization (K_{obs}^{dim}) compared to Swi6^{WT} (data not shown). This difference may reflect the different steric constraints placed on the ARK loop-CD interaction in the dimer vs. the oligomer (Figure 2d). The overall consequence is that Swi6^{EW} is less auto-inhibited and more bridging competent than Swi6^{WT}. Consistent with this interpretation, Swi6^{EW} binds ~3-fold more strongly to methylated nucleosomes and to H3K9me3 tail peptides compared to Swi6^{WT} even though in the context of the CD alone the same mutations do not affect binding of H3K9me3 tail peptides (data not shown).

The loop-CD interaction promotes heterochromatin assembly and gene silencing *in vivo*

The above analysis of Swi6^{EW} is consistent with the hypothesis that oligomerization of HP1 proteins is important for heterochromatin assembly and gene silencing *in vivo*^{31,32,34}. The data presented here implies that in Swi6 such oligomerization is mediated by the CD-loop interaction. To further test the impact of this

interaction *in vivo* we investigated the effects of disrupting the CD-loop interaction via the LoopX and AcidicX mutants. As these mutants concomitantly weaken oligomerization and nucleosome binding, we expected to observe loss-of-function effects *in vivo*. We constructed isogenic fission yeast strains in which these Swi6 mutants were introduced at the endogenous chromosomal location replacing the wild type gene. We then investigated whether the *swi6^{LoopX}* and *swi6^{AcidicX}* mutants affect silencing of a *ura4+* reporter gene inserted at the pericentromeric *imr* region (Fig. 6a, schematics)⁵⁰. We found that both mutants show defects in silencing (Fig. 6a). These effects are comparable to the *swi6+* deletion strain and are not due to a reduction of Swi6 protein level (Fig. 6b and Supplementary Fig. 9).

We next investigated the effects of these mutants on heterochromatin at the endogenous centromeric *dg* repeats. Previous work has shown that in the absence of the RNAi machinery, Swi6 is important for maintaining high levels of H3K9 methylation at the *dg* repeats⁵¹. It was shown, that, while deletion of RNAi components causes a small but reproducible decrease in H3K9 methylation, further deletion of *swi6* causes a much larger decrease in H3K9 methylation⁵¹. Interestingly, we find that the *loopX* and *acidicX* mutants also show large decreases in H3K9 methylation in the absence of the RNAi pathway (Fig 6c and Supplementary Fig. 9). Specifically, in a *dcr1Δ* background, the *swi6Δ* and the two mutants reduce methylation by greater than 50 fold, bringing the methylation level to near background.

All together, these data strongly imply that the loop-CD interaction identified in this study plays a central role in maintaining H3K9 methylated heterochromatin formation *in vivo*. Our results with the LoopX and AcidicX mutants are also consistent with previous work showing that mutations in these regions of Swi6 affect mitotic stability and mating type switching³³, both of which depend on the integrity of heterochromatin.

Conclusions and Implications

The conformational switch in Swi6 couples the assembly of Swi6 to recognition of specific features of the nucleosomal template such as H3K9 methylation and nucleosomal DNA. This coupling can ensure correct targeting to H3K9 methylated chromatin and help prevent aberrant spread of Swi6 in euchromatin. Interestingly, the same loop that stabilizes the auto-inhibited state of HP1 dimers, assists in binding nucleosomes when flipped into the open state. It is possible that these opposing roles of the ARK loop, which ensure that spreading is mutually exclusive with dimerization, provide a means for a more switch-like behavior of HP1 spreading.

The ability of Swi6 to exist in more than one discrete conformational state may allow it to interact with different regulators based on the specific nuclear process that it participates in. For example, factors that interact with the CSD-CSD interface through PxVxL-like motifs and other chromodomain containing factors that can interact with the ARK loop could alter the stability and structure of the Swi6-nucleosome platform (Fig. 6d). By this model, it is possible that anti-silencing proteins, like Epe1 in *S. pombe*⁵²⁻⁵⁴,

inhibit Swi6 spread by acting as a cap and stabilizing the auto-inhibited state of Swi6 on nucleosomes. In contrast, enhancers of silencing, like the SHREC complex in *S. pombe*^{14,55,56}, may stabilize the open conformation of Swi6 on the nucleosome. Recent studies imply that the ability of Swi6 to read the H3K9 methyl mark is incompatible with its ability to bind RNA transcripts generated as part of the RNAi silencing pathway⁵⁷. In this case, it is possible that RNA binding promotes the closed state of Swi6. Interestingly, the ARKGGG sequence is absent in the other *S. pombe* HP1 protein, Chp2, which is less abundant than Swi6, and this difference may explain some of the differences in the biological roles of the Chp2 and Swi6^{13,14,53}.

Post-translational modifications on the chromodomain loop could further regulate the different conformational states of HP1 proteins. In Swi6, the ARK loop stabilizes the auto-inhibited state even though the lysine is not methylated, presumably due to the high effective concentration of the ARK loop relative to its partner CD. However, the major human HP1 α isoform contains just the KG residues of the ARKGGG sequence found in Swi6 and, in this context, the lysine can be monomethylated *in vivo*³⁹. It is tempting to speculate that the methylation energetically compensates for the loss of the arginine residue while, at the same time, making the interaction more regulatable.

In summary, our thermodynamic, structural and genetic studies provide a molecular framework for understanding how HP1 proteins participate in diverse nuclear processes. Protein assemblies that are controlled by release of auto-inhibition have been

well-characterized in other cellular processes such as actin nucleation and protein tyrosine kinase activation⁵⁸⁻⁶¹. We anticipate that similarly sophisticated mechanisms govern the assembly, spread, and functions of HP1-mediated heterochromatin.

Methods

Methods are described in the Supplementary Information.

References

1. Eissenberg, J. C. & Elgin, S. C. The HP1 protein family: getting a grip on chromatin. *Current opinion in genetics & development* **10**, 204–10 (2000).
2. Lachner, M., O’Carroll, D., Rea, S., Mechtler, K. & Jenuwein, T. Methylation of histone H3 lysine 9 creates a binding site for HP1 proteins. *Nature* **410**, 116–20 (2001).
3. Peters, A. H. F. M. *et al.* Loss of the Suv39h Histone Methyltransferases Impairs Mammalian Heterochromatin and Genome Stability. *Cell* **107**, 323–337 (2001).
4. Nakayama, J., Rice, J. C., Strahl, B. D., Allis, C. D. & Grewal, S. I. Role of histone H3 lysine 9 methylation in epigenetic control of heterochromatin assembly. *Science (New York, NY)* **292**, 110–113 (2001).
5. Noma, K., Allis, C. D. & Grewal, S. I. Transitions in distinct histone H3 methylation patterns at the heterochromatin domain boundaries. *Science (New York, NY)* **293**, 1150–1155 (2001).
6. Grewal, S. I. S. & Jia, S. Heterochromatin revisited. *Nature reviews Genetics* **8**, 35–46 (2007).
7. Wallrath, L. L. & Elgin, S. C. Position effect variegation in *Drosophila* is associated with an altered chromatin structure. *Genes & development* **9**, 1263–77 (1995).
8. Hall, I. M. *et al.* Establishment and maintenance of a heterochromatin domain. *Science (New York, N.Y.)* **297**, 2232–7 (2002).
9. Danzer, J. R. & Wallrath, L. L. Mechanisms of HP1-mediated gene silencing in *Drosophila*. *Development (Cambridge, England)* **131**, 3571–80 (2004).
10. Bannister, A. J. *et al.* Selective recognition of methylated lysine 9 on histone H3 by the HP1 chromo domain. *Nature* **410**, 120–124 (2001).
11. Kellum, R. HP1 complexes and heterochromatin assembly. *Current topics in microbiology and immunology* **274**, 53–77 (2003).
12. Verschure, P. J. *et al.* In vivo HP1 targeting causes large-scale chromatin condensation and enhanced histone lysine methylation. *Molecular and cellular biology* **25**, 4552–4564 (2005).

13. Motamedi, M. R. *et al.* HP1 proteins form distinct complexes and mediate heterochromatic gene silencing by nonoverlapping mechanisms. *Molecular cell* **32**, 778–790 (2008).
14. Fischer, T. *et al.* Diverse roles of HP1 proteins in heterochromatin assembly and functions in fission yeast. *Proceedings of the National Academy of Sciences of the United States of America* **106**, 8998–9003 (2009).
15. Fanti, L. & Pimpinelli, S. HP1: a functionally multifaceted protein. *Current opinion in genetics & development* **18**, 169–174 (2008).
16. Vermaak, D. & Malik, H. S. Multiple roles for heterochromatin protein 1 genes in *Drosophila*. *Annual review of genetics* **43**, 467–92 (2009).
17. Zeng, W., Ball, A. R. & Yokomori, K. HP1: heterochromatin binding proteins working the genome. *Epigenetics : official journal of the DNA Methylation Society* **5**, 287–292 (2010).
18. Cheutin, T. *et al.* Maintenance of stable heterochromatin domains by dynamic HP1 binding. *Science (New York, NY)* **299**, 721–725 (2003).
19. Cheutin, T., Gorski, S. & May, K. In vivo dynamics of Swi6 in yeast: evidence for a stochastic model of heterochromatin. *Molecular and Cellular Biology* **24**, 3157–3167 (2004).
20. Jacobs, S. A. & Khorasanizadeh, S. Structure of HP1 chromodomain bound to a lysine 9-methylated histone H3 tail. *Science (New York, NY)* **295**, 2080–2083 (2002).
21. Nielsen, P. R. *et al.* Structure of the HP1 chromodomain bound to histone H3 methylated at lysine 9. *Nature* **416**, 103–7 (2002).
22. Yamada, T., Fukuda, R., Himeno, M. & Sugimoto, K. Functional domain structure of human heterochromatin protein HP1 (Hsalpha): involvement of internal DNA-binding and C-terminal self-association domains in the formation of discrete dots in interface nuclei. *Journal of Biochemistry*, **125**, 832–7 (1999).
23. Brasher, S. V *et al.* The structure of mouse HP1 suggests a unique mode of single peptide recognition by the shadow chromo domain dimer. *The EMBO journal* **19**, 1587–97 (2000).
24. Cowieson, N. P., Partridge, J. F., Allshire, R. C. & McLaughlin, P. J. Dimerisation of a chromo shadow domain and distinctions from the chromodomain as revealed by structural analysis. *Current biology : CB* **10**, 517–25 (2000).

25. Smothers, J. F. & Henikoff, S. The HP1 chromo shadow domain binds a consensus peptide pentamer. *Current biology* : *CB* **10**, 27–30 (2000).
26. Mendez, D. L. *et al.* The HP1a disordered C terminus and chromo shadow domain cooperate to select target peptide partners. *Chembiochem* : a *European journal of chemical biology* **12**, 1084–1096 (2011).
27. Zhao, T., Heyduk, T., Allis, C. D. & Eissenberg, J. C. Heterochromatin protein 1 binds to nucleosomes and DNA in vitro. *The Journal of biological chemistry* **275**, 28332–8 (2000).
28. Muchardt, C. *et al.* Coordinated methyl and RNA binding is required for heterochromatin localization of mammalian HP1alpha. *EMBO reports* **3**, 975–981 (2002).
29. Meehan, R. R., Kao, C.-F. & Pennings, S. HP1 binding to native chromatin in vitro is determined by the hinge region and not by the chromodomain. *The EMBO journal* **22**, 3164–74 (2003).
30. Nakayama, J., Klar, a J. & Grewal, S. I. A chromodomain protein, Swi6, performs imprinting functions in fission yeast during mitosis and meiosis. *Cell* **101**, 307–17 (2000).
31. Yamamoto, K. & Sonoda, M. Self-interaction of heterochromatin protein 1 is required for direct binding to histone methyltransferase, SUV39H1. *Biochemical and biophysical research communications* **301**, 287–292 (2003).
32. Hines, K. a *et al.* Domains of heterochromatin protein 1 required for *Drosophila melanogaster* heterochromatin spreading. *Genetics* **182**, 967–77 (2009).
33. Wang, G. *et al.* Conservation of heterochromatin protein 1 function. *Molecular and cellular biology* **20**, 6970–6983 (2000).
34. Canzio, D. *et al.* Chromodomain-Mediated Oligomerization of HP1 Suggests a Nucleosome-Bridging Mechanism for Heterochromatin Assembly. *Molecular cell* **41**, 67–81 (2011).
35. Schuck, P. On the analysis of protein self-association by sedimentation velocity analytical ultracentrifugation. *Analytical biochemistry* **320**, 104–124 (2003).
36. Vistica, J. *et al.* Sedimentation equilibrium analysis of protein interactions with global implicit mass conservation constraints and systematic noise decomposition. *Analytical biochemistry* **326**, 234–256 (2004).

37. FRIGON, R. P. & TIMASHEFF, S. N. MAGNESIUM-INDUCED SELF-ASSOCIATION OF CALF BRAIN TUBULIN .1. STOICHIOMETRY. *Biochemistry* **14**, 4559–4566 (1975).
38. FRIGON, R. P. & TIMASHEFF, S. N. MAGNESIUM-INDUCED SELF-ASSOCIATION OF CALF BRAIN TUBULIN .2. THERMODYNAMICS. *Biochemistry* **14**, 4567–4573 (1975).
39. LeRoy, G. *et al.* Heterochromatin protein 1 is extensively decorated with histone code-like post-translational modifications. *Molecular & cellular proteomics : MCP* **8**, 2432–2442 (2009).
40. Sampath, S. C. *et al.* Methylation of a histone mimic within the histone methyltransferase G9a regulates protein complex assembly. *Molecular cell* **27**, 596–608 (2007).
41. Ruan, J. *et al.* Structural basis of the chromodomain of Cbx3 bound to methylated peptides from histone h1 and G9a. *PLoS one* **7**, e35376 (2012).
42. Ishida, M. *et al.* Intrinsic Nucleic Acid-Binding Activity of Chp1 Chromodomain Is Required for Heterochromatic Gene Silencing. *Molecular cell* (2012).doi:10.1016/j.molcel.2012.05.017
43. Hiragami-Hamada, K. *et al.* N-terminal phosphorylation of HP1{alpha} promotes its chromatin binding. *Molecular and cellular biology* **31**, 1186–200 (2011).
44. Rice, S. *et al.* A structural change in the kinesin motor protein that drives motility. *Nature* **402**, 778–784 (1999).
45. Simon, M. D. *et al.* The site-specific installation of methyl-lysine analogs into recombinant histones. *Cell* **128**, 1003–12 (2007).
46. Kim, D. *et al.* Corecognition of DNA and a methylated histone tail by the MSL3 chromodomain. *Nature structural & molecular biology* **17**, 1027–9 (2010).
47. Dawson, M. a *et al.* JAK2 phosphorylates histone H3Y41 and excludes HP1alpha from chromatin. *Nature* **461**, 819–22 (2009).
48. Lavigne, M. *et al.* Interaction of HP1 and Brg1/Brm with the globular domain of histone H3 is required for HP1-mediated repression. *PLoS genetics* **5**, e1000769 (2009).
49. Richart, A. N., Brunner, C. I. W., Stott, K., Murzina, N. V & Thomas, J. O. Characterization of the chromoshadow domain-mediated binding of heterochromatin protein 1 α (HP1 α) to histone H3. *The Journal of biological chemistry* (2012).doi:10.1074/jbc.M111.337204

50. Ekwall, K., Cranston, G. & Allshire, R. C. Fission Yeast Mutants That Alleviate Transcriptional Silencing in Centromeric Flanking Repeats and Disrupt Chromosome Segregation. *Genetics* **153**, 1153–1169 (1999).
51. Sadaie, M., Iida, T., Urano, T. & Nakayama, J.-I. A chromodomain protein, Chp1, is required for the establishment of heterochromatin in fission yeast. *The EMBO journal* **23**, 3825–35 (2004).
52. Zofall, M. & Grewal, S. I. S. Swi6/HP1 recruits a JmjC domain protein to facilitate transcription of heterochromatic repeats. *Molecular cell* **22**, 681–692 (2006).
53. Sadaie, M. *et al.* Balance between distinct HP1 family proteins controls heterochromatin assembly in fission yeast. *Molecular and cellular biology* **28**, 6973–6988 (2008).
54. Braun, S. *et al.* The Cul4-Ddb1(Cdt)² ubiquitin ligase inhibits invasion of a boundary-associated antisilencing factor into heterochromatin. *Cell* **144**, 41–54 (2011).
55. Yamada, T., Fischle, W., Sugiyama, T., Allis, C. D. & Grewal, S. I. S. The nucleation and maintenance of heterochromatin by a histone deacetylase in fission yeast. *Molecular cell* **20**, 173–85 (2005).
56. Sugiyama, T. *et al.* SHREC, an effector complex for heterochromatic transcriptional silencing. *Cell* **128**, 491–504 (2007).
57. Keller, C. *et al.* HP1(Swi6) Mediates the Recognition and Destruction of Heterochromatic RNA Transcripts. *Molecular cell* (2012).doi:10.1016/j.molcel.2012.05.009
58. Mullins, R. D. How WASP-family proteins and the Arp2/3 complex convert intracellular signals into cytoskeletal structures. *Current opinion in cell biology* **12**, 91–96 (2000).
59. Huse, M. & Kuriyan, J. The conformational plasticity of protein kinases. *Cell* **109**, 275–282 (2002).
60. Harrison, S. C. Variation on an Src-like theme. *Cell* **112**, 737–740 (2003).
61. Padrick, S. B. & Rosen, M. K. Physical mechanisms of signal integration by WASP family proteins. *Annual review of biochemistry* **79**, 707–735 (2010).

Supplementary Figures and Figure Legends

Supplementary Figures and Figure Legends (1-9) are described in the Supplementary Information.

Acknowledgements

We would like to thank Julia Tretyakova for preparation of histone proteins and John Leonard for sample preparation for Cryo-EM of the nucleosome alone. We would also like to thank Wendell Lim, Matthew Simon, Karim Armache, Jesse Zalatan, Lisa Racki and members of the Narlikar laboratory for discussions and helpful comments on the manuscript. DC would like to thank Idelisse Ortiz Torres and Kristopher M. Kuchenbecker for useful scientific discussions and members of the Schuck laboratory for advice in the use of AUC approaches. This work was supported by a grant from the Hillblom foundation to D.C. and by grants from the American Cancer Society, Leukemia and Lymphoma Society and the NIH to G.J.N. The contribution of P.S. to this work was supported by the Intramural Research Program of NIBIB, National Institutes of Health. NN and EP were supported by the NIH grant AR053720.

Figure Legends

Figure 1: Dissecting Swi6 self-association equilibria

- a. Domain map of the Swi6 protein (N: N-terminal region; CD: chromodomain; H: Hinge Region; CSD: chromoshadow domain)
- b. Sedimentation Equilibrium (SE) AUC analysis of Swi6^{WT} self-association. Top panel: SE interference profiles at rotor speeds 6000 rpm (blue), 11000 rpm (green) and 18000 rpm (red). Loading concentration, in monomer units, was varied from 1.7 μ M to 32 μ M. Data shown are for 6.7 μ M. For clarity only every 20th data point is shown. Solid lines are best-fit distributions for global analysis using an isodesmic self-association model (see Methods). Bottom panel: Residuals of the fit.
- c. Sedimentation Velocity (SV) AUC analysis of Swi6^{WT} self-association. Top panel: Isotherm of weighted average sedimentation coefficient (s_w) as a function of total Swi6^{WT} protein concentration. Total loading concentration, in monomer units, was varied from 0.5 μ M to 73 μ M. Dashed line is best-fit for global analysis using an isodesmic self-association model. Bottom panel: Residuals of fit.
- d. Model of Swi6 self-association. The Swi6 monomer is represented by “S”. A two-step process: (1) a tight association of two Swi6 monomers with association constant ($K_{obs}^{dim} = [S_2]/[S][S]$) and (2) an isodesmic self-association of Swi6 dimers with identical chain elongation affinity constant ($K_{obs}^{iso} = [S_{n+2}]/[S_n][S_2]$). Table indicates the values of K_{obs}^{dim} and K_{obs}^{iso} at T=8°C from global analysis of SE and SV AUC data.
- e. Change in the overall weighted average sedimentation coefficient (s_w) as a function of 18-mer H3K9me3 and H3K9 peptides. Loading Swi6^{WT} concentration, in

- monomer units is $20\mu\text{M}$. At 24°C , sedimentation coefficients of Swi6^{WT} dimer and tetramer are $\sim 4\text{S}$ and $\sim 5.2\text{S}$, respectively.
- f. Swi6 chromodomain sequence modeled on crystal structure of drosophila HP1 chromodomain bound to H3K9me3 peptide (PDB: 1KNE). Both H3K9me3 peptide and ARK loop H3-tail mimic are in red. The hydrophobic cage is in yellow.
- g. Top panel: Alignment comparing the H3-tail (aa 4-14) to Swi6 (aa 72-97), $\text{dHP1}\alpha$, $\text{hHP1}\alpha$ and $\text{hHP1}\beta$. The conserved lysine (K) is in red and the phosphorylatable serines (S) in blue. Bottom panel: Model for mutually exclusive binding of methylated H3 tail peptide (green line with red circle denoting methylation) and the Swi6 ARK loop to the Swi6 CD.

Figure 2: Identification of an H3-tail mimic in Swi6 chromodomain that regulates both the isodesmic association of Swi6 dimers and the dimerization of Swi6 monomers

- a. Left: Schematic representation of the known and previously hypothesized Swi6 :H3 tail interactions. Right: Schematic representation of the hypothetical CD:CD interactions. The grey oval represent a region of negative potential generated by acidic the N-terminal of the CD. The brown oval represent the π -cation interactions generated by the three hydrophobic cage residues. Bottom: Nomenclature of the three mutants used in this study.
- b. Comparison of the isodesmic association constant (K_{obs}^{iso}) for Swi6^{WT} and $\text{Swi6}^{\text{LoopX}}$, $\text{Swi6}^{\text{CageX}}$, $\text{Swi6}^{\text{AcidicX}}$. $K_{obs}^{\text{iso}} = 0.009\mu\text{M}^{-1}$ for Swi6^{WT} , $0.003\mu\text{M}^{-1}$ for $\text{Swi6}^{\text{LoopX}}$, $0.005\mu\text{M}^{-1}$ for $\text{Swi6}^{\text{CageX}}$, $0.001\mu\text{M}^{-1}$ for $\text{Swi6}^{\text{AcidicX}}$. $1/K_{obs}^{\text{iso}} = 110\mu\text{M}$ for Swi6^{WT} ,

- 345 μ M for Swi6^{LoopX}, 195 μ M for Swi6^{CageX}, 960 μ M for Swi6^{AcidicX}. Errors bars (n \geq 3) represent s.e.m. Also see Supplementary Figure 4.
- c. Comparison of dimerization association constant (K_{obs}^{dim}) for Swi6^{WT} and Swi6^{LoopX}, Swi6^{CageX}, Swi6^{AcidicX}. $K_{obs}^{dim} = 20.5\mu\text{M}^{-1}$ for Swi6^{WT}, $1.5\mu\text{M}^{-1}$ for Swi6^{LoopX}, $3.8\mu\text{M}^{-1}$ for Swi6^{CageX}, $7.5\mu\text{M}^{-1}$ for Swi6^{AcidicX}. $1/K_{obs}^{dim} = 0.048\mu\text{M}$ for Swi6^{WT}, $0.68\mu\text{M}$ for Swi6^{LoopX}, $0.26\mu\text{M}$ for Swi6^{CageX}, $0.16\mu\text{M}$ for Swi6^{AcidicX}. Errors (n \geq 3) represent s.e.m. Also see Supplementary Figure 4.
- d. Model for the self-association of Swi6. In Swi6^{WT}, the dimer is stabilized by both the CSD and CD interfaces, and higher-order oligomeric states are stabilized by the loop-CD interactions between dimers. K^{conf} defines the equilibrium constant for the closed to open transition in the Swi6 dimer ($K^{conf} = [\text{open}]/[\text{closed}]$). K^{oligo} defines the isodesmic association constant for Swi6^{WT} oligomerization from the open state of the dimer. For Swi6^{WT}, $K_{obs}^{dim} = \frac{K^{csd}}{K^{conf}}$ and $K_{obs}^{iso} = K^{conf} \times K^{oligo}$.
- e. Affinity constant for H3K9me3 tail peptide. Left: Comparison of 18mer H3K9me3 peptide binding by Swi6^{WT} (blue), Swi6^{LoopX} (green) and Swi6^{AcidicX} (yellow) assayed by tryptophan fluorescence studies. $K = 0.08\mu\text{M}^{-1}$ for Swi6^{WT}, $0.5\mu\text{M}^{-1}$ for Swi6^{LoopX}, $0.01\mu\text{M}^{-1}$ for Swi6^{AcidicX}. $1/K = 12\mu\text{M}$ for Swi6^{WT}, $2\mu\text{M}$ for Swi6^{LoopX}, $90\mu\text{M}$ for Swi6^{AcidicX}. Right: Comparison of 15mer H3K9me3 peptide binding by Swi6^{WT} (blue), Swi6^{CageX} (grey) assayed by anisotropy fluorescence studies. $K =$

$0.1\mu\text{M}^{-1}$ for Swi6^{WT}, $0.002\mu\text{M}^{-1}$ for Swi6^{CageX}. $1/K = 9.5\mu\text{M}$ for Swi6^{WT}, $554\mu\text{M}$ for Swi6^{CageX}. Errors ($n \geq 3$) represent s.e.m.

Figure 3: The ARK loop in Swi6 chromodomain is immobilized in the closed conformation of the Swi6 dimer

- a. Rationale for EPR experiments with an MSL probe (yellow circle) located on the ARK loop: a closed state results in an immobile probe while an open-state yields a mobile probe. All experiments in this figure have an MSL probe at residue G95C of Swi6^{3S}.
- b. Comparative SV AUC (left panels) and EPR analyses (right panels) of Swi6^{probe-WT}, Swi6^{probe-AcidicX}, Swi6^{probe-LoopX} and Swi6^{probe-DimerX} proteins. c(M) is the molar mass distribution. Representative EPR spectra shown. The horizontal axis is the magnetic field and the vertical axis is the derivative of absorbance. Mobile and immobile components are shown by dashed arrows. Errors for the percent of probe immobilized is < 10%.
- c. Change in the percentage of immobilized probes as a function of increasing 18mer H3K9me3 (red), H3K9 (black) or H3K4me3 (white) peptides. Swi6^{probe-WT} monomer concentration: $20\mu\text{M}$.

Figure 4: Visualization of distinct Swi6 conformations and of the Swi6-H3K_c9me₃ nucleosome complex by EM

- a. Visualization of the CFP-Swi6. Representative 2D class average of negative stain EM images is shown. The cartoons represent the proposed global conformation of the fusion construct and are mainly intended to guide the eye. They are not intended to imply a symmetric arrangement. Scale bar is show.
- b. Visualization of the Swi6-CFP. Representative 2D class average of negative stain EM images is shown. As in a., the cartoons represent the proposed global conformations of the fusion construct. Scale bar is show.
- c. Two different views of a cryo-EM based 3D reconstruction of the complex of Swi6 with an H3K_c9me₃ core nucleosome (left), a cryo-EM based 3D reconstruction of a nucleosome with 60 bp of flanking DNA (flanking DNA is averaged out in 3D reconstruction) (middle), and difference map between the 3D reconstruction of the Swi6:H3K_c9me₃ nucleosome complex and the nucleosome alone (right). The nucleosome crystal structure (PDB 1KX5) was fitted into the 3D reconstruction using the Chimera Fit in Map function. H3 is highlighted in red. The isosurface of the 3D reconstruction of the nucleosome at high threshold is shown in dark blue, and low threshold in light blue.
- d. Difference density between Swi6:H3K_c9me₃ complex and nucleosome alone. Putative locations of Swi6 domains in the difference map are inferred based on the assumption that the difference density is mainly contributed by the bound Swi6 dimer. The structures of the chromodomain of Swi6 (CD, black; PDB 2RSO, aa 72-142) and the chromoshadow domain of Swi6 (CSD, red; PDB 1E0B) were manually

docked into the difference map. The hypothesized location of the Hinge region (H) is shown.

- e. Additional view of 3D reconstruction of the Swi6-H3K_c9me₃ nucleosome core particle to highlight proposed locations of the two unoccupied chromodomain (CD) sticky-ends.

Figure 5: Energetics of methylated nucleosome recognition by Swi6

- a. Fluorescence anisotropy studies of nucleosome binding by Swi6^{WT} (blue) and Swi6^{LoopX} (green).
- b. Summary of the dissociation constants (K_d) measured using the fluorescence anisotropy assay in (b) for Swi6^{WT}, Swi6^{LoopX}, Swi6^{DimerX} and Swi6^{EW} binding to H3K9 and H3K_c9me₃ nucleosomes.
- c. Fluorescence anisotropy studies of DNA binding by Swi6^{WT} (blue), Swi6^{LoopX} (green), Swi6^{ΔNCD} (white) in the absence of H3 peptide, and Swi6^{WT} in the presence of 18mer H3K9 (grey) and 18mer H3K9me₃ peptide (red). Affinity constants for 20mer DNA are: Swi6^{WT}, 0.066μM⁻¹; Swi6^{LoopX}, 0.016μM⁻¹; Swi6^{ΔNCD} 0.017μM⁻¹; Swi6^{WT} + 18mer H3K9 peptide 0.044μM⁻¹ Swi6^{WT} + 18mer H3K9me₃ peptide 0.2μM⁻¹. Errors ($n \geq 3$) in (b) and (c) represent s.e.m.
- d. Proposed model for how HP1/Swi6 alters conformation upon binding methylated nucleosomes. Swi6 is in equilibrium between an auto-inhibited, closed state and an open state. Binding to methylated H3 tails releases ARK loops to assist in engaging

nucleosomal DNA and concomitantly generates a conformation that is competent to spread by exposing two unoccupied chromodomains.

Figure 6: Swi6^{LoopX} and Swi6^{AcidicX} results in defects in pericentromeric heterochromatin silencing

- a. Top: Schematics of centromere 1 with the *ura4+* reporter gene inserted in the *inner most repeat (imr)* region. Bottom: Silencing assay of Swi6 mutants in the pericentromeric *ura4+* reporter strain background. Cells were plated on non-selective YS media (YS) and YS media with 5-FOA (YS + 5-FOA).
- b. Swi6^{LoopX} and Swi6^{AcidicX} proteins express at similar levels that Swi6^{WT}. Extracts from respective strains were separated on SDS-PAGE gels and probed for α -hexokinase and α -Swi6. α -Swi6 was raised against recombinant purified full-length protein. Quantification of the Swi6 band normalized for the α -hexokinase control is shown relative to the value obtained for Swi6^{WT}. Swi6^{AcidicX} has a faster mobility on a SDS-PAGE gel as expected from the faster mobility of recombinant Swi6^{AcidicX} (Supplementary Fig. 9).
- c. *swi6^{LoopX}* and *swi6^{AcidicX}* mutants strongly decrease H3K9 methylation levels at the centromeric *dg* repeat in a *dcr1 Δ* background. H3K9me2 fold enrichment over actin at the centromeric *dg* repeat for *swi6^{WT}* (brown), *dcr1 Δ swi6^{WT}* (blue), *dcr1 Δ swi6^{LoopX}* (green), *dcr1 Δ swi6^{AcidicX}* (yellow), *dcr1 Δ swi6 Δ* (white). Errors represent s.e.m from three independent IPs.

- d. Proposed model of multiple ways by which HP1 proteins can engage a methylated nucleosome template and how the HP1-chromatin platform can recruit a variety of other modifying factors that can either promote (yellow, red, blue and green cartoons) or inhibit (grey cartoon) heterochromatin spread.

Figure 1

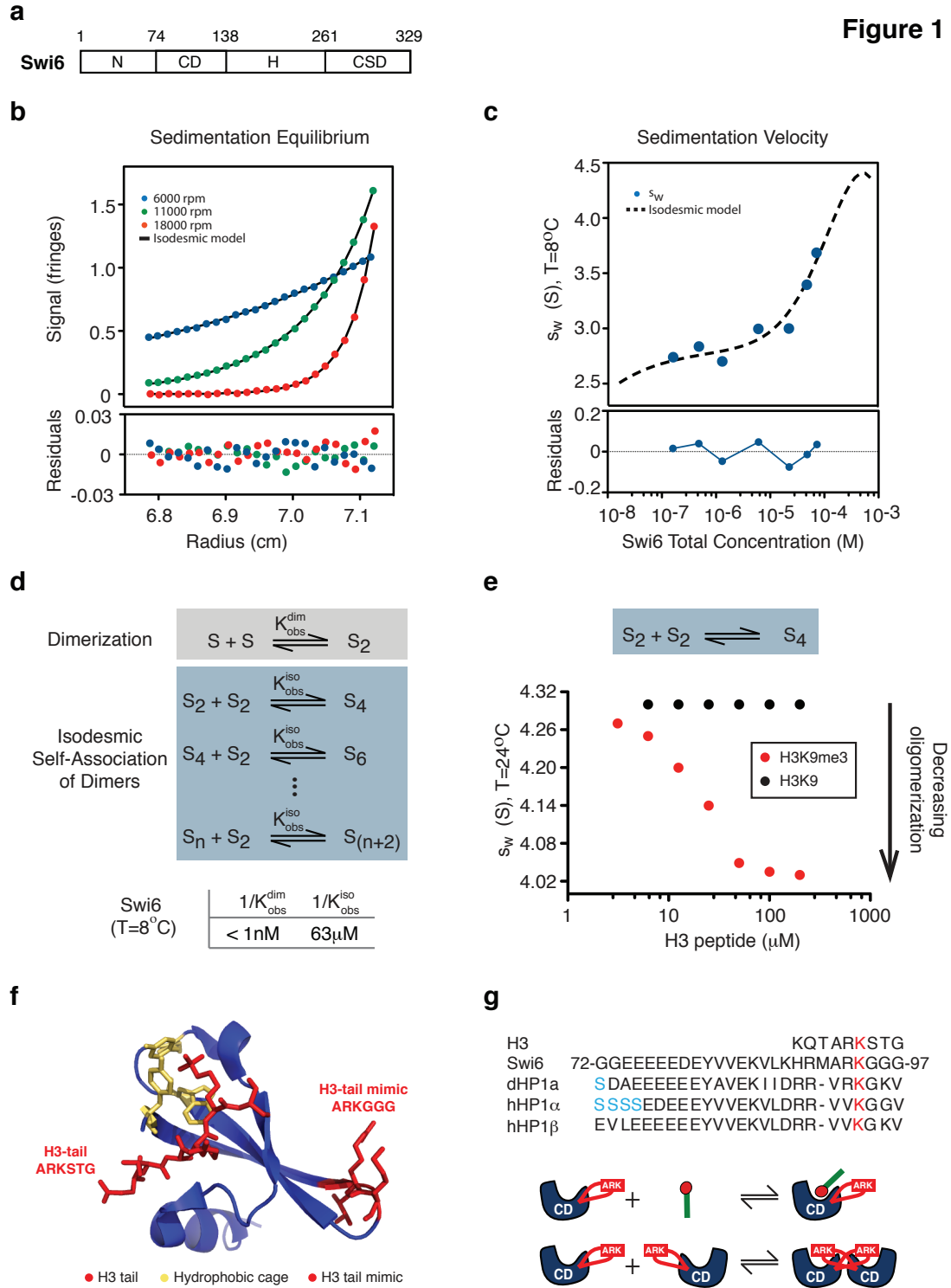


Figure 2

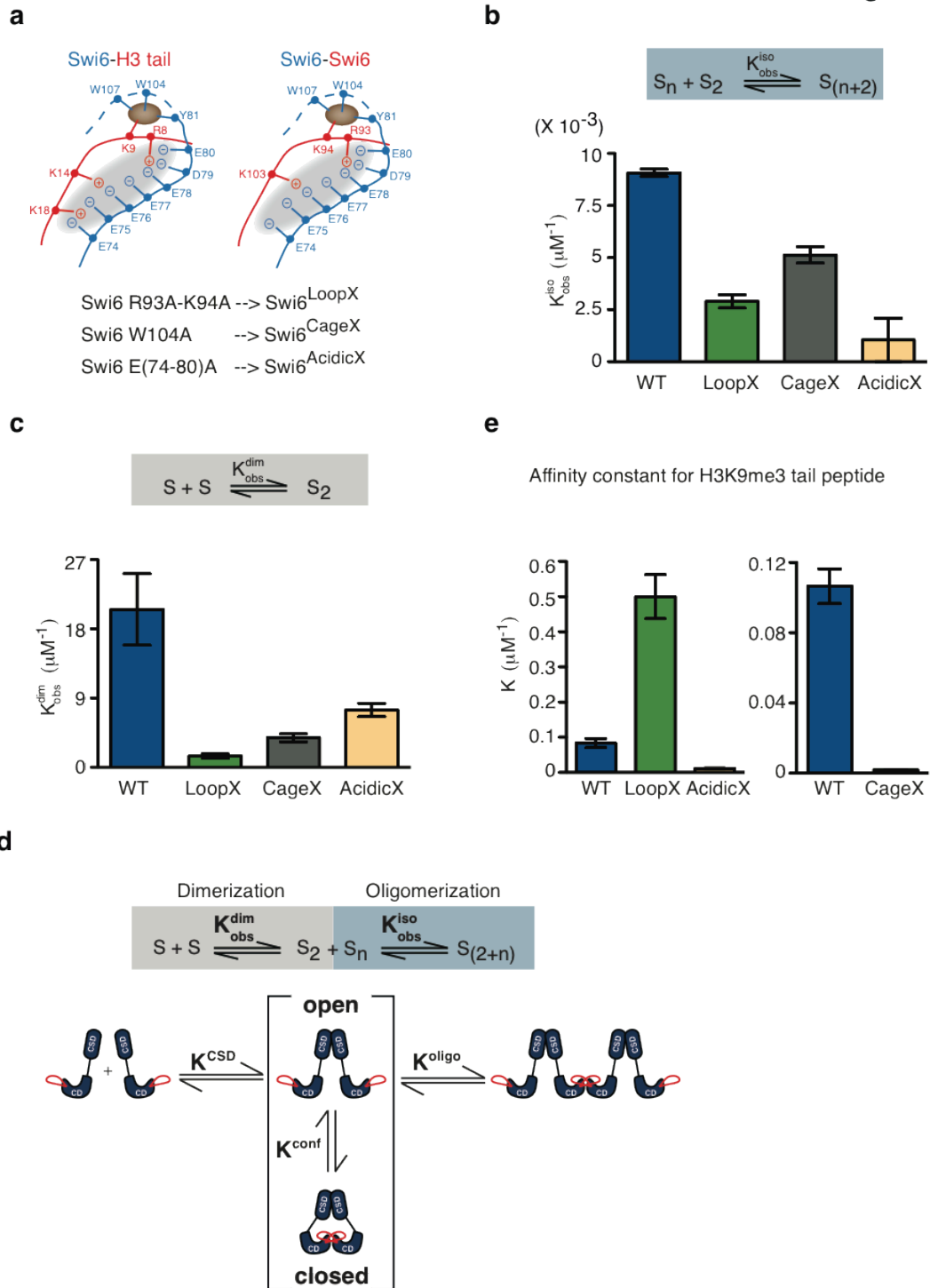


Figure 3

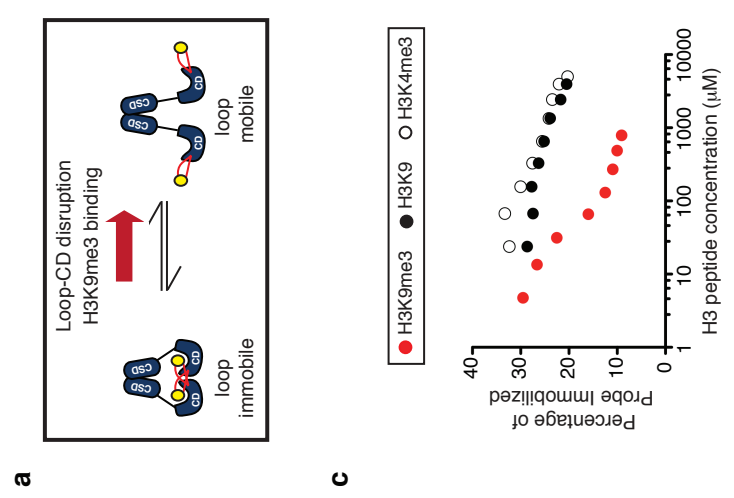
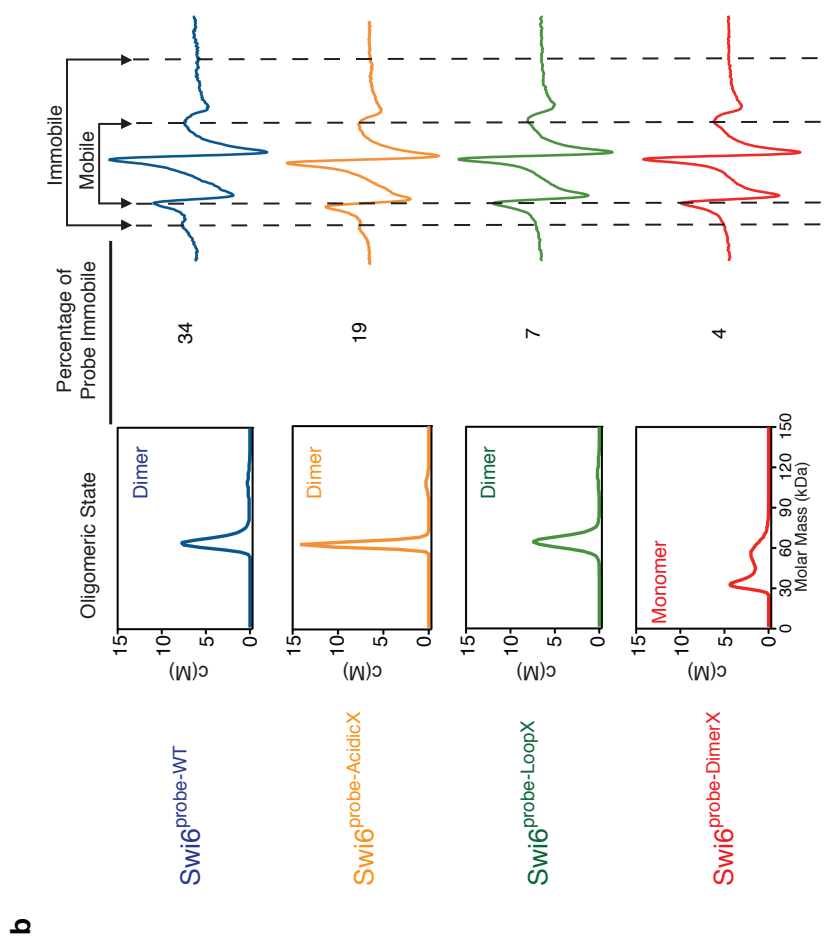


Figure 4

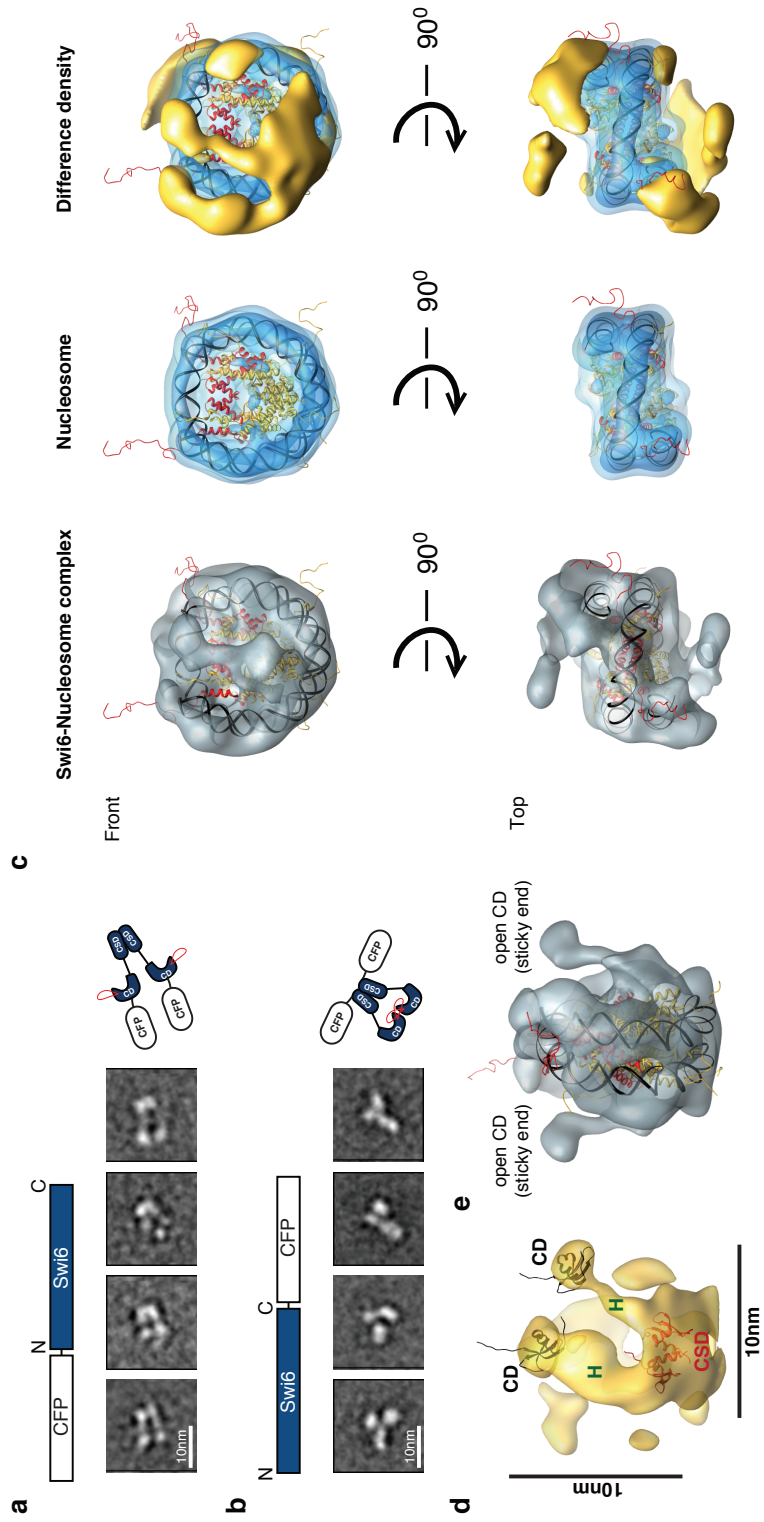


Figure 5

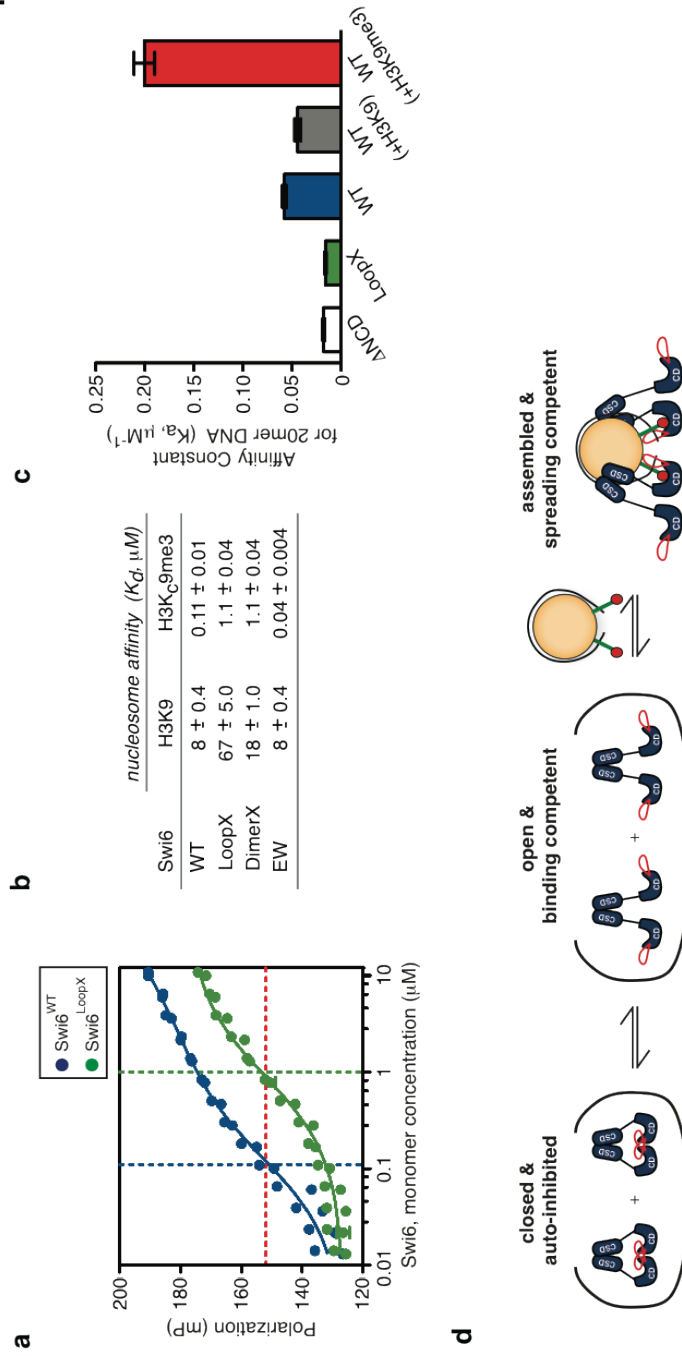
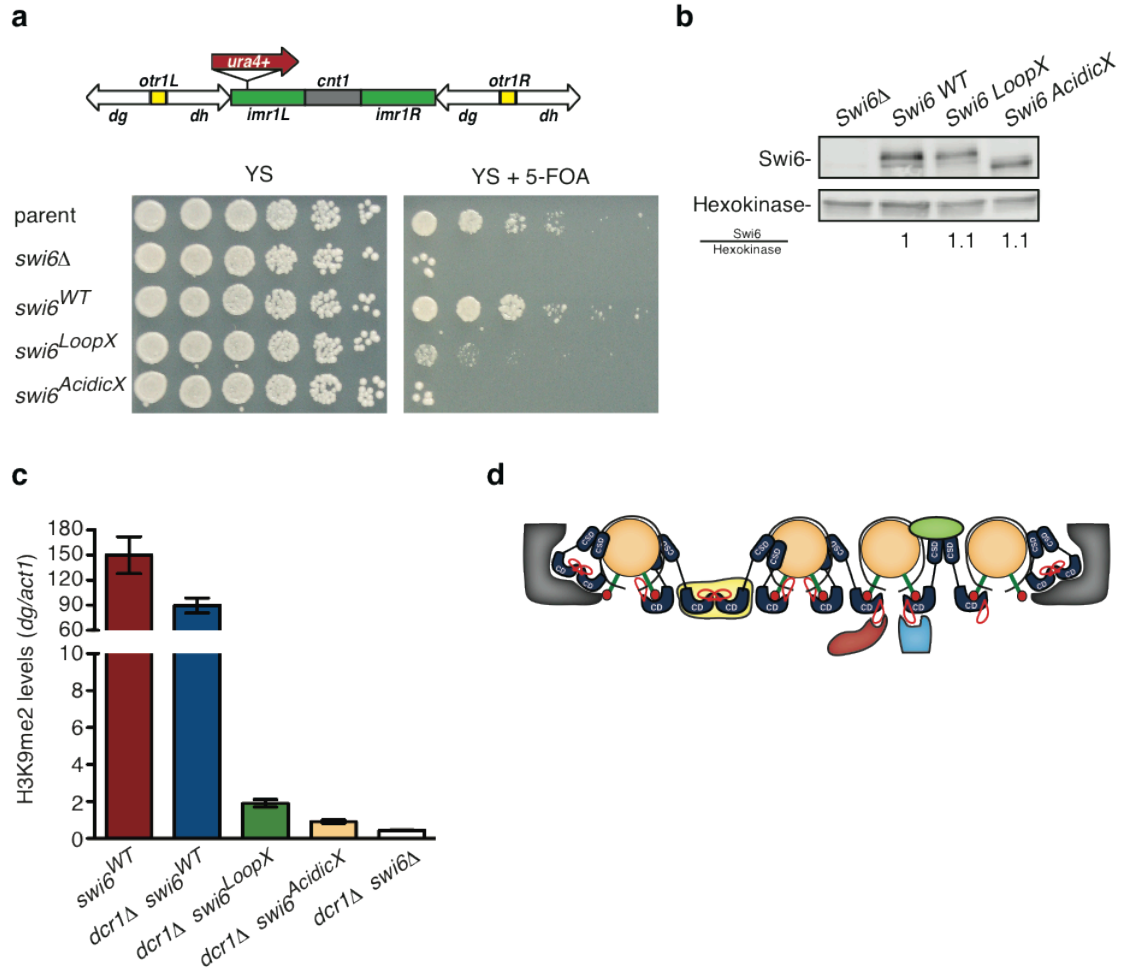


Figure 6



Supplementary Information

A conformational switch in HP1 allows conditional activation and drives heterochromatin assembly in vivo

Daniele Canzio, Maofu Liao, Nariman Naber, Ed Pate, Adam Larson, Shenping Wu, Diana B. Marina, Jennifer F. Garcia, Hiten D. Madhani, Roger Cooke, Peter Schuck, Yifan Cheng, Geeta J. Narlikar

Inventory of Supplementary Information

Supplementary Figures and Legends

Supplementary Figure 1: Analysis of Swi6^{WT} self-association

Supplementary Figure 2: Swi6^{WT} self-association data and global fit using a two-step isodesmic self-association model

Supplementary Figure 3: Swi6^{WT} self-association data and global fit using a monomer-dimer-tetramer model and monomer-trimer model

Supplementary Figure 4: Studies of the self-association process of Swi6^{WT}, Swi6^{LoopX}, Swi6^{AcidicX}, Swi6^{CageX}, Swi6^{ΔNCD}, Swi6⁽⁸⁰⁻³²⁹⁾ by SV AUC

Supplementary Figure 5: Characterization of cys-free Swi6^{3S} and Swi6^{probe} with MLS probe on either K94C or G95C residues

Supplementary Figure 6: Characterization of CFP-Swi6 and Swi6-CFP by negative stain EM and SV AUC studies

Supplementary Figure 7: Cryo-EM studies of the nucleosome core particle and the Swi6-H3K_c9me3 nucleosome complex

Supplementary Figure 8: Nucleosome binding studies of Swi6^{WT}, Swi6^{LoopX}, Swi6^{DimerX} and Swi6^{EW} and DNA binding studies for Swi6^{WT}, Swi6^{LoopX}, Swi6^{ΔNCD}

Supplementary Figure 9: *In vivo* characterization of *swi6*^{LoopX} and *swi6*^{AcidicX}

Supplementary Methods

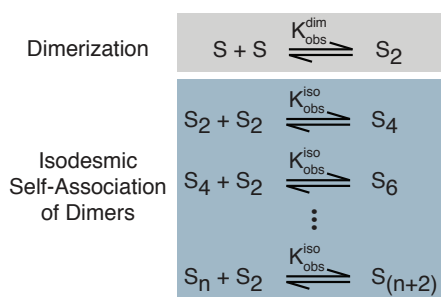
Supplementary Table

Supplementary Table 1: Table of all the Swi6 constructs used in this study

Supplementary Table 2: Table of all the *S. pombe* strains used in this study

a

Two-step isodesmic self-association model

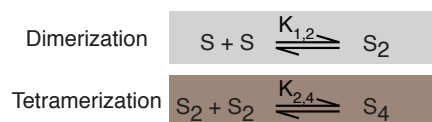


Data from T=8°C experiments

	Data Points	1/K _{obs} ^{dim} (nM)	1/K _{obs} ^{iso} (μM)	s(S ₂)	Global χ ²
SE (Abs) & SV	6851	< 0.68	74.1 (65.1 - 100)	3.73 (3.71 - 3.76)	2.44
SE (IF) & SV	7128	< 1.0	63.1 (56.2 - 79.4)	3.77 (3.74 - 3.87)	5.30

b

Monomer-dimer-tetramer model



Data from T=8°C experiments

	Data Points	1/K _{1,2} (nM)	1/K _{2,4} (μM)	s(S ₂)	Global χ ²
SE (IF) & SV	7128	< 1.0	62.4 (45.4 - 89.4)	3.71 (3.70 - 3.73)	8.67

c

Monomer-trimer model



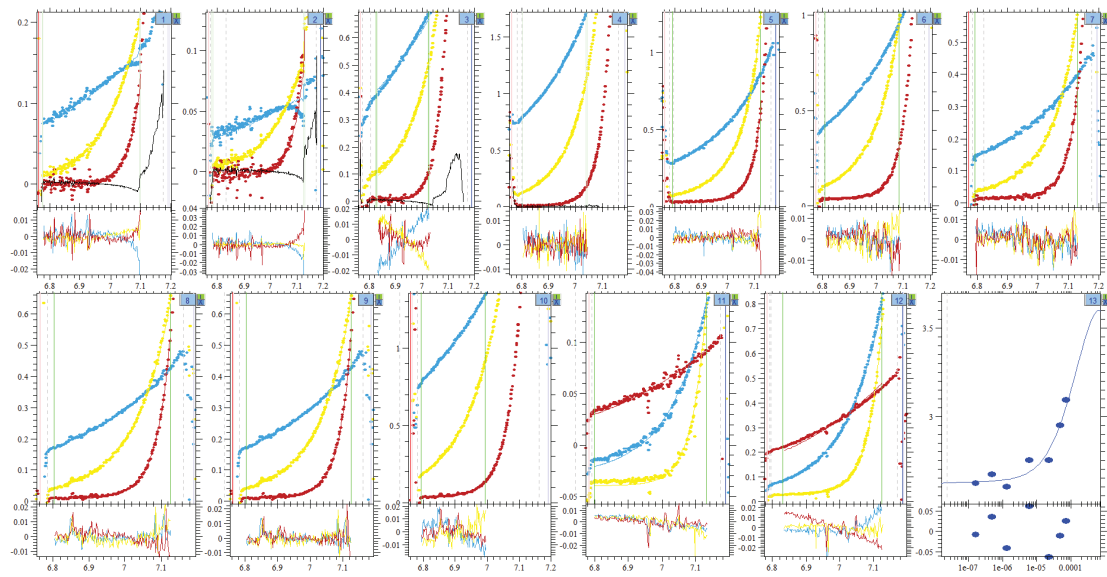
Data from T=8°C experiments

	Data Points	1/K (μM ²)	s(S ₃)	Global χ ²
SE (IF) & SV	7128	2.8 ⁻¹⁵ (7.9 ⁻¹⁶ - 6.3 ⁻¹⁵)	4.12 (4.06 - 4.18)	53.4

Supplementary Figure 1

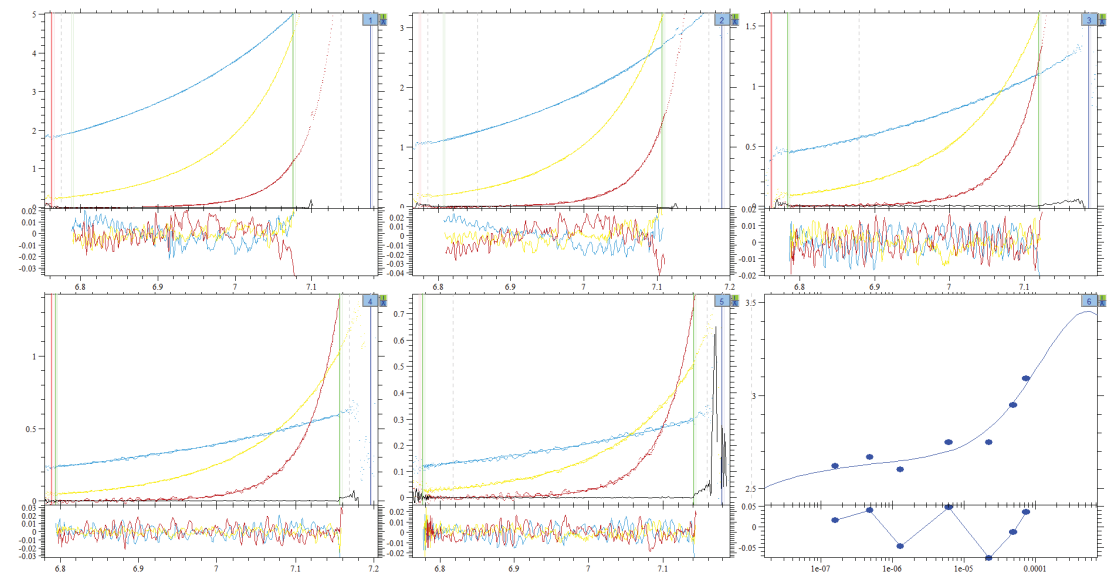
a

Sedimentation Equilibrium Absorbance optics (SE, Abs) & Velocity (SV), (T=8°C)
Global analysis using a two-step isodesmic self-association model



b

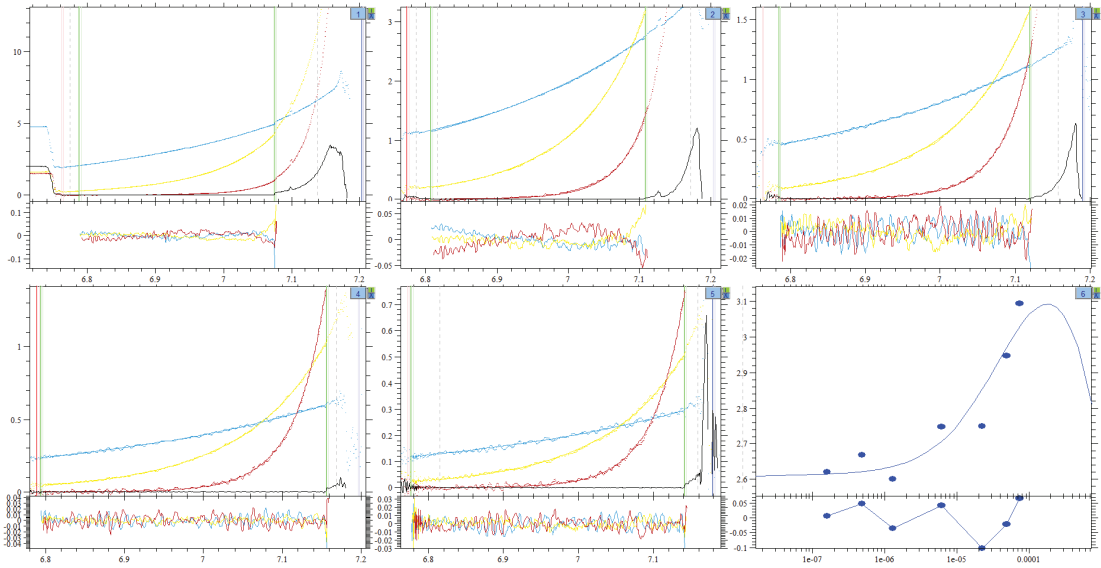
Sedimentation Equilibrium Interference optics (SE, IF) & Velocity (SV), (T=8°C)
Global analysis using a two-step isodesmic self-association model



Supplementary Figure 2

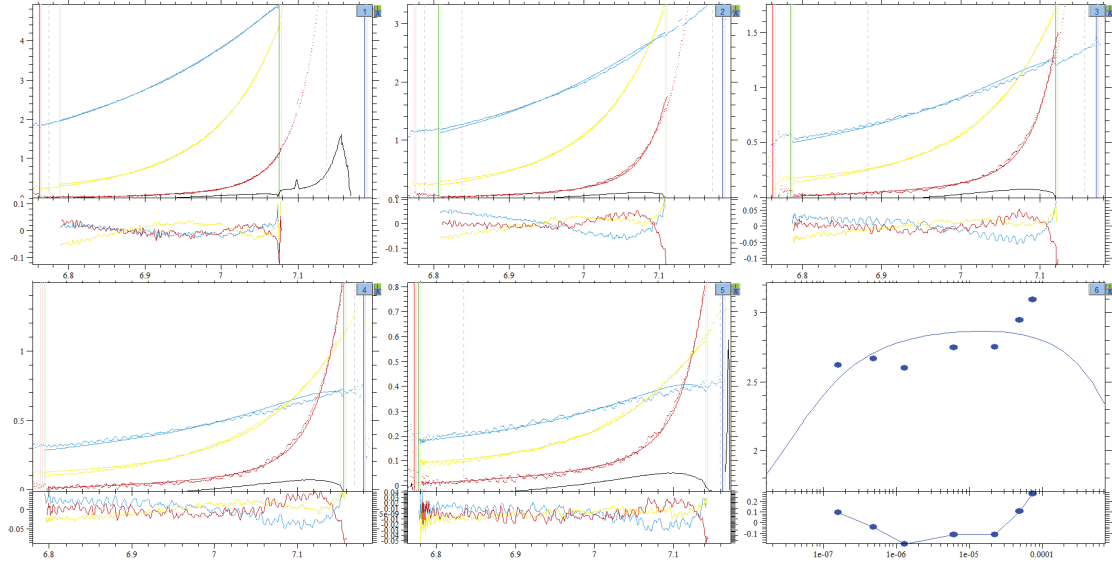
a

Sedimentation Equilibrium Interference optics (SE, IF) & Velocity (SV), ($T=8^{\circ}\text{C}$)
Global analysis using a monomer-dimer-tetramer model

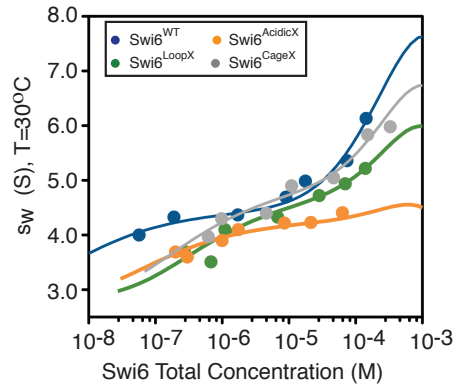


b

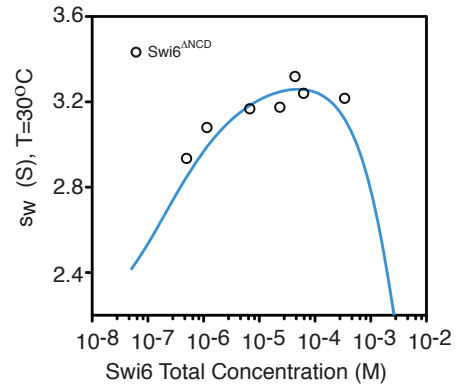
Sedimentation Equilibrium Interference optics (SE, IF) & Velocity (SV), ($T=8^{\circ}\text{C}$)
Global analysis using a monomer-trimer model



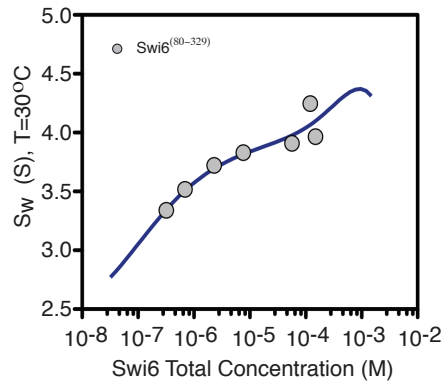
Supplementary Figure 3

a

	$s(S_2)$	$1/K_{obs}^{dim}$ (nM)	$1/K_{obs}^{iso}$ (μ M)
Swi6 ^{WT}	3.76 (\pm 0.03)	48 (\pm 11)	110 (\pm 2.1)
Swi6 ^{LoopX}	3.94 (\pm 0.04)	687 (\pm 140)	345 (\pm 38)
Swi6 ^{AcidicX}	3.52 (\pm 0.01)	134 (\pm 15)	960 (\pm 121)
Swi6 ^{CageX}	3.97 (\pm 0.03)	260 (\pm 36)	195 (\pm 15)

b

	$s(S_2)$	$1/K_{obs}^{dim}$ (nM)
Swi6 ^{ANCD}	2.78 (\pm 0.01)	370 (\pm 140)

c

	$s(S_2)$	$1/K_{obs}^{dim}$ (nM)	$1/K_{obs}^{iso}$ (μ M)
Swi6 ⁽⁸⁰⁻³²⁹⁾	3.24 (\pm 0.03)	165 (\pm 12)	754 (\pm 72)

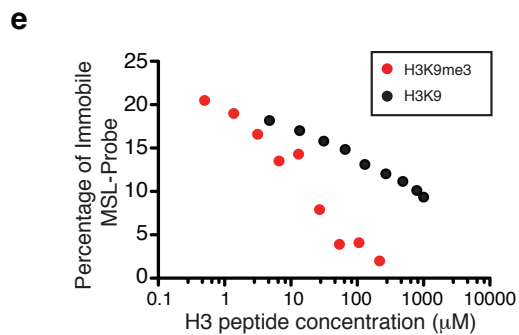
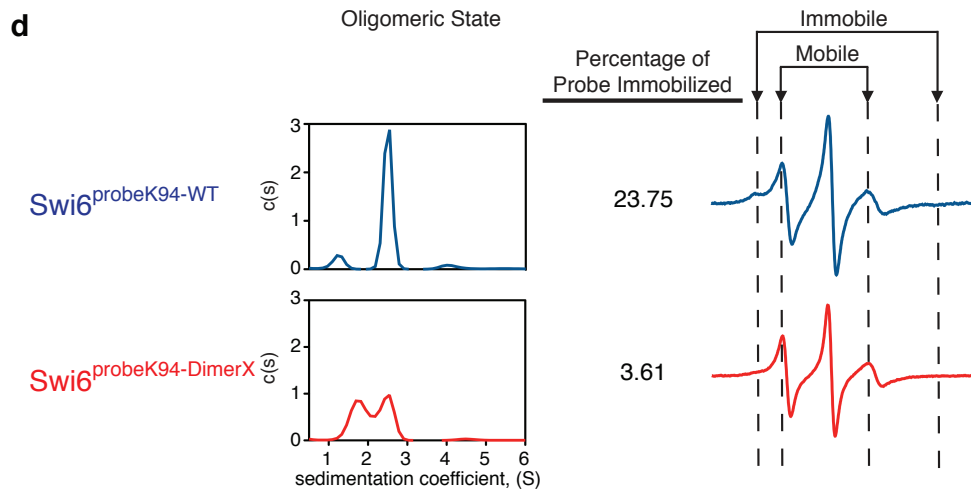
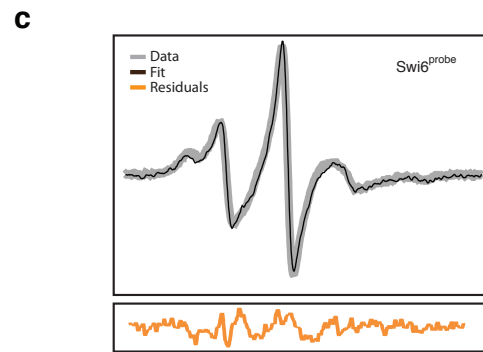
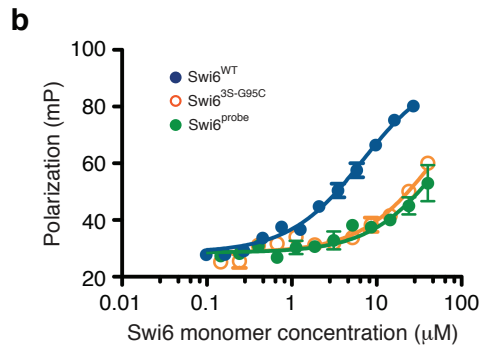
d

T=16°C	H3K9me3 18mer	$1/K_{obs}^{dim}$ (nM)	$1/K_{obs}^{iso}$ (μ M)
Swi6 ^{WT}	-	< 1	112 (89 - 140)
Swi6 ^{WT}	+	60 (13 - 144)	588 (213 - 3700)

Supplementary Figure 4

a

	Self-Association, SV T=24°C		H3K9me3 tail binding	Nucleosome Binding	
	1/K _{obs} ^{dim} (nM)	1/K _{obs} ^{iso} (μM)	K _d (μM)	H3K9 K _d (μM)	H3K _c 9me3 K _d (μM)
Swi6 ^{WT}	< 6	151 (113-220)	10 (± 1.4)	12 (± 1.7)	0.14 (± 0.01)
Swi6 ^{3S}	164 (48-370)	134 (60-460)	40 (± 4.7)	11 (± 1.4)	1.5 (± 0.12)

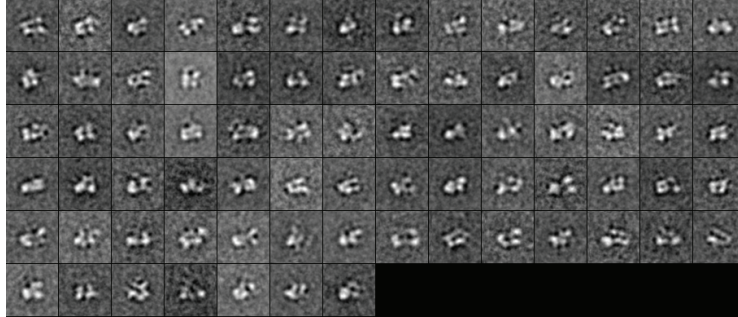


Supplementary Figure 5

a



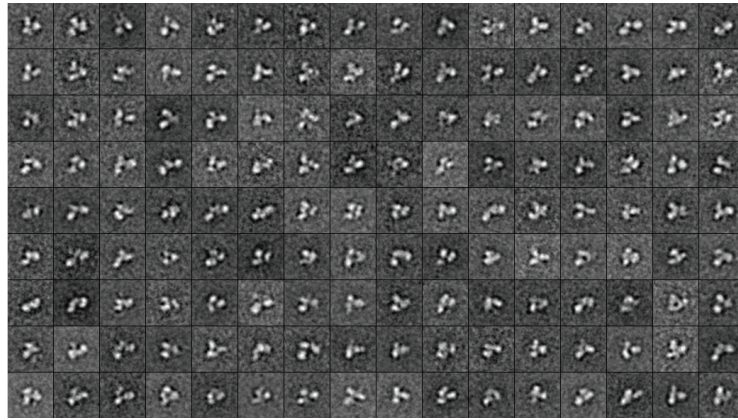
77 2D-class averages (4000 particles total)



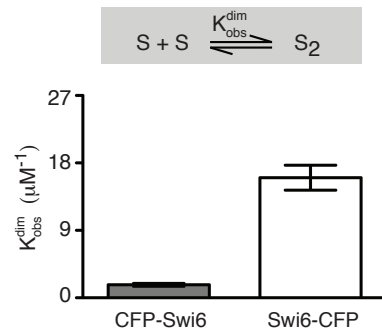
b



144 2D-class averages (3000 particles total)



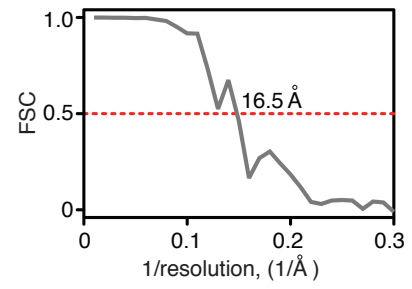
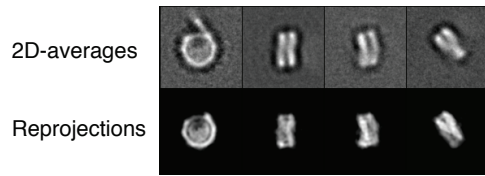
c



Supplementary Figure 6

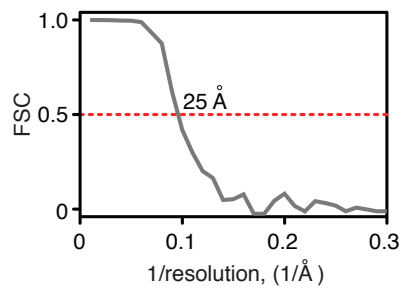
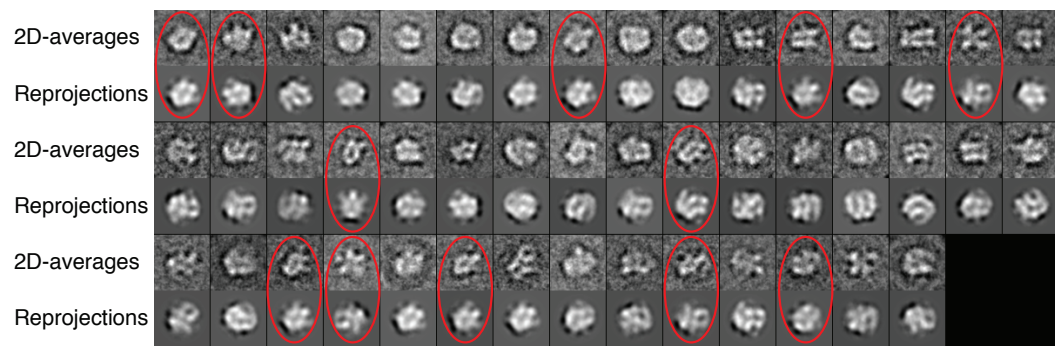
a

Nucleosome: cryo-EM

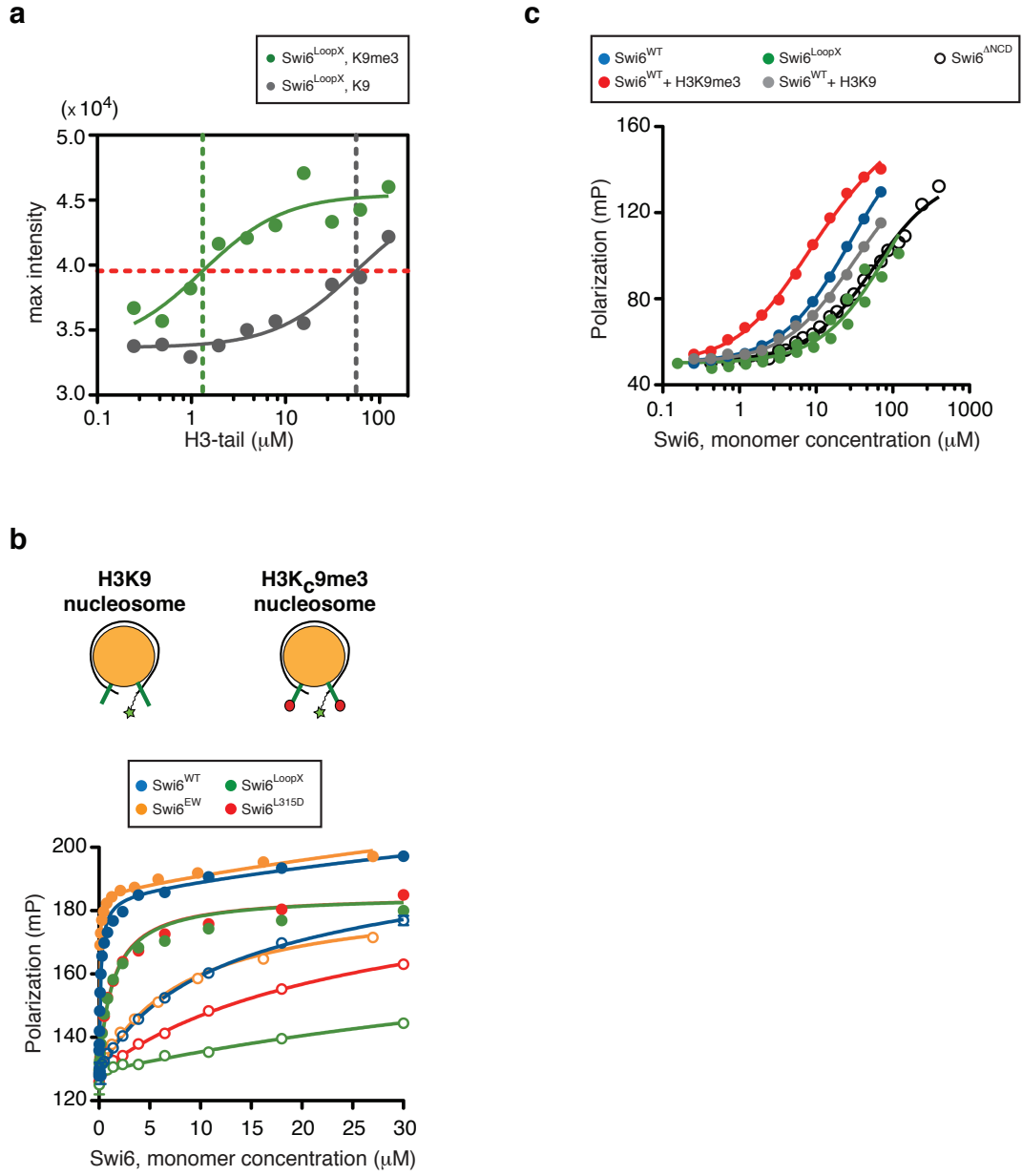


b

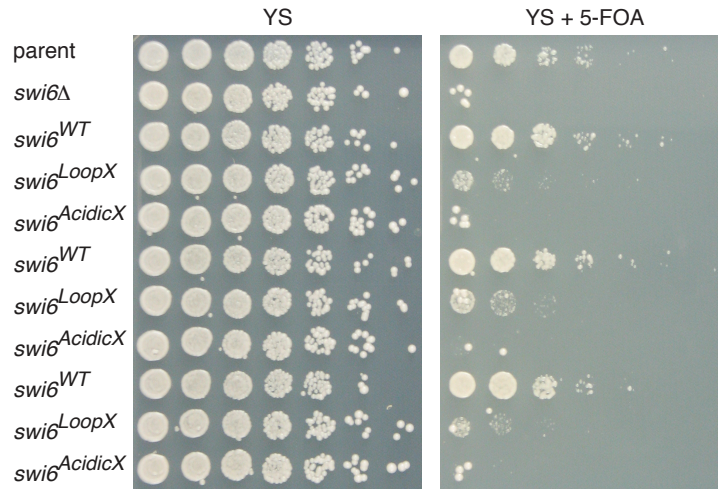
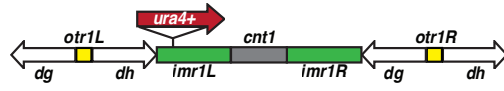
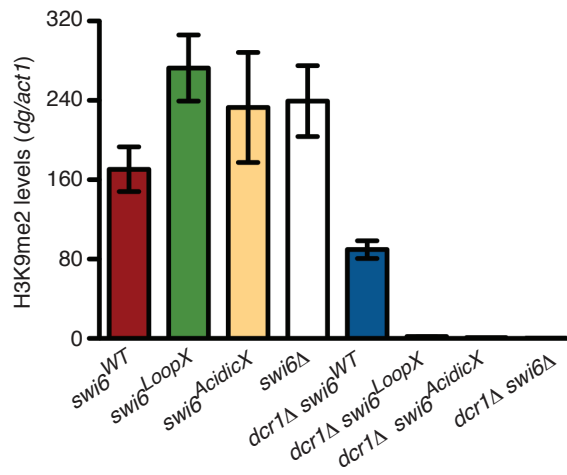
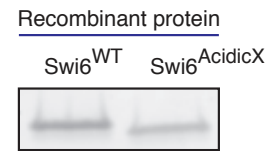
Swi6-H3K₉me3 Nucleosome complex: cryo-EM



Supplementary Figure 7



Supplementary Figure 8

a**b****c****Supplementary Figure 9**

Supplementary Figure Legends

Supplementary Figure 1: Analysis of Swi6^{WT} self-association

We fitted the data in Supplementary Figure 2 to three models shown here in (a), (b) and (c). Based on the best-fit χ^2 values, the two-step isodesmic model in (a) fits the data the best. In addition, the values obtained from the monomer-dimer-tetramer model in (b) are not substantially different from the values obtained using the isodesmic models in (a). This suggests that the oligomeric states defined by the monomer-dimer-tetramer model are most likely sampled by Swi6 and are more extensively incorporated into the isodesmic model. For all the analysis, the χ^2 value is a weighted, global reduced χ^2 , based on estimates of statistical errors in the data acquisition, and incorporates a weighting factor for the sedimentation velocity data. The 95% confidence intervals are in parenthesis. The value of the sedimentation coefficient of a Swi6 monomer was measured to be ~ 2.3 by using the monomeric Swi6^{DimerX} construct and was fixed in this analysis.

- a. (Left) Two-step isodesmic self-association model: (1) a tight association of two Swi6 monomers (S) with affinity constant (K_{obs}^{dim}) and (2) an isodesmic self-association of Swi6 dimers (S_2) with identical chain elongation affinity constant (K_{obs}^{iso}). (Right) Table describing the results of fitting the data (Supplementary Figure 2a and b) using a two-step self-association model. The $s(S_2)$ value indicates the best-fit sedimentation coefficient of a Swi6 dimer normalized to 20°C.
- b. (Left) A monomer-dimer-tetramer model: $K_{1,2}$ is the affinity constant for the dimerization step and $K_{2,4}$ for the tetramerization step. (Right) Table describing the

results of fitting the data (Supplementary Figure 2b) using a monomer-dimer-tetramer model. The $s(S_2)$ value indicates the best-fit sedimentation coefficient of a Swi6 dimer normalized to 20°C.

- c. (Left) A monomer-trimer model with association constant, $K_{1,3}$, for the monomer-trimer transition. (Right) Table describing the results of fitting the data (Supplementary Figure 2b) using a monomer-trimer model. The $s(S_3)$ value indicates the best-fit sedimentation coefficient of a Swi6 dimer normalized to 20°C.

Supplementary Figure 2: Swi6^{WT} self-association data and global fit using a two-step isodesmic self-association model

- a. Global fit using a two-step isodesmic self-association model of SE AUC data, acquired using absorbance optics, and SV AUC data. All the experiments were performed at 8°C. Results of the fit are shown in Supplementary Figure 1a. Residuals are in the bottom panels of each data set. For the SE data, the y-axis is absorbance units and x-axis is in radius (cm). For the SV data, the y-axis is the weighted average sedimentation coefficient (s_w) and the x-axis is total protein concentration in molar units.
- b. Global fit using a two-step isodesmic self-association model of SE AUC data, acquired using interference optics, and SV AUC data. All the experiments were performed at 8°C. Results of the fit are shown in Supplementary Figure 1a. Residuals are in the bottom panels of each data set. For the SE data, the y-axis is fringes units and x-axis is in radius (cm). For the SV data, the y-axis is the weighted

average sedimentation coefficient (s_w) and the x-axis is total protein concentration in molar units.

Supplementary Figure 3: Swi6^{WT} self-association data and global fit using a monomer-dimer-tetramer model and monomer-trimer model

- a. Global fit using a monomer-dimer-tetramer self-association model of SE AUC data, acquired using interference optics, and SV AUC data. All the experiments were performed at 8°C. Results of the fit are shown in Supplementary Figure 1b. Residuals are in the bottom panels of each data set. For the SE data, the y-axis is fringes units and x-axis is in radius (cm). For the SV data, the y-axis is the weighted average sedimentation coefficient (s_w) and the x-axis is total protein concentration in molar units.
- b. Global fit using a monomer-trimer self-association model of SE AUC data, acquired using interference optics, and SV AUC data. All the experiments were performed at 8°C. Results of the fit are shown in Supplementary Figure 1c. Residuals are in the bottom panels of each data set. For the SE data, the y-axis is fringes units and x-axis is in radius (cm). For the SV data, the y-axis is the weighted average sedimentation coefficient (s_w) and the x-axis is total protein concentration in molar units.

Supplementary Figure 4: Studies of the self-association process of Swi6^{WT},

Swi6^{LoopX}, Swi6^{AcidicX}, Swi6^{CageX}, Swi6^{ΔNCD}, Swi6⁽⁸⁰⁻³²⁹⁾ by SV AUC

- a. Representative Sedimentation Velocity AUC experiments for Swi6^{WT} and Swi6^{LoopX}, Swi6^{AcidicX}, Swi6^{CageX}. Data were fitted with a two-step isodesmic model. Table indicates the values measured. The value of the sedimentation coefficient of a Swi6 monomer $s(S_1)$ was measured to be ~ 2.3 by using the monomeric Swi6^{DimerX} construct and was fixed in this analysis. The $s(S_2)$ indicated is the sedimentation coefficient of the dimer normalized to standard conditions at 20°C. Error represent s.e.m. from three or more independent experiments.
- b. Representative Sedimentation Velocity AUC experiment for Swi6^{ΔNCD}. Data were fitted with monomer-dimer model. Table indicates the values measured. The sedimentation coefficient of monomer $s(S_1)$ was fixed to 1.7S using the scaling relationship that $s(S_2) \approx s(S_1) \times 2^{2/3}$ for dimer and monomer with similar frictional coefficient. The $s(S_2)$ indicated is the sedimentation coefficient of the dimer normalized to standard conditions at 20°C. Error represent s.e.m. from three independent experiments.
- c. Representative Sedimentation Velocity AUC experiment for Swi6⁽⁸⁰⁻³²⁹⁾. Data were fitted with a two-step isodesmic model. Table indicates the values measured. The sedimentation coefficient of monomer $s(S_1)$ was fixed to 2.0S using the scaling relationship that $s(S_2) \approx s(S_1) \times 2^{2/3}$ for dimer and monomer with similar frictional coefficient. The $s(S_2)$ indicated is the sedimentation coefficient of the dimer

normalized to standard conditions at 20°C. Error represent s.e.m. from three independent experiments.

- d. SV AUC studies of Swi6^{WT} at 16°C in the absence and presence of H3K9me18 tail peptide. The 68% confidence intervals are in parenthesis. The studies here are done differently than those in Fig. 1e. Instead of keeping Swi6 concentration constant and varying H3 tail peptide concentration as in Fig. 1e, here we kept peptide concentration constant at 250µM and varied the concentration of Swi6. In Figure 1e, the concentrations of Swi6 are above the K_d for the CSD-CSD interaction and therefore any weakening of the CD-loop interaction in the dimer will cause a detectable increase in the concentration of the monomer.

Supplementary Figure 5: Characterization of cys-free Swi6^{3S} and Swi6^{probe} with MLS probe on either K94C or G95C residues

- a. Characterization of the Swi6^{3S}: self-association properties by SV AUC, H3K9me3 15mer peptide binding by fluorescence anisotropy and nucleosome binding by fluorescence anisotropy. All the experiments were performed at 24°C. 95% confidence interval in parenthesis. Errors represent s.e.m.
- b. Fluorescence anisotropy studies of 15mer H3K9me3 peptide binding by Swi6^{WT} (blue), Swi6^{3S-G95C} (orange) and Swi6^{probe} (MSL on G95C, green). Affinities for 15mer H3K9me3 peptide for the above three constructs are 7µM, 50µM and 60µM respectively.

- c. Representative fit of an EPR spectrum: data (grey) acquired at 4°C for Swi6^{probe} (MSL on G95C), fit (black), residuals (orange). The percentage of probe immobile was determined by deconvolution of the spectrum into a mobile and immobile component (see methods).
- d. Comparative SV AUC and EPR analyses at 4°C of Swi6^{ProbeK94-WT} and Swi6^{ProbeK94-DimerX}. These proteins are labeled with an MSL probe at residue K94C. c(s) is the sedimentation coefficient distribution. In the EPR spectra, the horizontal axis is the magnetic field and the vertical axis is the derivative of absorbance. Mobile and immobile components are shown by dashed arrows.
- e. Change in the percent MSL probe immobilized for Swi6^{ProbeK94-WT} (MSL on K94C residue) at 4°C as a function of 18mer H3K9me3 or H3K9 peptide. Swi6 monomer concentration: 20µM.

Supplementary Figure 6: Characterization of CFP-Swi6 and Swi6-CFP by negative stain EM and SV AUC studies

- a. 2D class averages of CFP-Swi6 (77 classes) obtained from a total of 4000 particles.
- b. 2D class averages of Swi6-CFP (144 classes) obtained from a total of 3000 particles.
- c. Quantification of the dimerization association constant (K_{obs}^{dim}) at 30°C. $K_{obs}^{dim} = 1.74\mu\text{M}^{-1}$ ($1/K_{obs}^{dim} = 0.57\mu\text{M}$) for CFP-Swi6 and $K_{obs}^{dim} = 16\mu\text{M}^{-1}$ ($1/K_{obs}^{dim} = 0.062\mu\text{M}$) for Swi6-CFP. Errors (n=3) represent s.e.m.

For the analysis of both CFP-Swi6 and Swi6-CFP SV AUC data, we assumed that the shape of a monomeric Swi6 with a CFP-tag, at either the C- or N-terminus, would not differ drastically. We determined the value of the sedimentation coefficient of monomeric Swi6-CFP ($\sim 3S$) by floating both $s(S_1)$ and $s(S_2)$ in the analysis of the Swi6-CFP SV data, and then used that value for the CFP-Swi6 protein as well.

Supplementary Figure 7: Cryo-EM studies of the nucleosome core particle and the Swi6-H3K₉me₃ nucleosome complex

- a. Left: Representative view of 2D-class averages and correspondent reprojections of the cryo-EM structure of the nucleosome. The nucleosome used had a 60bp flanking DNA in addition to the 147bp that wrap around the octamer. Right: Fourier Shell Correlation (FSC) curve of 3D reconstruction of the nucleosome. The resolution of the 3D reconstruction is estimated from FSC=0.5 as $\sim 16.5\text{\AA}$.
- b. Top: View of 2D-class averages and correspondent reprojections of the cryo-EM structure of the Swi6-H3K₉me₃ nucleosome complex. The 2D-class averages and correspondent reprojections that better show the presence of additional densities on either side of the nucleosome are circled in red. Bottom: Fourier Shell Correlation (FSC) curve of 3D reconstruction of the Swi6-H3K₉me₃ nucleosome. The resolution of the 3D reconstruction is estimated from FSC=0.5 as $\sim 25\text{\AA}$.

Supplementary Figure 8: Nucleosome binding studies of Swi6^{WT}, Swi6^{LoopX},

Swi6^{DimerX} and Swi6^{EW} and DNA binding studies for Swi6^{WT}, Swi6^{LoopX}, Swi6^{ΔNCD}

- a. Tryptophan fluorescence studies of Swi6^{LoopX} with H3K9me3 (green) and H3K9 (grey) tail peptide. The red dashed line indicates the half-maximum intensity. The green dashed line indicates the measured K_d (1.3 μ M) for the methylated peptide. The grey dashed line indicates the measured K_d (56.3 μ M) for the unmethylated peptide.
- b. Fluorescence anisotropy studies of nucleosome binding by Swi6^{WT} (blue), Swi6^{LoopX} (green), Swi6^{DimerX} (red) and Swi6^{EW} (orange). Top: Schematics of the unmodified (H3K9) and methyl lysine analog (MLA) H3Kc9me3 mononucleosomes assembled on the 147 bp 601 sequence. The fluorescein probe (green star) is attached by a flexible linker at one end of the 147 bp DNA. Bottom: Filled circles are for MLA nucleosomes; open circles are for unmodified nucleosomes. Summary of the dissociation constants (K_d) measured are in Figure 5b.
- c. Fluorescence anisotropy studies of 20 bp DNA binding by Swi6^{WT} (blue), Swi6^{LoopX} (green), Swi6^{ΔNCD} (white), Swi6^{WT} + 100 μ M H3K9 18-mer peptide (grey) and Swi6^{WT} + 100 μ M H3K9me3 18-mer peptide (red). Summary of the association constants (K_a) measured are in Figure 5c.

Supplementary Figure 9: *In vivo* studies of $swi6^{WT}$, $swi6^{LoopX}$, $swi6^{AcidicX}$

- a. Top: Schematics of centromere 1 with the *ura4+* reporter gene inserted in the *inner most repeat (imr)* region. Bottom: Silencing assay comparing three independent isolates of $swi6^{WT}$, $swi6^{LoopX}$, $swi6^{AcidicX}$ in the pericentromeric *ura4+* reporter strain background. Cells were plated on non-selective YS media (YS) and YS media with 5-FOA (YS + 5-FOA).
- b. $swi6^{LoopX}$ and $swi6^{AcidicX}$ mutants strongly decrease H3K9 methylation levels at the centromeric *dg* repeat in a *dcr1Δ* background. Errors represent s.e.m from three independent IPs.
- c. SDS-PAGE gel of $Swi6^{WT}$ and $Swi6^{AcidicX}$ recombinantly expressed in *E. coli*. $Swi6^{AcidicX}$ runs faster due to the substitution of the negative charge stretch of glutamates with alanines. This same effect is observed for the *S. pombe* proteins in Figure 6b.

Supplementary Methods

Protein cloning and purification

Full length Swi6 was cloned into pET30a (Novagen), mutants were made using site directed mutagenesis and proteins were purified from *E. coli* as described previously¹. Except for the CFP-tagged proteins, all other Swi6 protein purifications yield final proteins that are devoid of N- or C-terminal tags. Protein concentrations of all Swi6 construct samples were measured by UV absorption at 280 nm and calculated using the experimentally determined extinction coefficient (see Analytical Ultracentrifugation section). To ensure that there was not any DNA contamination, we measured the 260/280 ratio for every purified protein. On average, the value of the 260/280 ratio was ~ 0.5.

Nucleosomes Assembly

For all studies with nucleosomes, except the cryoEM studies of nucleosomes alone, core mononucleosomes were assembled on 147 bp of DNA using the 601 positioning sequence, containing a Pst1 site 18 bp in from the 5' end. For the cryoEM of nucleosomes alone, 207 bp of DNA containing the 601 sequence at one end was used. The DNA was amplified by PCR and gel purified. The DNA fragment was assembled into mononucleosomes with recombinant *Xenopus laevis* histones by salt dialysis over 48-60 hrs². Reconstituted mononucleosomes were purified using a glycerol gradient. Methyl Lysine Analog (MLA) containing nucleosomes were prepared as before³. All histone octamer assemblies, nucleosome assemblies and nucleosome purifications were performed in the presence of 2 mM DTT to maintain the MLA modification.

Mononucleosomes were quantified by ethidium bromide staining and using DNA standards.

Tryptophan Fluorescence Studies

The association between Swi6 proteins and the H3 peptides were measured based on following the increases in the internal fluorescence of W104 (one of the three residues in the aromatic cage) using an ISS K2 fluorimeter at 30°C. The H3 peptide used was an 18mer (amino acid 1 to 18). Samples containing 200nM Swi6 protein in 20mM HEPES pH 7.5, 150mM KCl and 1 mM DTT were mixed with increasing concentrations of each H3 peptide, tri-methylated or unmethylated at lysine 9. After an incubation for 10min at 30°C, the fluorescence of W104 was measured with the incident wavelength of 295 nm, and the emission spectrum was collected between 300 and 380 nm. The fluorescence intensity F_{obs} at 330 nm was plotted as a function of peptide concentration. A 1:1 binding model was fit to the data using Graphpad Prism and the following set of equations:

$$F_{obs} = \frac{(F_{max}[H3_p] + F_{min}K_d)}{([H3_p] + K_d)}$$

F_{max} is the fluorescence at saturating peptide, F_{min} is the fluorescence in the absence of peptide and $[H3_p]$ represents the H3 tail peptide. The obtained K_d values were averaged over two or three independent sets of data. To compare the binding of WT and mutant Swi6, F_{obs} was converted to fraction bound with the following equations:

$$F_{obs} = \frac{(F_{obs} - F_{min})}{(F_{max} - F_{min})}$$

Fr_{bound} was then plotted versus $[H3_p]$ using the following equation:

$$Fr_{bound} = \frac{([H3_p])}{([H3_p] + K_d)}$$

Fluorescence Polarization (FP) Studies

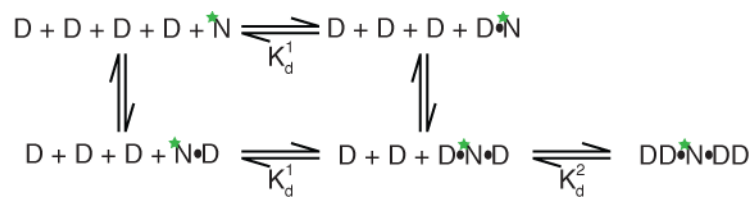
Fluorescence polarization based measurements of binding to H3 tail peptides, DNA and nucleosomes were performed in buffer containing 20 mM HEPES pH 7.5, 150 mM KCl, 1mM DTT and 0.01% NP40 at 24°C. 5-10 nM of peptide, DNA or nucleosomes were used and Swi6 concentrations were varied. The binding reaction was incubated for 30 min at room temperature and fluorescence polarization was measured using a Molecular Devices HT Analyst with excitation and emission wavelengths of λ_{ex} =480nm and λ_{em} =530nm, respectively. The H3 peptide used was a 15mer (amino acid 1 to 15) labeled at the N-terminus with a fluorescein probe (FAM). The peptide was synthesized by Genscript Piscataway, NJ, USA. The 20mer DNA used in the DNA binding assay was 5' labeled with 5,6 carboxy-fluorescein (IDT). The DNA to assemble fluorescent nucleosomes was labeled on one end by amplifying the sequence using PCR with a primer covalently linked to 6-carboxyfluorescein by a 6-carbon linker (IDT). All the data were analyzed using Graphpad Prism.

The peptide and DNA binding data were fit by the following equation:

$$F_{obs} = \frac{(F_{max}[Swi6] + F_{min}K_d)}{([Swi6] + K_d)}$$

F_{obs} is the fluorescence polarization signal observed, F_{min} is the fluorescence polarization signal for the probe alone (peptide or DNA), and F_{max} is the fluorescence polarization signal at saturating $[Swi6]$. The obtained K_d values were averaged over three or more independent sets of data.

The following model was used to fit the nucleosome binding data to account for Swi6-Swi6 oligomerization that is scaffolded by the Swi6-nucleosome complex. Because the fluorescent probe is located only on one-end of the DNA (green star), we made the assumption that changes in fluorescence polarization reflects binding of Swi6 on one-side of the nucleosome. We hypothesized that binding to the other side occurs independently and it is invisible to our assay:



D indicates a Swi6 dimer, $D \cdot N \cdot D$ is the Swi6 nucleosome complex, and $D \cdot D \cdot N \cdot D \cdot D$ is the Swi6 nucleosome complex bound by additional Swi6 dimers. The FP nucleosome data were fitted using the following equation:

$$F_{obs} = \frac{(F_0 K_d^1 K_d^2 + F_1 [Swi6] K_d^2 + F_2 [Swi6]^2)}{(K_d^1 K_d^2 + [Swi6] K_d^2 + [Swi6]^2)}$$

where F_{obs} is the fluorescence polarization signal observed, F_0 is the fluorescence polarization signal for the nucleosome alone, F_1 is the fluorescence polarization signal of the saturated Swi6-nucleosome complex, F_2 is the fluorescence polarization signal of due to the oligomerization of Swi6 scaffolded by the Swi6-nucleosome complex, K_d^1 is the dissociation constant for the Swi6-nucleosome complex, and K_d^2 is the dissociation constant for Swi6-Swi6 scaffolded by the Swi6:nucleosome complex. Data comparing Swi6 WT to the mutants were globally analyzed: the F_0 , F_1 , and F_2 were fix among all proteins while the K_d^1 and K_d^2 were floated.

Analytical Ultracentrifugation (AUC) Studies

Swi6 proteins were individually dialyzed into 20 mM HEPES pH 7.5, 150 mM KCl and 1 mM DTT overnight. Swi6 proteins were quantified by UV absorption at 280nm. We experimentally determined Swi6^{WT} extinction coefficient by recording both interference fringes and UV absorbance at 280nm for a given Swi6 sample. We then converted the number of interference fringes observed into mg Swi6/ml using an average refractive increment of 4.1 fringes/mg/ml. Using this estimated concentration and the absorbance value at 280nm, we then calculated the extinction coefficient at 280nm to be 36,880 M⁻¹ cm⁻¹. Simultaneous detection of protein by UV at multiple wavelengths allowed for the determination of the extinction coefficients at 230nm and 250nm (13,650 M⁻¹ cm⁻¹ and 221000 M⁻¹ cm⁻¹, respectively).

All sedimentation experiments were conducted using an analytical ultracentrifuge (Beckman Coulter, Brea, CA) equipped with either sole absorption optical scanner (Optima XLA) or both absorption and interference optics scanner (Optima XLI). Global analysis of SE and SV isotherm data was performed using the SEDPHAT software. Error estimates were calculated based on replicates of three or more experiments and confidence intervals based on F-statistics and the error projection method. Partial-specific volume (v), solution density (ρ), solution viscosity (η) were calculated in SEDNTERP.

Sedimentation Equilibrium (SE): Sedimentation equilibrium experiments were conducted at 8°C in an Optima XLI/A at rotor speeds of 6K, 11K, and 18K rpm in double-sector centerpieces with sample volumes of 170 μ l. Absorbance data, at wavelengths of 280, 250, and 230nm, and IF data were acquired from samples at five different loading concentrations at all rotor speeds. Global analysis of data at different wavelengths and rotor speeds was conducted with the software SEDPHAT, using Boltzmann exponentials representing the predicted concentration profiles of each species in chemical equilibrium, with amplitudes at all radii constrained by the mass action law:

$$c_{tot} = c_1 + nKc_1^n + \sum_{i=1}^{\infty} (n + im)Kc_1^n (Lc_1^n)^i$$

in combination with the method of implicit mass conservation, using the bottom position of each solution column as an adjustable parameter. In the above equation, c_{tot} is the

total protein concentration, c_1 is the concentration of Swi6 monomer, n is the number of Swi6 subunits that self-associate in the first-step of association ($n=2$ for dimer formation), m is the molecularity of the chain elongation unit ($m=2$ for a dimeric chain elongation unit), K is the association constant for Swi6 dimerization (Kd_{obs}^{dim}), L is the association constant for Swi6 isodesmic chain elongation (Kd_{obs}^{iso})⁴. Summation of terms was carried out to a relative numerical precision of 10^{-6} .

Sedimentation Velocity (SV): Samples volumes of 400 μ l at an overall final OD between 0.1 and 1.0, were pipetted into double-sector centerpieces, and inserted in an 8-hole rotor, which was placed in the temperature pre-equilibrated AUC chamber. An additional incubation period of 1-2 hours was added with the rotor at rest and under vacuum for temperature equilibration. For experiments performed at 4°C, the samples were left equilibrating under vacuum overnight. Runs were performed at a rotor speed of 50,000 rpm for more than 12 hours. Scans were collected following UV at 230, 250 and 280nm, scanned with a radial step size of 0.003 cm in continuous mode, and/or using the interference system. Data were analyzed using a $c(s)$ continuous distribution of Lamm equation solutions with the software SEDFIT, followed by integration and assembly into an isotherm of weighted-average s-values. The isotherm was modeled in SEDPHAT with mass action based models for the weighted-average s-value

$$s_w(c_{tot}) = \left[c_1 s_1 + n K c_1^n s_n + \sum_i (n + im) K c_1^n (L c_1^m)^i s_n \left(\left(\frac{n+im}{n} \right) \right)^k \right] \frac{1}{c_{tot}} (1 - k_s c_{tot} M_1)$$

assuming a power law for the sedimentation coefficients of oligomeric species with $\alpha = 0.566$ (consistent with increasingly elongated oligomers; this value was pre-determined from the global fit of SE and SV on an extensive data set), in combination with an overall hydrodynamic non-ideality term of magnitude $k_s = 0.01$ ml/g. As in the equation above, c_{tot} is the total protein concentration, c_1 is the concentration of Swi6 monomer, n is the number of Swi6 subunits that self-associate in the first-step of association ($n=2$ for dimer formation), m is the molecularity of the chain elongation unit ($m=2$ for a dimeric chain elongation unit), K is the association constant for Swi6 dimerization (Kd_{obs}^{dim}), L is the association constant for Swi6 isodesmic chain elongation (Kd_{obs}^{iso}), s_1 is the sedimentation coefficient of Swi6 monomer and s_n is the sedimentation coefficient of Swi6 dimer ($n=2$).

Rationale for different temperatures:

(i) To obtain a model for Swi6 self-association we performed SE and SV AUC studies at 8°C. SE experiments are ~1 week long, so a temperature of 8°C was used to stabilize the protein. Global analysis of both SE and SV AUC at 8°C allowed us to obtain a thermodynamic information for Swi6 self-association as well as hydrodynamic parameters for Swi6 monomer, dimer and oligomers that were used in all the SV experiments performed at higher temperatures.

(ii) To compare dimerization properties between Swi6 mutants, we had to performed the experiments at 30°C because dimerization is too tight at lower temperatures.

(iii) The EPR experiments were done at 4°C to stabilize the probe labeled Swi6 proteins. Therefore the corresponding AUC experiments were also done at 4°C.

Electron Paramagnetic (EPR) Studies

EPR measurements were performed with a Bruker Instruments EMX EPR spectrometer (Billerica, MA). First derivative, X-band spectra were recorded in a high-sensitivity microwave cavity using 50-s, 100-Gauss wide magnetic field sweeps. The instrument settings were as follows: microwave power, 25 mW; time constant, 164 ms; frequency, 9.83 GHz; modulation, 1 Gauss at a frequency of 100 kHz. Each spectrum used in the data analysis was an average of 10-40 50 seconds sweeps from an individual experimental preparation. Swi6^{3S} was labeled by reacting the sole cysteine residue (either K94C or G95C) with the EPR probe 4-maleimido-2,2,6,6-tetramethyl-1-piperidinyloxy (MSL, Sigma Aldrich, St. Louis, MO). The protein was first dialyzed overnight in a buffer containing 20mM HEPES, 150mM KCl, pH7.5. It was then incubated with MSL using a 2-fold molar excess of MSL to protein concentration. The mixture was then left to react for 4 hrs at 4°C. The excess label was removed by a microcon concentrator (mwt cut off 10 kDa), followed by an additional overnight dialysis step into the above buffer. The protein sample was incorporated into a 25µl capillary and the EPR spectrum was recorded. The temperature of the sample was controlled by blowing dry air (warm or cool) into the cavity and monitored using a thermistor placed close to the experimental sample. To stabilize the Swi6^{probe} WT and mutants we performed the EPR and AUC experiments at 4°C.

The spectra were deconvoluted into mobile and immobile spectral components using the protocols of Purcell *et al*⁵.

Electron Microscopy (EM) and Image Processing

Negative Stain EM of CFP-Swi6 and Swi6-CFP: Proteins were dialyzed overnight in 20 mM HEPES pH 7.5, 150 mM KCl and 1mM DTT. 2.5mL of CFP-Swi6 at 0.34 μ M and of Swi6-CFP at 0.1 μ M was absorbed to a glow-discharged copper grid coated with carbon film for 30 seconds followed by conventional negative stain with 0.75% uranyl formate. Images were collected using a Tecnai T12 microscope (FEI company, Hillsboro, OR) with a LaB₆ filament and operated at 120 kV accelerating voltage. All images were recorded at a magnification of 67,000 with an UltraScan 4096 x 4096 pixel CCD camera (Gatan Inc, USA).

All images were 2x2 pixel binned to the final pixel size of 3.46 Å before any further processing. A total of 5000 and 3000 particles for CFP-Swi6 and Swi6-CFP respectively were selected from ~50 images using the display program SamViewer (written by Maofu Liao). All subsequent image processing was performed using SPIDER⁶ and FREALIGN⁷.

Cryo-EM Studies of the nucleosome and Swi6-nucleosome complex: Cryo-EM data were collected using Tecnai TF20 electron microscope equipped with a field emission gun (FEI Company, USA) and operated at 120kV (for the nucleosome) or at 200kV (for the Swi6-nucleosome complex). Images were collected at a nominal magnification of 62 kV using a TemF816 8K x 8K CMOS camera (TVIS, Germany).

Nucleosome alone: All images were binned by a factor of 2 (2.39 Å/pixel) for further processing. Defocus values were determined for each micrograph using CTFFIND⁸ and

ranged from -1.5 μ m to -3 μ m. A total of 13629 particles were selected and classified into 100 2D-class averages. 3D reconstructions were calculated and refined using GeFREALIGN⁷. The initial model was generated by filtering the atomic structure of the nucleosome (PDB 1KX5) to 35Å (command `pdb2mrc` from EMAN package)⁹. The resolution was estimated to be ~16.5Å, based on Fourier Shell Correlation (FSC) = 0.5 criteria. This same resolution was also obtained when the atomic structure of the nucleosome (PDB 1KX5) was filtered to greater than 35Å.

Swi6:H3K_c9me3 nucleosome complex: Swi6 was dialyzed overnight in 20 mM HEPES pH 7.5, 150 mM KCl and 1mM DTT. The binding reaction was set such that a) both nucleosome and Swi6 concentrations were above the K_d value measured by FP and b) the Swi6 concentration was sufficient to titrate all the nucleosomes as assayed by native gel shift. Those same conditions were used previously to measure the stoichiometry of the complex by SV AUC and are known to result in homogenous samples.

A total of 5,000 particles were selected and classified into 200 2D-class averages and all were included in the final 3D reconstruction. The cryo-EM 3D reconstruction of the nucleosome alone was low pass filtered to 35Å and used as the initial model for 3D refinement of the complex. 2D symmetry was applied during the refinement for the reasons described in the main text. The resolution of the final 3D reconstruction was estimated to be ~25Å, based on Fourier Shell Correlation (FSC) = 0.5 criteria. This same resolution was also obtained when the cryo-EM 3D reconstruction of nucleosome alone was low pass filtered to greater than 35Å. 3D reconstructions were visualized by UCSF

Chimera. The “Fit in Map” function of Chimera was used to dock the atomic structure of the nucleosome (PDB 1KX5) into the 3D volume¹⁰.

Silencing Assays

The strains were grown overnight to saturation and diluted to OD₆₀₀ of 1 at the highest dilution. Serial dilutions were performed with dilution factor of 5 and cells were grown on non-selective (YS) and 5-FOA (2 grams/liter of 5-fluoroorotic acid) containing media for *ura4+* reporter at 30°C for 2-3 days.

Quantifying Swi6 protein levels *in vivo*

Swi6 protein levels were quantified using polyclonal antibodies raised in Rabbits by injecting recombinant Swi6.

Chromatin Immunoprecipitation

The ChIP assay was performed as described previously¹¹. Cells were lysed at 4 °C by bead beating 7 times for 1 min each with 2 min rests on ice. Chromatin fraction was sonicated 20 times for 30s each with 1-min rest in between cycles using Bioruptor.

Ab1220 (Abcam) was used for H3K9me2 ChIP and Protein A Dynabeads were used in the washing steps.

References for Methods:

1. Canzio, D. *et al.* Chromodomain-mediated oligomerization of HP1 suggests a nucleosome-bridging mechanism for heterochromatin assembly. *Molecular cell* **41**, 67–81 (2011).
2. Luger, K., Rechsteiner, T. J. & Richmond, T. J. Preparation of nucleosome core particle from recombinant histones. *Methods In Enzymology* **304**, 3–19 (1999).
3. Simon, M. D. Installation of site-specific methylation into histones using methyl lysine analogs. *Current protocols in molecular biology / edited by Frederick M. Ausubel ... [et al.] Chapter 21*, Unit 21.18.1–10 (2010).
4. Vistica, J. *et al.* Sedimentation equilibrium analysis of protein interactions with global implicit mass conservation constraints and systematic noise decomposition. *Analytical biochemistry* **326**, 234–256 (2004).
5. Purcell, T. J. *et al.* Nucleotide pocket thermodynamics measured by EPR reveal how energy partitioning relates myosin speed to efficiency. *Journal of molecular biology* **407**, 79–91 (2011).
6. Frank, J. *et al.* SPIDER and WEB: processing and visualization of images in 3D electron microscopy and related fields. *Journal of structural biology* **116**, 190–199 (1996).
7. Li, X., Grigorieff, N. & Cheng, Y. GPU-enabled FREALIGN: accelerating single particle 3D reconstruction and refinement in Fourier space on graphics processors. *Journal of structural biology* **172**, 407–412 (2010).
8. Mindell, J. A. & Grigorieff, N. Accurate determination of local defocus and specimen tilt in electron microscopy. *Journal of structural biology* **142**, 334–347 (2003).
9. Ludtke, S. J., Baldwin, P. R. & Chiu, W. EMAN: semiautomated software for high-resolution single-particle reconstructions. *Journal of structural biology* **128**, 82–97 (1999).
10. Pettersen, E. F. *et al.* UCSF Chimera--a visualization system for exploratory research and analysis. *Journal of computational chemistry* **25**, 1605–12 (2004).
11. Rougemaille, M., Shankar, S., Braun, S., Rowley, M. & Madhani, H. D. Ers1, a rapidly diverging protein essential for RNA interference-dependent heterochromatic silencing in *Schizosaccharomyces pombe*. *The Journal of biological chemistry* **283**, 25770–3 (2008).

Supplementary Table 1: List of Swi6 constructs used in this study

Name	Construct	Mutations
Swi6 ^{WT}	Full-length	WT sequence
Swi6 ^{LoopX}	Full-length	R94A-K94A
Swi6 ^{DimerX}	Full-length	L315D
Swi6 ^{AcidicX}	Full-length	E(74-80)A
Swi6 ^{CageX}	Full-length	W104A
Swi6 ^{EW}	Full-length	V82E-Y131W
Swi6 ^{3S}	Full-length	C121S-C124S-C310S
Swi6 ^{3S-G95C}	Full-length	Swi6 ^{3S} with G95C
Swi6 ^{Probe-WT}	Full-length	Swi6 ^{3S} with probe on G95C
Swi6 ^{Probe-LoopX}	Full-length	Swi6 ^{3S} with probe on G95C and R94A-K94A mutations
Swi6 ^{Probe-DimerX}	Full-length	Swi6 ^{3S} with probe on G95C and L315D mutation
Swi6 ^{Probe-AcidicX}	Full-length	Swi6 ^{3S} with probe on G95C and E(74-80)A mutation
Swi6 ^{ProbeK94-WT}	Full-length	Swi6 ^{3S} with with probe on K94C
Swi6 ^{ProbeK94-DimerX}	Full-length	Swi6 ^{3S} with with probe on K94C and L315D mutation
Swi6 ^{ANCD}	aa 138-329	WT sequence
Swi6 ⁽⁸⁰⁻³²⁹⁾	aa 80-329	WT sequence
CFP-Swi6	CFP-fusion at N-terminus	Swi6 WT sequence
Swi6-CFP	CFP-fusion at C-terminus	Swi6 WT sequence

Supplementary Table 2: List of *S. pombe* strains used in this study

Name	Genotype
PM0251	P(h+), ura4-DS/E, ade6-M210, leu1-32, imr1L(NcoI)::ura4, otr1R(Sph1)::ade6
PM1978	PM0251, <i>swi6</i> Δ::KanMX
PM1981	PM0251, <i>swi6</i> ::KanMX
PM1945	PM0251, <i>swi6</i> (R93A-K94A)::KanMX
DC19	PM0251, <i>swi6</i> (E74-80A)::KanMX
DC27	PM0251, <i>swi6</i> Δ::KanMX::KanMX, <i>dcr1</i> Δ::NatMX
DC30	PM0251, <i>swi6</i> ::KanMX::KanMX, <i>dcr1</i> Δ::NatMX
DC32	PM0251, <i>swi6</i> (R93A-K94A)::KanMX::KanMX, <i>dcr1</i> Δ::NatMX
DC35	PM0251, <i>swi6</i> (E74-80A)::KanMX::KanMX, <i>dcr1</i> Δ::NatMX

Chapter 4:

Characterization of the self-association and ligand binding
properties of Swi6 domains in isolation

Introduction

HP1 proteins contain three recognized protein domains: 1) a chromodomain (CD), 2) an evolutionarily related chromoshadow domain (CSD), and 3) a poorly defined hinge (H) region between the CD and CSD (Vermaak and Malik, 2009). We, and others, have studied the functions of the individual domains to understand how their activities are integrated into the full-length protein to allow stable recognition of the physiological template, H3K9 methylated chromatin. Below is the summary of unpublished data regarding each of the domains of Swi6.

Results and Implications

The chromodomain (CD)

The chromodomain (CD) is part of a family of proteins that contain a specialized hydrophobic cage, formed by aromatic residues, that bind methyl marks on histones with high specificity but micromolar affinity (Bannister et al., 2001; Jacobs and Khorasanizadeh, 2002; Nielsen et al., 2002). In Chapter 2 and 3, we have shown that the CD of Swi6 also bears an interface for CD-CD mediated Swi6 self-association. In particular, in Chapter 3, we show that such interface relies on a loop (the ARK loop) that contains a sequence that mimics that H3 tail sequence. Unbound Swi6 dimers mainly exist in an autoinhibited state where the ARK loop from one CD blocks H3K9 methyl binding recognition of the other CD. The same loop that stabilizes the auto-inhibited state of Swi6 dimers, when flipped into the open state, assists in binding nucleosomes and in promoting self-association of Swi6 dimers.

a. The acidic stretch in the CD plays multiple functions in Swi6

Located on the N-terminal of the CD, there is a stretch of acidic residues (amino acid 74-80) that, in Chapter 3, we show to be important for both H3 tail and ARK loop binding (Figure 1a and b). Our data are consistent with previously published work on the binding of the H3 tail by HP1 (Hiragami-Hamada et al., 2011).

Here we show that a CD construct lacking 6 out of the 7 acidic residues (aa 80-138) dimerizes with an affinity constant of $\sim 2\text{mM}$ (Figure 1c). Extension of this construct to the rest of the acidic residues in the stretch (aa 1-138), increases both CD-CD dimerization and H3K9me3 tail binding by 3-fold (Figure 1c and d). These data are in agreement with the data shown in Chapter 3 for the full-length protein, Swi6^{WT} and Swi6^{AcidicX}.

Interestingly, in comparing Swi6^{WT}, Swi6^{AcidicX} and Swi6^{EW} binding to nucleosomes and to a 20mer DNA, we noticed that mutating the acidic stretch to alanines in Swi6^{AcidicX} decreases Swi6's ability to discriminate between methylated and unmethylated nucleosomes by ~ 20 fold (Figure 1e). These same mutations, though, result in increasing binding for a 20mer DNA by ~ 4 fold (Figure 1e). The opposite effect was observed for Swi6^{EW} (Figure 1e). This mutant has an extra glutamate on position 82, one amino acid away from the acidic stretch (See Chapter 2 for more details). This mutant increases Swi6 ability to discriminate between methylated and unmethylated nucleosomes by ~ 3 fold but also decreases binding to the 20mer DNA by

~ 2 fold (Figure 1e). It is tempting to speculate that the V82E mutation in the Swi6^{EW} (See Chapter 2 for more details) adds to the nearby acidic stretch of residues.

All together, the data presented here so far argue that the acidic stretch in Swi6 CD has at least two functions in the formation of the Swi6-nucleosome complex: (1) to increase the affinity for nucleosomes by directly interacting with residues of the H3 tail; and (2) to prevent Swi6 dimers from binding nucleosomes in non-specific modes, thus increasing the overall specificity for methylated nucleosome templates (for more discussion on specific and non-specific modes of binding see also Chapter 2).

b. Methylation of ARK loop peptides increases affinity to the CD

If the ARK loop would sit in the CD mimicking the H3 tail (Figure 2a) then, a simple prediction of this model is that the CD should show specificity for the degree of methylation on lysine 94 on the ARK loop. We indeed observed that Swi6 CD (aa 80-138) is able to specifically discriminate for Swi6 peptides that containing me3, me2, me1 or me0 at lysine 94 (Figure 2b). Interestingly, the magnitude of the specificity between me3 and the rest of the peptides is consistent with the magnitude of CD specificity for H3 tail peptides measured by us and others (Yamada et al., 2005; Canzio et al., 2011).

The chromoshadow domain (CSD)

The chromoshadow domain (CSD) is involved in dimerization of HP1 proteins and is important for the silencing function of HP1 proteins (Yamada et al., 1999; Brasher et

al., 2000; Cowieson et al., 2000) and in reading PxVxL pentapeptide motifs and other sequences present in different protein partners (Smothers and Henikoff, 2000; Mendez et al., 2011).

a. Thermodynamic analysis of CSD dimerization

CSD dimerization is important for HP1 function *in vivo* (Yamada et al., 1999; Brasher et al., 2000; Cowieson et al., 2000). While it is believed that such an effect is mainly due to the CSD domain functioning as a hub for many other protein factors involved in heterochromatin assembly, we have shown that the CSD dimerization is also important for binding to nucleosomes (See following section).

Based on these observations, it appears clear that regulation of the CSD domain is crucial for heterochromatin assembly. To better understand the nature the CSD dimerization (Figure 3a), we have performed Analytical Ultracentrifugation (AUC) studies to assess its thermodynamic properties (for methods, see Methods Chapter 3). We observed that the CSD dimer is very stable ($T_m \sim 70^\circ\text{C}$, data not shown) and that the interaction between the two monomers is mainly enthalpically driven given that the affinity strongly decreases with an increase in temperature (Figure 3b). We observed a similar temperature dependent effect on dimerization in the context of the full-length protein (data not shown); however, because of the ARK loop also contributes to the stability of the dimer, dimerization in full-length Swi6 is tighter than the CSD domain alone. Interestingly, contrary to the CSD dimerization, we observed that the isodesmic association of Swi6 dimers slightly increases with increasing temperatures (Figure 1c and 3c). This suggests that oligomerization of dimers may be entropically driven .

Ligands that interact with the CSD domain might regulate the stability of the dimer. While some HP1 protein partners might stabilize the CSD dimer to increase its affinity for chromatin, others might block or destabilize such an interaction to promote release of HP1 from chromatin.

b. Biochemical evidence of the CSD interface binding the nucleosome surface

Histone H3 contains a PxVxL-like motif which has been shown previously to be recognized by the CSD of HP1 (Dawson et al., 2009; Lavigne et al., 2009; Richart et al., 2012). Such a motif is located near the entry/exit site (Figure 4a), and it has been speculated that the nearby DNA must be distorted for the CSD to bind (Richart et al., 2012).

In Chapters 2 and 3, we have shown that (1) the CSD domain contributes energetically to nucleosome binding, and (2) its dimerization is important for Swi6 to discriminate between methylated and unmethylated nucleosomes. We further showed that Swi6^{DimerX} binds methylated nucleosomes with an affinity similar to the sole methylated H3 tails, thus suggesting that Swi6^{DimerX} only binds to the H3 tail in the context of the nucleosome (Figure 4b). We observed a similar effect for a construct of Swi6 that lacks the CSD dimer domain, Swi6¹⁻²⁶¹ (Figure 4b). To directly test whether the CSD domain of Swi6 binds the PxVxL-like motif in H3, we measured its binding by the Swi6⁽¹³⁸⁻³²⁹⁾ (HCSD construct) using fluorescence anisotropy (Figure 4c). We observed that Swi6⁽¹³⁸⁻³²⁹⁾ binds specifically to such motif and that mutation of the valine to alanine, reduces the binding by at least 10-folds.

This data, together with our analysis of the Swi6^{LoopX} and Swi6^{DimerX} in Chapter 3, suggest that the ARK loop and the CSD dimer cooperate to bind to their respective epitopes on the nucleosomes surface, nucleosomal DNA and the H3 PxVxL-like motif respectively. Further evidence of such coupling, is the fact that also LoopX protein binds nucleosomes with an affinity similar to its affinity for the sole H3K9me3 tail (Figure 4c). Interestingly, while Swi6^{LoopX} still retains specificity for methylated nucleosomes, the Swi6^{DimerX} and Swi6¹⁻²⁶¹ do not. We speculate that dimerization of the CSD and its interaction with PxVxL-like motif in H3 might be an additional mechanism by which HP1 proteins engage the nucleosome surface in a mode that promotes binding to the methyl mark (See Chapter 2 for further discussion).

c. Structural evidence that the CSD interface binding the nucleosome surface

Consistent with our biochemical data, is the Cryo-EM structure of the Swi6-nucleosome complex presented in Chapter 4. We observed that the CSD dimer of Swi6 appears engaged with the nucleosome. We also observed that, in contrast to the nucleosome alone structure where density for all the DNA is observed, in the Swi6-nucleosome structure a small amount of DNA density is missing near the entry/exit site (Figure 4c). We speculate that this missing DNA could reflect local DNA distortion due to Swi6.

Finally, we used negative stain EM to locate Swi6^{DimerX} on the nucleosome surface. Compared to Swi6^{WT}, we noticed that Swi6^{DimerX} binds methylated nucleosome in an orientation far away from the H3 tail (Figure 4d). This observation is consistent with our biochemical measurements, suggesting that the CSD dimer plays a fundamental role in

anchoring the Swi6 dimer into its specific orientation and that mutation of such interface in Swi6^{DimerX} drastically reduces the ability of Swi6 to discriminate in favor of methylated nucleosomes (Figure 4b).

Based on all the above data, we propose a model in which the ARK loop in Swi6, together with the hinge region, might serve the purpose to locally disrupt the DNA at the entry/exit site to allow the CSD dimer to bind the PxVxL-like motif in H3. Given that the ARK loop degenerates in higher eukaryotes, it is tempting to speculate that other mechanisms might have evolved to assist HP1 binding to chromatin. One such mechanism might be the use of chromatin remodeling enzymes to locally distort the nucleosome. This hypothesis is consistent with published evidence that both ACF1 and Brg1/Brm remodeling activities are needed to assist HP1 loading onto chromatin both *in vitro* and *in vivo* (Eskeland et al., 2007; Lavigne et al., 2009).

The Hinge region (H)

The H region is thought to be required for binding of HP1 proteins to DNA, as observed *in vitro* (Yamada et al., 1999; Meehan et al., 2003). Such effect raises the possibility that the hinge contributes to affinity rather than to methyl mark specificity.

a. Hinge contribution to Swi6 DNA binding

Using fluorescence polarization methods, we measured binding of Swi6 full-length WT and mutants, and Swi6 domains to either a 20mer or 47mer DNA. We observed that the hinge region alone (H, Swi6¹³⁸⁻²⁶¹) or in the context of the CSD domain (HCSD,

Swi6¹³⁸⁻³²⁹) cannot fully recapitulate the DNA binding affinity of Swi6 WT (WT, Swi6¹⁻³²⁹) for both a 20mer and a 47mer piece of DNA (Figure 5a and b). As shown in Chapter 3, mutations in the ARK loop (R93K94 to A93A94, Swi6^{LoopX}) reduces DNA binding of Swi6 to the level of the Hinge region alone as predicted by a model where the ARK loop together with the Hinge binds DNA (Figure 5a, b and Chapter 3). Interestingly enough, when the Swi6^{DimerX}, Swi6¹⁻²⁶¹ and Swi6⁸⁰⁻³²⁹ were assayed for binding to 20mer DNA, they did not show any effect in DNA binding (Figure 5a). If only based on the model from Chapter 3, these constructs were predicted to have an increase in binding to DNA given that they are mainly in an open state (Chapter 3). These data are consistent with a model where a 20mer DNA can bind to either the close or the open state with similar affinities (Figure 5c). Either mode of binding still requires both the Hinge regions and the ARK loop. We speculate that when a 20mer DNA binds to the close state, then the binding occurs between the Hinge of protomer 1 and the ARK loop of protomer 2 (Figure 5c). When such binding occurs in the open state, then it is the Hinge and the ARK loop from the same protomer that contact the DNA.

When the Swi6¹⁻²⁶¹ was compared to Swi6 WT to bind a 47mer piece of DNA, then Swi6 WT shows a 2 to 3 fold increase in binding (Figure 5b). This effect could be explained with the model that a 47mer DNA is long enough to bridge the two protomers of a Swi6 dimer (Figure 5d). By this model, Swi6 WT would have a higher affinity for a 47mer DNA than Swi6¹⁻²⁶¹.

b. Hinge contribution to Swi6 self-association

In measuring Swi6 self-association, we noticed that a construct of Swi6 that contains the N, the CD, and the Hinge region (Swi6¹⁻²⁶¹) dimerizes 7-fold better than the same construct lacking the Hinge region (Swi6¹⁻¹³⁸) (Figure 1c). Also, Swi6⁽¹⁻²⁶¹⁾ dimerization is similar in magnitude to the K_{obs}^{iso} in full-length Swi6 (Figure 1c). A simple explanation of this observation is that the Hinge region assists the ARK loop in promoting Swi6 self-association. This energetic coupling between the ARK loop and the Hinge region in Swi6 self-association is similar to what we earlier described for DNA binding. Future structural work will reveal how those two regions of the protein are able to couple both self-association and polynucleotide binding activity of HP1 proteins.

References

- Bannister, A.J., Zegerman, P., Partridge, J.F., Miska, E.A., Thomas, J.O., Allshire, R.C., and Kouzarides, T. (2001). Selective recognition of methylated lysine 9 on histone H3 by the HP1 chromo domain. *Nature* *410*, 120–124.
- Brasher, S. V, Smith, B.O., Fogh, R.H., Nietlispach, D., Thiru, A., Nielsen, P.R., Broadhurst, R.W., Ball, L.J., Murzina, N. V, and Laue, E.D. (2000). The structure of mouse HP1 suggests a unique mode of single peptide recognition by the shadow chromo domain dimer. *The EMBO Journal* *19*, 1587–1597.
- Canzio, D., Chang, E.Y., Shankar, S., Kuchenbecker, K.M., Simon, M.D., Madhani, H.D., Narlikar, G.J., and Al-Sady, B. (2011). Chromodomain-mediated oligomerization of HP1 suggests a nucleosome-bridging mechanism for heterochromatin assembly. *Molecular Cell* *41*, 67–81.
- Cowieson, N.P., Partridge, J.F., Allshire, R.C., and McLaughlin, P.J. (2000). Dimerisation of a chromo shadow domain and distinctions from the chromodomain as revealed by structural analysis. *Current Biology : CB* *10*, 517–525.
- Dawson, M.A., Bannister, A.J., Göttgens, B., Foster, S.D., Bartke, T., Green, A.R., and Kouzarides, T. (2009). JAK2 phosphorylates histone H3Y41 and excludes HP1 alpha from chromatin. *Nature* *461*, 819–822.
- Eskeland, R., Eberharter, A., and Imhof, A. (2007). HP1 binding to chromatin methylated at H3K9 is enhanced by auxiliary factors. *Molecular and Cellular Biology* *27*, 453–465.
- Hiragami-Hamada, K., Shinmyozu, K., Hamada, D., Tatsu, Y., Uegaki, K., Fujiwara, S., and Nakayama, J.-I. (2011). N-terminal phosphorylation of HP1 {alpha} promotes its chromatin binding. *Molecular and Cellular Biology* *31*, 1186–1200.
- Jacobs, S. a, and Khorasanizadeh, S. (2002). Structure of HP1 chromodomain bound to a lysine 9-methylated histone H3 tail. *Science (New York, N.Y.)* *295*, 2080–2083.
- Lavigne, M., Eskeland, R., Azebi, S., Saint-André, V., Jang, S.M., Batsché, E., Fan, H.-Y., Kingston, R.E., Imhof, A., and Muchardt, C. (2009). Interaction of HP1 and Brg1/Brm with the globular domain of histone H3 is required for HP1-mediated repression. *PLoS Genetics* *5*, e1000769.
- Meehan, R.R., Kao, C.-F., and Pennings, S. (2003). HP1 binding to native chromatin in vitro is determined by the hinge region and not by the chromodomain. *The EMBO Journal* *22*, 3164–3174.
- Mendez, D.L., Kim, D., Chruszcz, M., Stephens, G.E., Minor, W., Khorasanizadeh, S., and Elgin, S.C.R. (2011). The HP1a disordered C terminus and chromo shadow domain

cooperate to select target peptide partners. *ChemBiochem : a European Journal of Chemical Biology* *12*, 1084–1096.

Nielsen, P.R., Nietlispach, D., Mott, H.R., Callaghan, J., Bannister, A., Kouzarides, T., Murzin, A.G., Murzina, N. V, and Laue, E.D. (2002). Structure of the HP1 chromodomain bound to histone H3 methylated at lysine 9. *Nature* *416*, 103–107.

Richart, A.N., Brunner, C.I.W., Stott, K., Murzina, N. V, and Thomas, J.O. (2012). Characterization of chromoshadow domain-mediated binding of heterochromatin protein 1 α (HP1 α) to histone H3. *The Journal of Biological Chemistry* *287*, 18730–18737.

Smothers, J.F., and Henikoff, S. (2000). The HP1 chromo shadow domain binds a consensus peptide pentamer. *Current Biology : CB* *10*, 27–30.

Vermaak, D., and Malik, H.S. (2009). Multiple roles for heterochromatin protein 1 genes in *Drosophila*. *Annual Review of Genetics* *43*, 467–492.

Yamada, T., Fischle, W., Sugiyama, T., Allis, C.D., and Grewal, S.I.S. (2005). The nucleation and maintenance of heterochromatin by a histone deacetylase in fission yeast. *Molecular Cell* *20*, 173–185.

Yamada, T., Fukuda, R., Himeno, M., and Sugimoto, K. (1999). Functional domain structure of human heterochromatin protein HP1(Hs α): involvement of internal DNA-binding and C-terminal self-association domains in the formation of discrete dots in interphase nuclei. *J Biochem* *125*, 832–837.

Figure Legends:

Figure 1: The role of the acidic stretch in the CD of Swi6

- a. Top: Schematics of Swi6 domains and their correspondent amino acid numbers.
Bottom: Alignment of key residues in the CD in Swi6, dHP1, hHP1.
- b. Left: Schematic representation of the known and previously hypothesized Swi6:H3 tail interactions. Right: Schematic representation of the hypothetical CD:CD interactions. The grey oval represent a region of negative potential generated by acidic the N-terminal of the CD. The brown oval represent the π -cation interactions generated by the three hydrophobic cage residues.
- c. Left: Model of Swi6 self-association. The Swi6 monomer is represented by “S”. A two-step process: (1) a tight association of two Swi6 monomers with association constant ($K_{obs}^{dim} = [S_2]/[S][S]$) and (2) an isodesmic self-association of Swi6 dimers with identical chain elongation affinity constant ($K_{obs}^{iso} = [S_{n+2}]/[S_n][S_2]$). Table indicates the values of K_{obs}^{dim} and K_{obs}^{iso} at T=8°C from global analysis of SE and SV AUC data. Right: Analysis of the self-association properties of different Swi6 constructs obtained by SV AUC.
- d. Quantification of H3K9me3 15mer binding by fluorescence polarization. K_d 2 μ M and 7.52 μ M for Swi6⁽¹⁻¹³⁸⁾ Swi6⁽⁸⁰⁻¹³⁸⁾.
- e. Comparison of nucleosome specificity and DNA binding between Swi6^{WT}, Swi6^{AcidicX}, Swi6^{EW}.

Figure 2: Methylation of the ARK loop its increases affinity for the CD

- a. Simulation of Swi6 CD (PDB 2RSO) dimerization.

- b. Fluorescence polarization studies of Swi6⁽⁸⁰⁻¹³⁸⁾ binding to Swi6 peptides containing different degree of methylation on K94 of the ARK loop.

Figure 3: Thermodynamic analysis of Swi6 chromoshadow domain

- a. Swi6 chromoshadow domain (CSD) structure (PDB 1E0B). In yellow is the residue L315 that when mutated to aspartate disrupts Swi6 dimerization (L315D, Swi6^{DimerX}).
- b. Temperature dependence studies of the CSD dimerization by SE and SV AUC. Except the data at 8°C that were obtained by sedimentation equilibrium (SE), all the others were done by SV AUC.
- c. Isodesmic association of Swi6 WT dimers measured at different temperatures by SV AUC.

Figure 4: The chromoshadow domain of Swi6 binds the nucleosome

- a. Zooming into the structure of the nucleosome (PDB 1KX5). In red is the PxVxL-like on histone H3.
- b. Comparison between Swi6^{WT}, Swi6^{LoopX}, Swi6^{DimerX}, Swi6⁽¹⁻²⁶¹⁾ for H3K9me3 tail, H3K_c9me3 and H3K9 nucleosome binding.
- c. Fluorescence anisotropy binding of Swi6⁽¹³⁸⁻³²⁹⁾ to a PxxVxL and PxxAxL H3 peptides (FAM-PGTVALREIRRYQ and FAM-PGTAALREIRRYQ). K_d 150μM and 1154μM for PxxVxL and PxxAxL peptide respectively. Average of n=2.
- d. Comparison of nucleosome alone structure with Swi6-H3K_c9me3 nucleosome complex to highlight possible missing DNA density (dashed circles) in the Swi6-H3K_c9me3 complex. This structure is the Cryo-EM structure presented in Chapter 3.

- e. 3D reconstruction of the Swi6^{DimerX} and Swi6^{WT} in complex with the nucleosome.
Both structures are negative stain EM based.

Figure 5: Contribution of the Hinge region to DNA binding

- a. Fluorescence anisotropy studies of DNA binding by Swi6^{WT}, Swi6^{LoopX}, Swi6^{Dimer X}, Swi6⁽¹⁻¹²⁶⁾, Swi6⁽⁸⁰⁻³²⁹⁾, Swi6⁽¹³⁸⁻³²⁹⁾, Swi6⁽¹³⁸⁻²⁶¹⁾. Affinity constants for 20mer DNA are: Swi6^{WT}, 0.066 μ M⁻¹; Swi6^{LoopX}, 0.016 μ M⁻¹; Swi6^{Dimer X}, 0.067 μ M⁻¹; Swi6⁽¹⁻¹²⁶⁾, 0.06 μ M⁻¹; Swi6⁽⁸⁰⁻³²⁹⁾, 0.07 μ M⁻¹; Swi6⁽¹³⁸⁻³²⁹⁾, 0.017 μ M⁻¹; Swi6⁽¹³⁸⁻²⁶¹⁾, 0.022 μ M⁻¹. Data for Swi6⁽¹³⁸⁻²⁶¹⁾ is average of n=2; errors (n \geq 3) and represent s.e.m.
- b. Fluorescence anisotropy studies of DNA binding by Swi6^{WT}, Swi6^{LoopX}, Swi6⁽¹⁻¹²⁶⁾, Swi6⁽¹³⁸⁻²⁶¹⁾. Affinity constants for 47mer DNA are: Swi6^{WT}, 0.3 μ M⁻¹; Swi6^{LoopX}, 0.04 μ M⁻¹; Swi6⁽¹⁻¹²⁶⁾, 0.1 μ M⁻¹; Swi6⁽¹³⁸⁻²⁶¹⁾, 0.04 μ M⁻¹. Data for Swi6⁽¹³⁸⁻²⁶¹⁾ is average of n=2; errors (n \geq 3) and represent s.e.m.
- c. Schematics of DNA binding by Swi6 when the DNA is 20bp long. Swi6 binds DNA in either its closed or open state with the same affinity. In either case, both the hinge and the ARK loop in the CD help stabilize the 20mer DNA. In the case of the closed state, we speculate that the DNA is stabilized by contacts from the hinge region of one monomer and the ARK loop of the other.
- d. Schematics of DNA binding by Swi6 when the DNA is 47bp long. Swi6 binds DNA in either its closed or open state with the same affinity. In either case, both the hinge and the ARK loop in the CD help stabilize the 20mer DNA. A 47mer DNA is long enough to be stabilized by a binding site that overlaps both monomers.

FIGURE 1

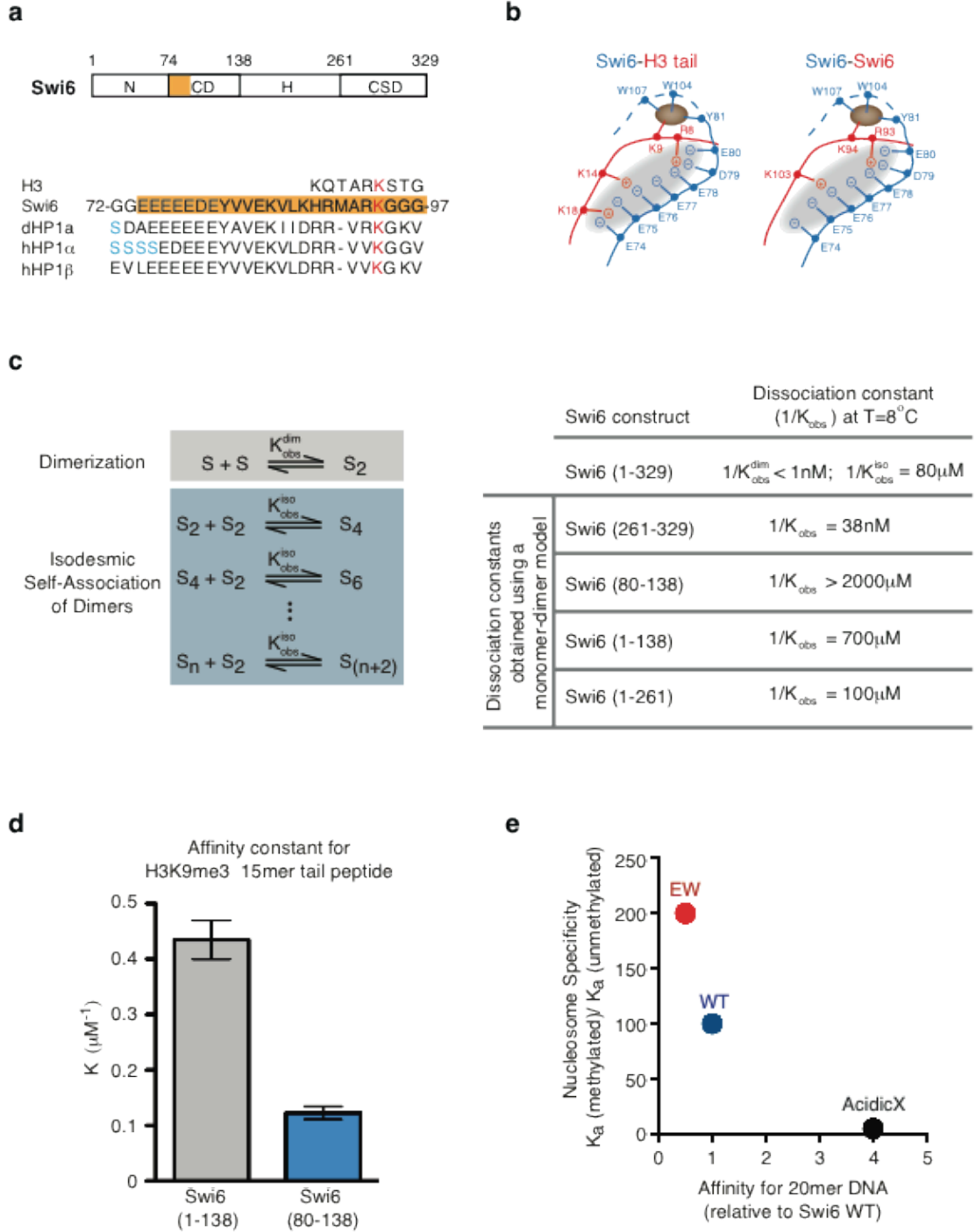
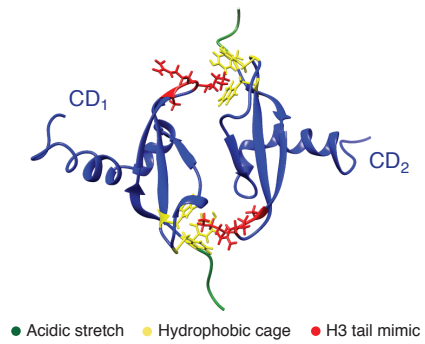
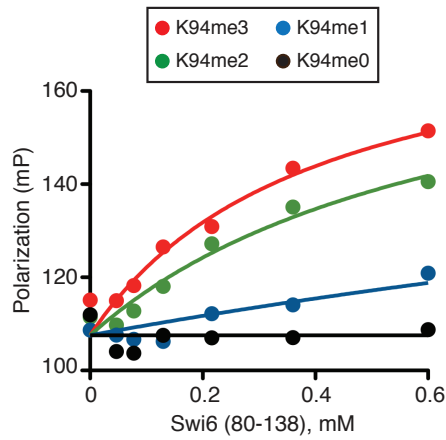


FIGURE 2

a

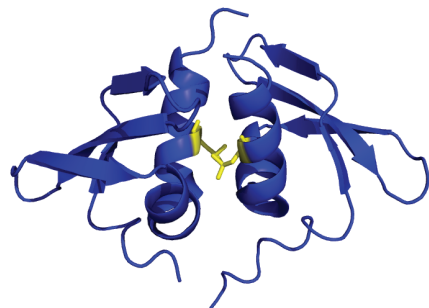


b



Swi6 peptide sequence:
KHRMAR^{K₉₄}GGGYEYLL

	<i>K_d</i> , mM
me3	0.4
me2	0.7
me1	3.2
me0	> 40

FIGURE 3**a****b**

Temperature dependence on the isodesmic self-association of Swi6 (261-329)

Temperature	$1/K_{\text{obs}}$	95% confidence interval
8°C	38nM	3.4nM - 116nM
25°C	100nM	54nM - 150nM
30°C	250nM	220nM - 290
37°C	3700nM	2100nM - 6100nM

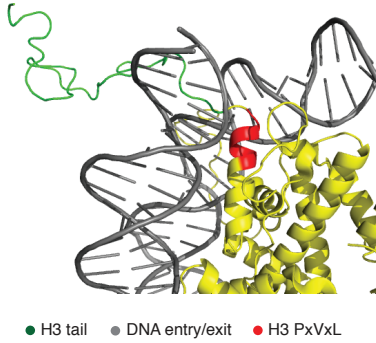
c

Temperature dependence on the isodesmic self-association of Swi6 (1-329)

Temperature	$1/K_{\text{obs}}^{\text{iso}}$	95% confidence interval
8°C	80 μ M	65 μ M - 104 μ M
16°C	78 μ M	62 μ M - 105 μ M
24°C	68 μ M	58 μ M - 82 μ M
30°C	58 μ M	51 μ M - 67 μ M

FIGURE 4

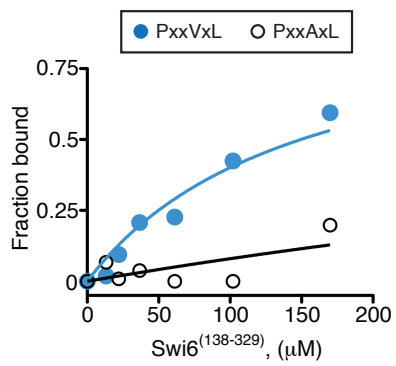
a



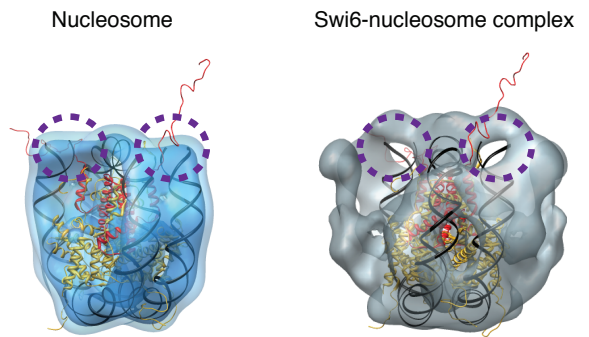
b

Swi6	<i>H3 tail affinity</i>	<i>nucleosome affinity</i>		
	(K_d , μM)	H3K ₉ me3	H3K ₉ me3	H3K ₉
WT	12 ± 1.8	0.11 ± 0.01	8 ± 0.4	
LoopX	2 ± 0.2	1.1 ± 0.04	67 ± 5.0	
DimerX	2.7 ± 0.3	1.1 ± 0.04	18 ± 1.0	
1-261	3 ± 0.6	0.5 ± 0.2	8 ± 3.4	

c



d



e

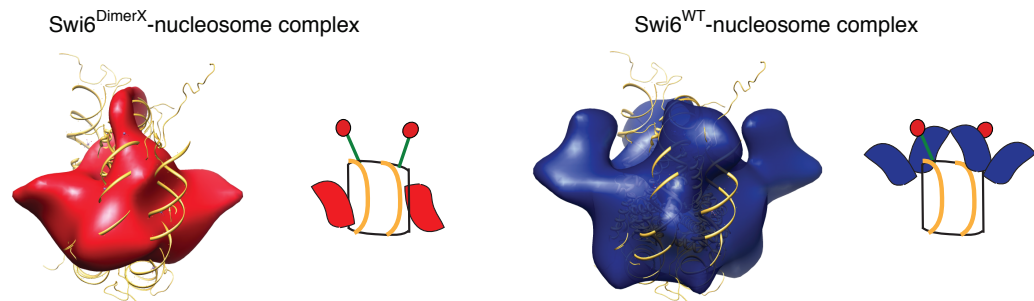
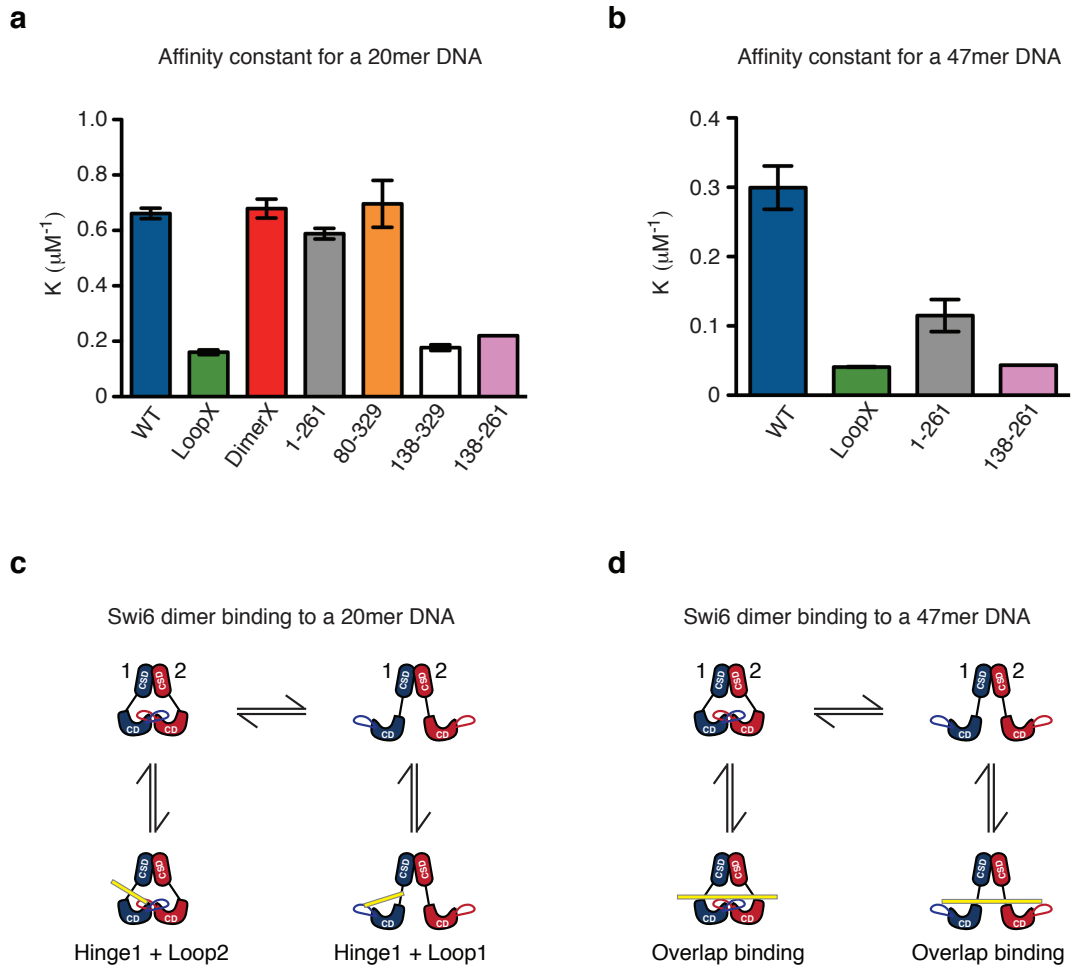


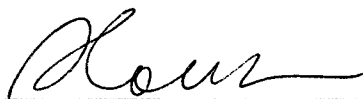
FIGURE 5



Publishing Agreement

It is the policy of the University to encourage the distribution of all theses, dissertations, and manuscripts. Copies of all UCSF theses, dissertations, and manuscripts will be routed to the library via the Graduate Division. The library will make all theses, dissertations, and manuscripts accessible to the public and will preserve these to the best of their abilities, in perpetuity.

I hereby grant permission to the Graduate Division of the University of California, San Francisco to release copies of my thesis, dissertation, or manuscript to the Campus Library to provide access and preservation, in whole or in part, in perpetuity.



Author Signature

12/22/12
Date